Isotopic Patterns in Modern Global Precipitation

KAZIMIERZ ROZANSKI, LUIS ARAGUÁS-ARAGUÁS, AND ROBERTO GONFIANTINI

International Atomic Energy Agency, P.O. Box 100, 1400-Vienna, Austria

The International Atomic Energy Agency (IAEA), in cooperation with the World Meteorological Organization (WMO), has been conducting a world-wide survey of hydrogen ($^2H/^1H$) and oxygen ($^{18}O/^{16}O$) isotope composition of monthly precipitation since 1961. At present, 72 IAEA/WMO network stations are in operation. Another 82 stations belonging to national organizations continue to send their results to the IAEA for publication. The paper focuses on basic features of spatial and temporal distribution of deuterium and ^{18}O in global precipitation, as derived from the IAEA/WMO isotope database. The internal structure and basic characteristics of this database are discussed in some detail. The existing phenomenological relationships between observed stable isotope composition of precipitation and various climate-related parameters such as local surface air temperature and amount of precipitation are reviewed and critically assessed. Attempts are presented towards revealing interannual fluctuations in the accumulated isotope records and relating them to changes of precipitation amount and the surface air temperature over the past 30 years.

INTRODUCTION

Decisive improvements in mass-spectrometry techniques shortly after World War II [*Nier*, 1947; *Nier et al.*, 1947; *McKinney et al.*, 1950] enabled precise measurements of the natural abundances of oxygen-18 and deuterium in meteoric waters. First publications on this subject appeared within a few years [*Dansgaard*, 1953, 1954; *Epstein and Mayeda*, 1953; *Friedman*, 1953]. The first attempt to summarize the available information on the isotopic composition of freshwaters worldwide (including precipitation) was published by Craig in 1961 [*Craig*, 1961].

In the same year the International Atomic Energy Agency (IAEA), in cooperation with the World Meteorological Organization (WMO), initiated a world-wide survey of the isotope composition of monthly precipitation. The programme was launched with the primary objective of collecting systematic data on isotope content of precipitation on a global scale (deuterium, oxygen-18 and tritium), characterizing their spatial and temporal variability and, consequently, providing basic isotope data for the use of environmental isotopes in hydrogeological investigations. It appeared soon that the collected data are also very useful in other water-related fields such as oceanography, hydrometeorology and climatology.

The operation of the network started with more than 100 meteorological stations in 65 countries and territories, collecting monthly composite precipitation samples for isotope analyses. The number of stations varied and reached a maximum of about 220 stations in 1963-64. After a revision in 1977, operation of some stations was stopped. During the past decade, the number of IAEA/WMO network stations was oscillating around eighty. Approximately the same number of stations belonging to national organizations continued to send their results to the IAEA for publication. Since 1990, approximately 15 new stations have been incorporated in the network, mainly representing regions with poor data coverage. Detailed technical procedures for the collection and shipment of samples, to be followed by the stations, and a standardized data reporting format were introduced from the beginning of operation of the network. The isotope analyses are performed in the IAEA laboratory and in laboratories of cooperating institutions in Member States. In addition to the isotope data, certain meteorological variables are also recorded (type and amount of precipitation, surface air temperature, vapor pressure) and reported to the IAEA.

The isotope and meteorological data are published regularly by the IAEA in the form of data books [*IAEA*, 1969, 1970, 1971, 1973, 1975, 1979, 1983, 1986, 1990] and are also available on magnetic tape or on floppy disks. Information on isotopic composition of precipitation includes the tritium content (reported as $^3H/^1H$ ratios, expressed in Tritium Units) and the stable isotope ratios ($^2H/^1H$ and $^{18}O/^{16}O$), all with their analytical errors as stated by the laboratories performing the analyses. Basic statistical treatment of the data accumulated till 1978 is available as a separate volume [*IAEA*, 1981]. A revised and extended version of this treatment, covering the data gathered up to the end of 1987, was published by the IAEA in 1992 [*IAEA*, 1992].

The basic characteristics of the network, as at the end of 1987, are summarized in Figures 1 to 3. The total number of stations ever operated is 379. Both tritium and stable isotopes are available for approximately 64 percent of the stations. Of the 251 stations for which the stable isotope data are available, 219 have an oxygen-18 record

Climate Change in Continental Isotopic Records
Geophysical Monograph 78

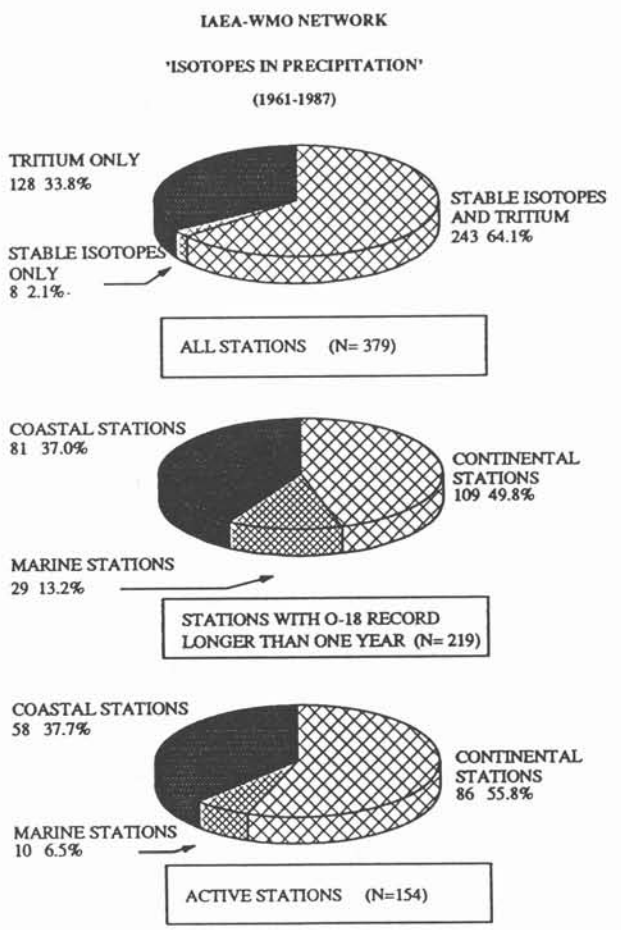

Fig. 1. General structure of the IAEA/WMO global network "Isotopes in Precipitation".

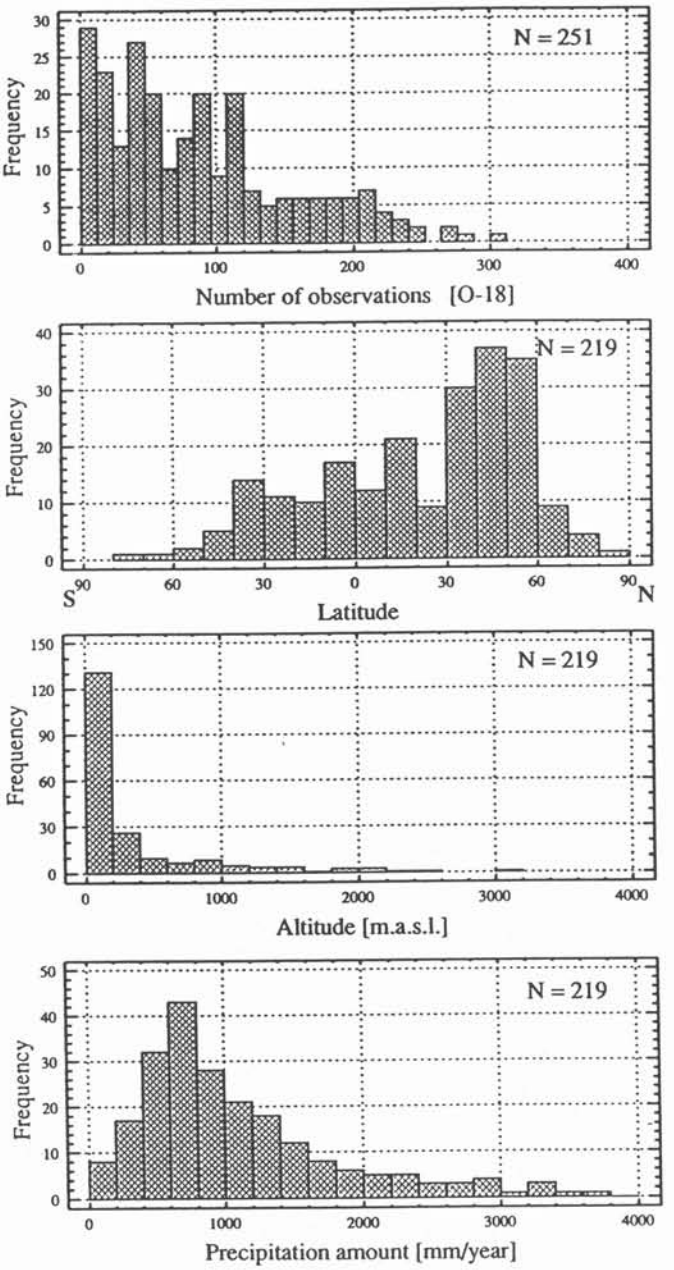

Fig. 2. (a) Frequency distribution histogram of the length of ^{18}O records available for the IAEA/WMO stations, as at the end of 1987; (b) Latitudinal distribution of the network stations for which a minimum of one year of ^{18}O record is available; (c) Frequency distribution histogram of the network stations with respect to altitude of their location; (d) Frequency distribution histogram of the network stations with respect to the amount of annual precipitation.

longer than one complete year (at least 12 monthly ^{18}O values). Only these stations were considered in this study. Although only one year of ^{18}O record may not always properly reflect average conditions at a given station, we have decided to include in the discussion also these relatively short records in order to improve spatial coverage with the data. Geographical distribution of the network stations is rather inhomogeneous (Figure 3); more than 50 percent are located in mid- northern latitudes, between 30°N and 60°N (Figure 2). Only 16 out of 219 stations are located in high latitudes (< 60°). The low-altitude stations (up to 200 m a.s.l.) constitute about 60 percent of the selected stations. Mountainous regions (above 1000 m a.s.l.) are represented by 24 stations. The length of the available oxygen-18 record also varies considerably (Figure 2). For 64 out of 219 stations, the record is shorter than 3 years. There are 32 stations for which at least 20 years of ^{18}O record is available. The Vienna station has the longest ^{18}O record (348 monthly data, 31 years of operation).

To date, approximately 180,000 isotope and meteorological values have been accumulated in the IAEA database. Critical analysis of the quality of stored information has recently been carried out, resulting in removing inconsistent data, obvious outliers, typing errors, etc. Altogether 530 stable isotope, 28 tritium and 325 meteorological data have been removed in this way from the database. Similar analysis carried out recently for several southern hemisphere stations revealed that a substantial part of the stable isotope record for Rarotonga, Kaitaia and Invercargill are unreliable, most probably due to evaporation of precipitation samples after collection [*Taylor*,

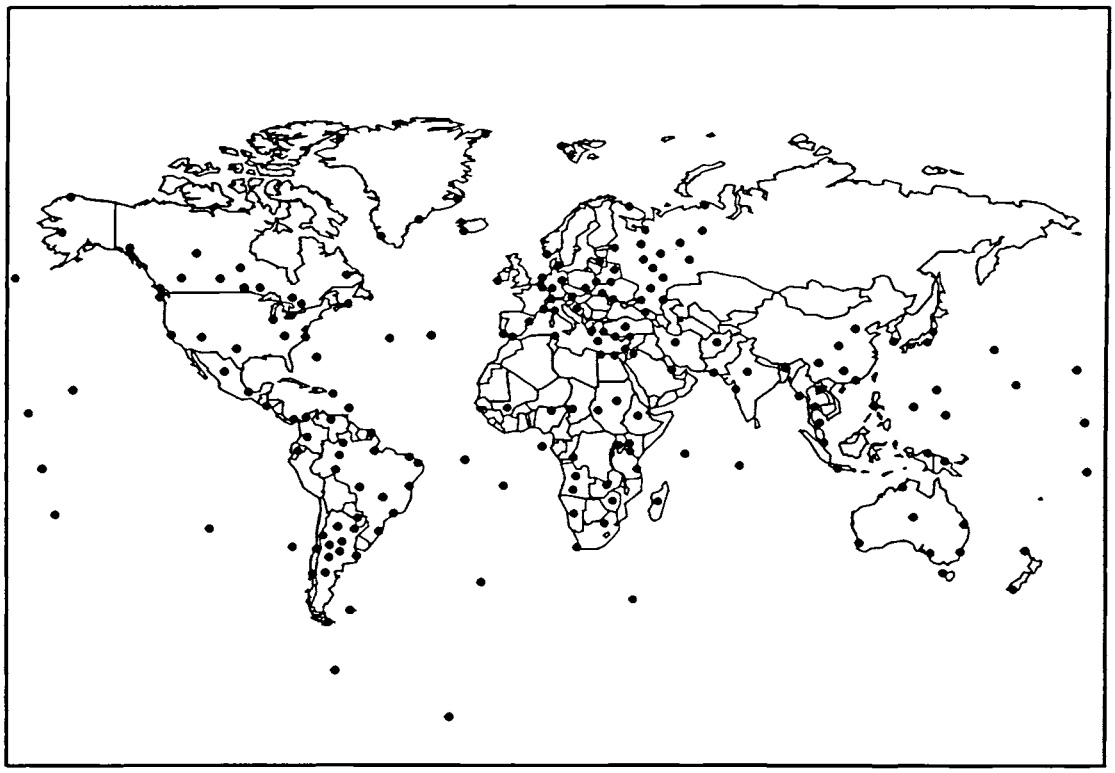

Fig. 3. Geographical distribution of the IAEA/WMO network stations for which a minimum of one complete year of stable isotope record is available.

1990]. These erroneous results were also removed from the database. Although some errors may still be present in the record, we believe that the overall quality of the database is now substantially improved. The revised statistical treatment mentioned above has been based on this cleaned database.

The stable isotope ratios of water, $^2H/^1H$ and $^{18}O/^{16}O$, are expressed by convention as parts per thousand deviation relative to the standard V-SMOW (Vienna Standard Mean Ocean Water). Delta notation, δ^2H or $\delta^{18}O$, commonly used to report the measured isotope variations, is defined by the following equation:

$$\delta = \left(\frac{R_{SAMPLE}}{R_{STANDARD}} - 1 \right) \times 1000 \quad [‰] \qquad (1)$$

where R_{SAMPLE} and $R_{STANDARD}$ stand for the isotope ratios $^2H/^1H$ or $^{18}O/^{16}O$ of the sample and the standard, respectively.

GLOBAL DISTRIBUTION PATTERNS

The early data gathered by the IAEA/WMO network were reviewed by Dansgaard [*Dansgaard*, 1964]. He gave a salient phenomenological evaluation of these data, relating the observed distribution of heavy isotopes to a number of environmental parameters characterizing the given sampling site, such as latitude, altitude, distance to the coast, amount of precipitation, surface air temperature. The reviews which followed [*Yurtsever and Gat*, 1981; *Gonfiantini*, 1982, *Gonfiantini*, 1985] essentially confirmed the early findings of Dansgaard. It was soon realized that the above mentioned empirical relationships (so called "effects") can in fact be considered as a measure of the average degree of rain-out of moisture from the given air mass, on the way from the source region to the site of precipitation.

The theoretical approaches to explain the observed isotope variations in meteoric waters evolved from the "isolated air mass" models based on Rayleigh condensation with immediate removal of precipitation or with a part of the condensate being kept in the cloud during the rain-out process [*Dansgaard*, 1964; *Friedman et al.*, 1964; *Craig and Gordon*, 1965; *Gat and Dansgaard*, 1972; *Taylor*, 1972; *Merlivat and Jouzel*, 1979; *Siegenthaler and Matter*, 1983; *Van der Straaten and Mook*, 1983; *Covey and Haagenson*, 1984; *Jouzel and Merlivat*, 1984; *Gedzelman*, 1988; *Johnsen et al.*, 1989]. The Rayleigh condensation concept has also been used in connection with classical equations of water vapor transport in the atmosphere, to model regional isotope fields [*Eriksson*, 1965; *Rozanski et al.*, 1982; *Sonntag et al.*, 1983; *Fisher and Alt*, 1985; *Fisher*, 1990; *Gedzelman and Lawrence*, 1990; *Ingraham and Craig*, this volume]. The global-scale modelling of deuterium and oxygen-18 distribution patterns in precipitation was recently carried out with the aid of general circulation models (GCMs) of the atmosphere [*Joussaume et al.*, 1984a,b; *Jouzel at al.*, 1987a; *Jouzel et al.*,1991). It appears that major characteristics of the global isotope fields are properly reproduced by the currently available GCMs.

A considerable amount of theoretical and applied work carried out

during the past three decades resulted in a fairly good understanding of the processes controlling the isotopic evolution of atmospheric waters at different levels of the water cycle. It became apparent that, like many other atmospheric properties, the isotopic composition of atmospheric water vapor and, consequently, of precipitation exhibits a broad spectrum of temporal variations with characteristic periods ranging from minutes up to hundreds or thousands of years.

Isotope studies of individual storm events, initiated by *Dansgaard* [1953] and continued by many other authors [e.g. *Gambell and Friedman*, 1965; *Miyake et al.*, 1968; *Ambach et al.*, 1975; *Gedzelman and Lawrence*, 1982; *Rindsberger et al.*, 1990], revealed that stable isotope composition of successive portions of precipitation collected during single rain event may vary dramatically. *Rindsberger et al.* [1990] in the regional study of individual rain events in Israel found that quite often the pattern of evolution of $\delta^{18}O$ in time is V- or W-shaped: a sharp decrease of the δ values was usually observed with a minimum value sometime in the middle of the shower. The most depleted isotope values corresponded usually to the period of most intense rain. This pattern was attributed to the passage of the frontal system(s). The range of in-storm $\delta^{18}O$ variations was quite large, reaching in some cases 10 to 12 per mil. Similar results were obtained by other authors [*Gambell and Friedman*, 1965; *Miyake et al.*, 1968; *E.M. Adar* - unpublished data, 1992]. The general conclusion of these studies was that the isotopic composition of precipitation from a given storm depends strongly on meteorological history of the air in which the precipitation is produced and through which it falls.

Precipitation samples collected on the per-event basis also reveal a strong linkage between their isotope signature and the storm's path, structure and evolution [*Rindsberger et al.*, 1983; *Gedzelman and Lawrence*, 1990; *Nativ and Riggio*, 1990]. For instance, detailed analysis of meteorological processes producing precipitation over northeastern United States led Gedzelman and co-workers [*Gedzelman and Lawrence*, 1982; *Lawrence et al.*, 1982] to the conclusion that the further south the storm track and the warm front, the lower δD value of precipitation. They also demonstrated that convective clouds produce precipitation with higher δ values than stratiform clouds with the same base and top.

A distinction should be made between liquid (rain) and solid (snow, hail) precipitation. Whereas isotopic composition of snow or hail collected at the ground reflects in-cloud conditions, raindrops undergo evaporation and isotopic exchange with atmospheric vapor on their fall down to the surface. Theoretical estimates [*Miyake et al.*, 1968; *Jouzel*, 1986], laboratory experiments [*Steward*, 1975] as well as isotope analyses of parallel samples of water vapor and rain collected at the ground [*Schoch-Fischer et al.*, 1984; *Jacob and Sonntag*, 1991] indicate that isotope exchange of raindrops with surrounding moisture is efficient enough to bring isotopic composition of rain close to the equilibrium value at the ground-level temperature. Substantial evaporative enrichment of raindrops beneath the cloud is mainly observed for light rains falling in relatively dry atmosphere.

The information available to date about deuterium and oxygen-18 content of global precipitation will be reviewed and discussed below in some detail. The review is based on the IAEA/WMO database (1961-1987, stations with at least a one-year record of oxygen-18). In some cases we use in the discussion more recent data sets as well as other published data, not included in the network. Regional maps of ^{18}O content in precipitation are shown in Figures 4 to 9. For each station two values are reported: long-term arithmetic and long-term weighted mean $\delta^{18}O$ (weighing by the amount of precipitation).

One should keep in mind that the IAEA/WMO database, represented by monthly composite samples of precipitation, provides only statistically averaged, episodic information about isotopic composition of atmospheric water vapor, resulting from successive precipitation events, each usually with highly variable isotope characteristics.

Latitudinal distribution

The annual mean values of ^{18}O content in precipitation are plotted in Figure 10a as a function of latitude. The available data from high-latitude regions (mainly Greenland and Antarctica) are also schematically indicated on the figure. They represent in most cases freshly collected snow [*Lorius and Merlivat*, 1977; *Peel et al.*, 1988; *Johnsen et al.*, 1989; *Petit et al.*, 1991; *A. D. Fisher* - unpublished data, 1991].

The distribution shown in Figure 10a can be qualitatively understood in view of the fact that the major global source of water vapor is the tropical ocean; approximately 65 percent of the global evaporation flux over the oceans originates between 30°S and 30°N [*Peixoto and Oort*, 1983]. Poleward transport of this vapor is connected with gradual rain-out and the resulting reduction of total precipitable water in the atmosphere. This process can be modelled using the above mentioned Rayleigh approach. In fact, *Fisher* [1990] was able to reproduce fairly well the $\delta^{18}O$ distribution shown in Figure 10a using a zonally-averaged global isotope model with distributed water vapor sources. The remarkable spread of the data shown in Figure 10a has several sources: (1) precipitation collected at mid-latitude continental stations is in general more depleted in heavy isotopes than at coastal or marine stations located at the same latitude (see discussion below). This effect is especially obvious in the northern hemisphere; (2) a strong vertical gradient in the isotope content of atmospheric moisture [*Taylor*, 1972; *Ehhalt*, 1974; *Rozanski and Sonntag*, 1982] results in an apparent tendency to observe precipitation more depleted in heavy isotopes with increasing elevation of the sampling site. Perhaps the most characteristic example of this effect is the Izobamba station located in the Andes close to the equator (elevation 3058 m a.s.l.), which exhibits the isotope composition of precipitation typical for mid-latitude regions; (3) some tropical maritime stations tend to show excessive depletion in the heavy isotope content when compared with coastal or continental stations located within the same latitude belt, due to pronounced amount effect; (4) regional temperature anomalies may result in the average isotopic composition of precipitation falling off the general latitudinal trend. For instance, some coastal stations in the North Atlantic region (Reykjavik, Lista, Isfjord, Valentia) are characterized by relatively enriched $\delta^{18}O$ values, probably due to the positive temperature anomaly caused by the presence of the Gulf Stream. A substantial contribution of local vapor sources for some of the stations in the region, as suggested by *Johnsen et al.* [1989], may also contribute to the observed effect.

The role of temperature in establishing the latitudinal gradient in the heavy isotope composition of precipitation is illustrated in Figure 10b. It shows the 3-month averages of $\delta^{18}O$ (winter and summer

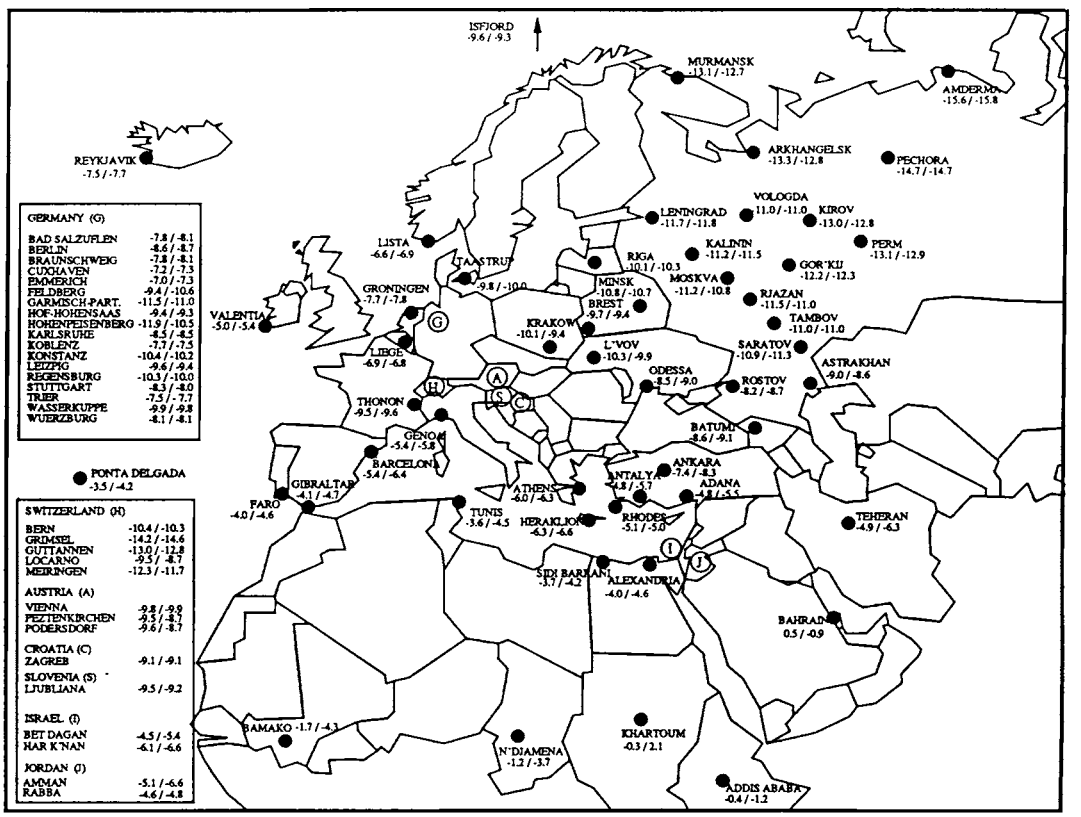

Fig. 4. Geographical distribution of the IAEA/WMO network stations in Europe. The stations are identified by name. For each station the long-term arithmetic mean (first number) and the weighted mean (second number) $\delta^{18}O$ values are indicated.

months, respectively) for continental and coastal stations, as a function of latitude. Reduced temperatures of the lower atmosphere over mid and high latitudes during winter months result in a substantial reduction of the total precipitable water in the atmosphere. For instance, for the latitude band of 40°N to 50°N the zonally-averaged total precipitable water drops from 25 kg m^{-2} in summer (JJA) to 12 kg m^{-2} during winter (DJF), with the values close to equator remaining essentially constant throughout the whole year [*Peixoto and Oort*, 1983]. This leads to a larger effective rain-out of the air masses resulting in a greater depletion of the heavy isotope content of precipitation during winter. As can be seen in Figure 10b, seasonal differences of the isotope signal are more pronounced in the northern hemisphere, reflecting the role of continents in establishing seasonal thermal gradients.

Continentality

The regional maps shown in Figures 4 to 9 reveal a great variety of distribution patterns of $\delta^{18}O$ over the continents. Detailed discussion of this distribution is beyond the scope of this paper. Here, we will focus only on the major features. In general, the distribution of $\delta^{18}O$ mimics the topography of the continents; mountainous chains are marked by more negative $\delta^{18}O$ values. This feature is called altitude effect. Also, there is an apparent tendency to observe more negative $\delta^{18}O$ values in precipitation with increasing distance from the coast. This feature is known as a "continental effect".

Basically the same mechanism is responsible for both effects: gradual removal of moisture from air masses which move inland or are orographically uplifted, coupled with preferential removal of the heavy isotopes during condensation process. This implies that the ocean is a major source of water vapor over the continents. Such an assumption might, however, not always be fulfilled, e.g. in the vicinity of large continental water bodies or in the interior of continents, where the re-evaporated moisture plays an important role in the atmospheric water balance [*Salati et al.*, 1979; *Sonntag et al.*, 1983; *Ingraham and Taylor*, 1986].

Systematic studies of isotopic composition of near-ground atmospheric water vapor carried out in Europe [*Schoch-Fischer et al.*, 1984; *Rozanski*, 1986; *Jacob and Sonntag*, 1991] and in the northeast United States [*White and Gedzelman*, 1984] revealed a strong positive correlation between δD of the vapor and the specific humidity of air. *Sonntag et al.* [1983] demonstrated that, under certain assumptions, the monthly and seasonal mean values of the specific humidity measured at ground level can be converted to the total precipitable water, using only ground-level characteristics of the atmosphere. Further, they showed that the ratio of total precipitable water measured over the continent to that over the vapor source region (monthly or seasonal averages) is a good measure of the average degree of rain-out of the air masses moving inland, and, consequently, can be used to calculate the average isotopic depletion of the vapor

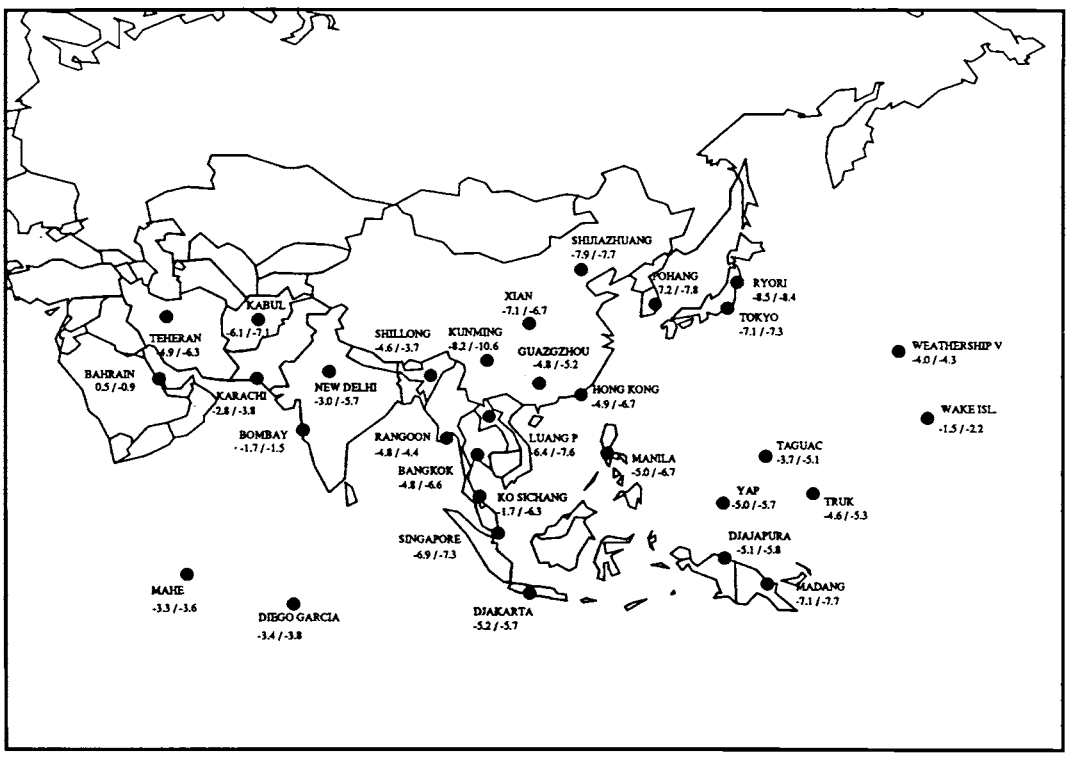

Fig. 5. Geographical distribution of the IAEA/WMO network stations in Asia and Far East. The stations are identified by name. For each station the long-term arithmetic mean (first number) and the weighted mean (second number) $\delta^{18}O$ values are indicated.

and precipitation over the continents.

Perhaps the most characteristic example of the continental effect is supplied by the available data for the European continent (Figure 11a). The seasonal and annual mean $\delta^{18}O$ values for selected European stations are plotted as a function of the distance from the Atlantic coast. The Atlantic coast was chosen due to predominant westerly circulation over western and central Europe [*Korzun*, 1974; *Peixoto and Oort*, 1983]. Two stations representing major source regions for the vapor entering the European continent are also shown in Figure 11a (Weathership E and Ponta Delgada). A distinct, gradual depletion of ^{18}O content in precipitation is observed with increasing distance from the coast. The overall depletion reaches 8 per mil over a distance of about 4500 km. The extent of the ^{18}O depletion varies seasonally: in winter it is much more pronounced than in summer. This effect has been explained by seasonal differences of water balance over the continent. In summer, the plant cover returns to the atmosphere substantial amounts of water during the transpiration process. This backward flux of vapor reduces the inland gradient of total precipitable water [*Peixoto and Oort*, 1983] and the resulting effective degree of rain-out of air masses moving eastward, which in turn reduces the extent of isotopic depletion of precipitation during summer months [*Rozanski et al.*, 1982]. The gradual isotopic depletion with increasing distance from the Atlantic coast seems to persist till the Ural Mountains. Unfortunately, no reliable data are so far available for western and central Siberia.

An apparent nonlinearity of the continental effect, limited to the winter months, is also seen in Figure 11a. A substantially larger slope of the best fit line (approximately 3.8‰ per 1000 km) is observed till the longitude band of about 17°E to 20°E, as compared with the average slope further east (about 1.6‰ per 1000 km). The decrease of the slope has been explained by additional moisture supply from the south (Mediterranean Sea, Black Sea, Caspian Sea), substantially contributing to water balance over eastern Europe during winter months [*Sonntag et al.*, 1983]. In fact, *Rozanski et al.* [1982] were able to reproduce the seasonal mean δD values in European precipitation only till the above mentioned longitude band, assuming that the Atlantic Ocean is the only source of water vapor over Europe. Significant south-north component in the horizontal vapor flux over eastern Europe during winter months is visible also on the global maps of the zonal and meridional horizontal vapor flow [*Korzun*, 1974; *Kuznetsova*, 1990] and on maps of total precipitable water [*Peixoto and Oort*, 1983].

Like western and central Europe, the South American continent is under the prevailing influence of the Atlantic ocean [*Ratisbona*, 1976]. The Andes constitute in fact an effective barrier against air masses transporting moisture from the Pacific Ocean. This fact has important consequences for spatial distribution of $\delta^{18}O$ in precipitation over this continent (Figure 7). For the Amazon Basin, the continental gradient of $\delta^{18}O$ in precipitation over the distance of the first 2000 kilometers from the coast is substantially smaller when compared to Europe (Figure 11b). It reaches approximately 1.5‰ per 1000 km, compared to about 2.0‰ per 1000 km for Europe,

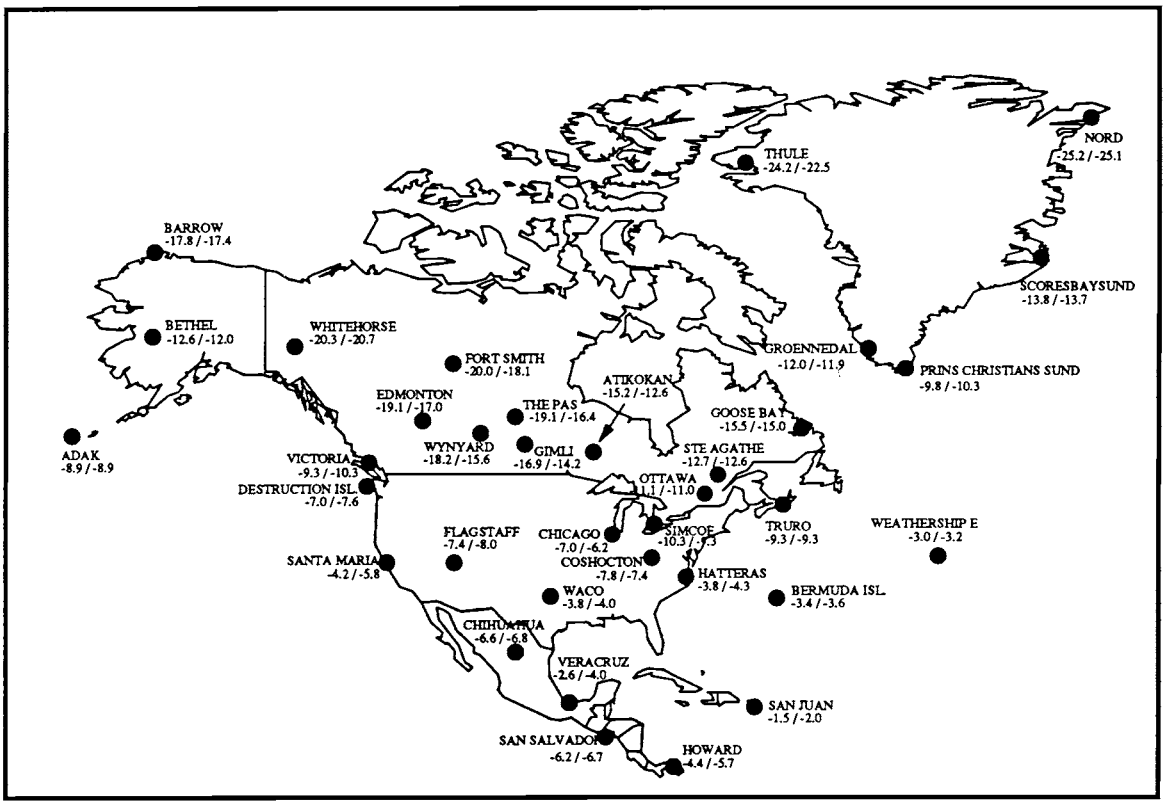

Fig. 6. Geographical distribution of the IAEA/WMO network stations in the north American continent. The stations are identified by name. For each station the long-term arithmetic mean (first number) and the weighted mean (second number) $\delta^{18}O$ values are indicated.

when long-term annual mean $\delta^{18}O$ values are considered. This reduced "continentality" of the isotope signal has been explained by intense recycling of moisture within the basin by the evapotranspiration [*Salati et al.*, 1979; *Gat and Matsui*, 1991]. Two other features of the data points presented in Figure 11b are worth being mentioned here: (1) the continental gradient of $\delta^{18}O$ in precipitation over the basin becomes very small west of Manaus; during the rainy period $\delta^{18}O$ is stabilized already at a distance of about 1000 kilometers from the coast. Such an effect can be observed in Europe only during summer, however at much greater distance from the coast (Figure 11a). This points to a high intensity of recycling of moisture by evapotranspiration in the Amazon Basin; (2) there are relatively large seasonal fluctuations of $\delta^{18}O$ in precipitation already at the entrance to the Amazon Basin (station Belém) which are then propagated westward. Origin of these variations remains unclear. *Matsui et al.* [1983] noted that very low $\delta^{18}O$ in precipitation and in atmospheric moisture at Belém are associated with the passage of the Intertropical Convergence Zone (ITCZ) over the region. The Izobamba station, shown for comparison in Figure 11b, reveals much higher isotope depletion than the stations located within the basin. It results from orographic uplift of the air masses on the eastern slopes of the Andes.

The data coverage for the North American continent (Figure 6) is not as good as for Europe. On the other hand, spatial distribution patterns of $\delta^{18}O$ and δD in precipitation over this continent are substantially more complex, reflecting seasonally varying influence of the air masses of different origin: (1) Gulf of Mexico and subtropical Atlantic in the south-east; (2) subtropical Pacific in the south-west; (3) north Pacific in the west and north-west, and (4) Arctic in the north [*Bryson and Hare*, 1974]. This results in a strong apparent linkage between isotope signature of precipitation and the air mass trajectories as reported by several authors [*Lawrence et al.*, 1982; *Fritz et al.*, 1983; *Nativ and Riggio*, 1990; *Lawrence and White*, 1991; *Friedman et al.*, 1992]. On a regional scale, a distinct continental effect recorded in surface and shallow ground waters has been observed by *Ingraham and Taylor* [1986] along a traverse through Northern California and by *Yonge et al.*, [1989] in southwestern Canada.

Isotope data for the African continent are scarce (Figure 8). Three sources of vapour can in principle contribute to precipitation collected over the continent: the Atlantic Ocean, the Indian Ocean and the Mediterranean Sea. The contribution of the Mediterranean is limited to North Africa. Precipitation patterns over Western and Central Africa are controlled by seasonal shift of the ITCZ with associated NE or SE trade winds and permanent monsoonal flow originating in the southern subtropical Atlantic [*Lacaux et al.*, 1992]. Eastern Africa receives most of its precipitation from the Indian Ocean. For the stations located between 0 and 15°N the rainy period usually lasts from June to September, whereas the south-east of Africa receives most of its precipitation between November and April. It is interesting to compare the stations lying along the trajectory of the Atlantic monsoonal flow (Kano, N'djamena,

Fig. 7. Geographical distribution of the IAEA/WMO network stations in the south American continent. The stations are identified by name. For each station the long-term arithmetic mean (first number) and the weighted mean (second number) $\delta^{18}O$ values are indicated.

Geneina, Khartoum). An apparent increase of $\delta^{18}O$ with increasing distance from the coast is observed. Surprisingly enough, the Addis Ababa station, situated at an elevation of 2360 m a.s.l., reveals the highest ^{18}O enrichment of precipitation among the stations of the region. Most of the data points cluster along the Global Meteoric Water Line (cf. Figure 27) which excludes substantial evaporative enrichment of rain collected at this station.

It has been suggested [*Sonntag et al.*,1979] that rainforest of the Congo Basin may represent an important source of moisture for the regions situated north and north-east of the basin thus leading to relatively high $\delta^{18}O$ and δD values of Addis Ababa precipitation. Because the transpiration proceeds without isotope differentiation [*Zimmermann et al.*, 1967], the moisture released in this process will be isotopically much heavier than the atmospheric water vapor of maritime origin. Consequently, rain produced from such recycled moisture can easily reach positive $\delta^{18}O$ and δD values, which often happens at Addis Ababa. Further, more detailed studies of rain and atmospheric moisture in the region would be needed to verify this hypothesis.

Recently, *Joseph et al*, [1992] proposed an alternative explanation for the apparent east-west gradient in ^{18}O content of precipitation and shallow ground waters observed in the Sahelo-Sudanese Zone in Africa (between 10°N and 17°N), which includes the network stations discussed above. They suggest that a major supply of moisture for this region is from the Indian Ocean. The vapor is transported westward by the zonal flows of East African Jet and Tropical Easterly Jet. In their model, the rain collected at Addis Ababa during the rainy period represents in fact first condensation stage of maritime moisture brought by the Indian monsoon.

Seasonality

The regular seasonal variations of deuterium and ^{18}O content of monthly precipitation, with precipitation isotopically depleted in

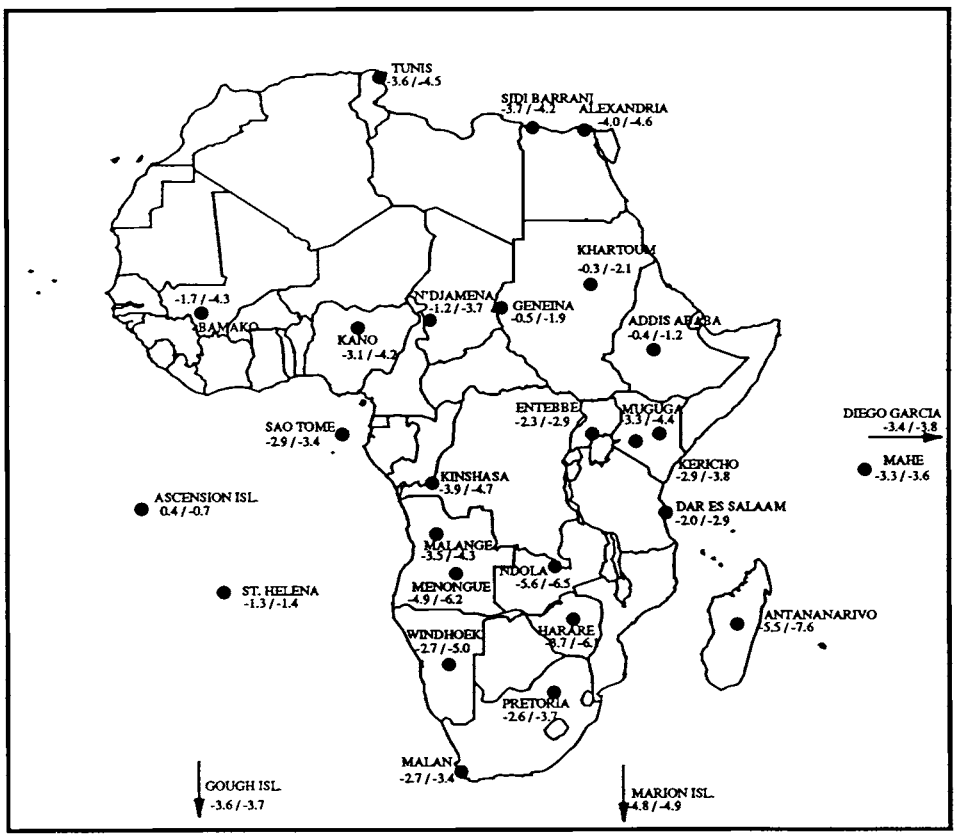

Fig. 8. Geographical distribution of the IAEA/WMO network stations in Africa. The stations are identified by name. For each station the long-term arithmetic mean (first number) and the weighted mean (second number) $\delta^{18}O$ values are indicated.

winter and enriched in summer, are common at mid- and high-latitude stations of the IAEA/WMO network. These seasonal differences are due to several factors: (1) seasonally changing temperature at mid- and high latitudes, with only minor fluctuations in the tropics. It results in seasonal variations of the total precipitable water in the atmosphere at these latitudes due to a varying degree of rain-out of the air masses transported poleward. This, in turn, via the Rayleigh mechanism, induces seasonality in the isotope signal observed in precipitation; (2) seasonally modulated evapotranspiration flux over the continents induces seasonal differences in the atmospheric water balance; (3) seasonally changing source areas of the vapor and/or different storm trajectories.

The seasonal fluctuations of $\delta^{18}O$ and δD, observed at many tropical island stations, have a different origin. In this case, the ^{18}O and deuterium content in precipitation is usually well correlated with the amount of precipitation (see discussion below). Isotopically depleted precipitation is observed during the rainy period.

Figure 12 illustrates the seasonal variability of $\delta^{18}O$ and temperature records for selected stations of the network. Groups of stations representing marine, coastal and continental environments at low, mid- and high latitudes are shown. It is obvious that the continental stations reveal much higher seasonal variations of both $\delta^{18}O$ and temperature than is the case for marine or coastal stations.

The gradual enhancement of seasonal variations of the isotope and temperature records with increasing distance from the coast is illustrated by Figure 13, showing the long-term monthly means of $\delta^{18}O$ and temperature for several European stations. The amplitude of $\delta^{18}O$ signal increases from about $2.5‰$ at the coast (the Valentia station) to approximately $10‰$ at the station Moskva, 3200 km inland. The above discussed substantial reduction of the continental effect during summer is also visible in Figure 13a. The large amplitude of seasonal variations of the heavy isotope composition of precipitation at more continental sites in Europe has been attributed to a combined effect of: (1) reduced continental isotope gradient in precipitation during summer due to recycling of atmospheric moisture by evapotranspiration, and (2) seasonally changing thermal gradient between the source regions (subtropical Atlantic) and the continent, leading to a larger degree of rain-out of air masses during winter months [*Rozanski et al.*, 1982].

The amount effect

The apparent correlation between the amount of monthly precipitation and its isotopic composition was first observed by *Dansgaard* [1964] and named the "amount effect". Figure 14a illustrates this relationship for tropical marine stations of the network (islands) located between 20°S and 20°N. The long-term monthly and annual means of $\delta^{18}O$ are plotted there as a function of the average

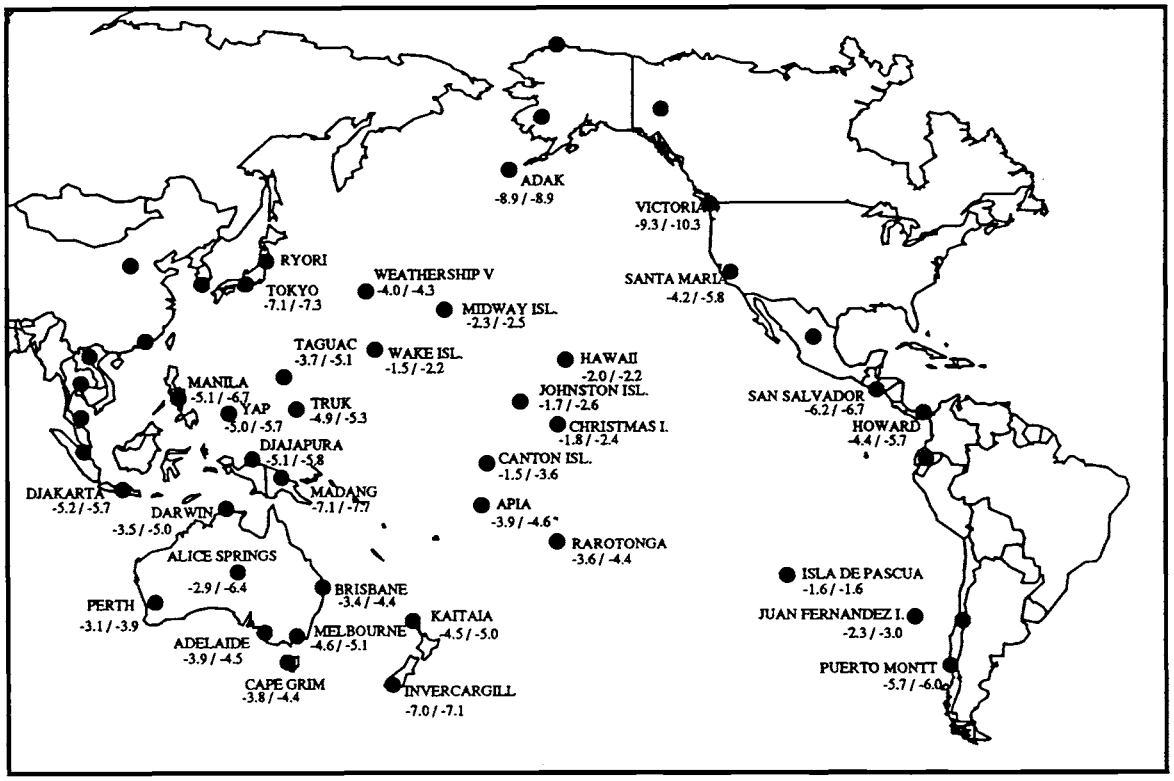

Fig. 9. Geographical distribution of the IAEA/WMO network stations in the Pacific region. The stations are identified by name. For each station the long-term arithmetic mean (first number) and the weighted mean (second number) $\delta^{18}O$ values are indicated.

monthly precipitation. The same isotope data are plotted on Figure 14b as a function of surface air temperature (monthly and annual means). Apparently, there is a strong inverse relationship between the mean monthly or annual $\delta^{18}O$ of precipitation and the amount of monthly precipitation for these stations whereas the correlation with the mean monthly (annual) surface air temperature is virtually nonexistent.

Figure 15 shows seasonal variations of $\delta^{18}O$, temperature and amount of precipitation at two tropical island stations: Apia (13.80°S, 171.7°W) and Taguac, Guam Island (13.55°N, 144.83°E). Both stations experience only minor fluctuations of temperature throughout the year. The $\delta^{18}O$ is inversely correlated with the amount of monthly precipitation: the correlation coefficient is equal to 0.55 for Apia and 0.71 for Taguac [*IAEA*, 1992].

The inverse relationship between precipitation $\delta^{18}O$ (δD) values and precipitation intensity in a single storm was reported by several authors [*Matsuo and Friedman*, 1967; *Miyake et al.*, 1968, *Mook et al.*, 1974; *Ambach et al.*, 1975]. This led *Yapp* [1982] to the development of a cloud model simulating isotopic composition of precipitation during convective showers, in which the precipitation rate at a given height is controlled mainly by the vertical velocity of ascending air mass. He was able to reproduce monthly mean δD values of precipitation recorded at two tropical islands (Wake Island and Johnston Island), as a function of rain intensity recorded at these stations. He further showed that the amount effect may be explicable, in part, as a consequence of the extent of rain-out process of deep convective clouds because a rough correspondence was noted between monthly mean precipitation intensity and precipitation amount at these two tropical, oceanic island sites.

Another process contributing to the amount effect is connected with isotope exchange and partial evaporation of raindrops below the cloud base. Already *Dansgaard* [1964] noted that during months with low precipitation, evaporative enrichment of raindrops may play an important role (low relative humidity beneath the cloud base) which is not the case during the rainy period. On the other hand, heavy showers will tend to modify the heavy isotope content of atmospheric moisture beneath the cloud towards a more negative value via the isotope exchange with falling raindrops. This, in turn, should help to preserve the in-cloud isotope signatures (low $\delta^{18}O$ and δD values) of raindrops collected at the ground.

For some tropical continental stations the apparent correlation between the heavy isotope composition and the amount of precipitation seems to be controlled not only by local rain-out processes but also by changes of the isotopic composition of the vapor in the source region. The Manaus station (3.12°S, 60.00°W) may serve as a good example of such a situation (Figure 16). Gradual decrease of $\delta^{18}O$ values observed between February and May at this station coincide with the maximum of precipitation, suggesting the typical amount effect. However, at the same time the ITCZ crosses the eastern margin of the Amazon Basin, pushing isotopically depleted

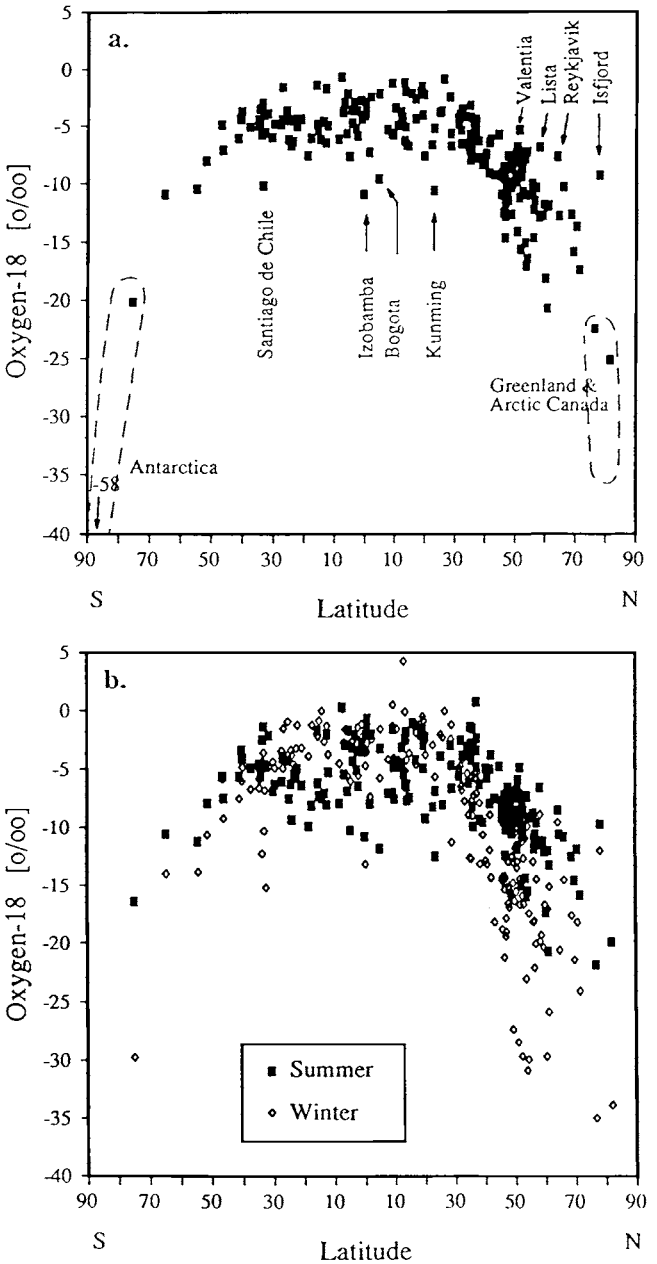

Fig. 10. (a) Long-term annual mean ^{18}O content in precipitation, derived from the database of the IAEA/WMO global network, plotted as a function of latitude. The $\delta^{18}O$ data for polar regions, gathered outside the network, are schematically indicated by contour lines [*Johnsen et al.*, 1989; *Lorius and Merlivat*, 1977; *Peel et al.*, 1988; *Petit et al.*, 1991; *D. A. Fisher* - unpublished data, 1991]; (b) Long-term seasonal mean ^{18}O content in precipitation, derived from the database of the network, plotted as a function of latitude. Summer season: June, July, August (NH) and December, January, February (SH). Winter season: December, January, February (NH) and June, July, August (SH).

moisture inland [*Matsui et al.*, 1983]. This negative isotope signal is visible also in the Izobamba station some 2000 km westward (Figure 16).

Figure 17 illustrates seasonal variations of $\delta^{18}O$, temperature and amount of monthly precipitation at two stations controlled by a monsoon climate: New Delhi (28.58°N, 77.20°E) and Hong Kong (22.32°N, 114.10°E). Contrary to tropical oceanic islands (Figure 15), the temperature at these stations reveals a distinct seasonal trend, with the maximum corresponding to monsoon period. Interestingly, the $\delta^{18}O$ is inversely correlated with monthly temperature with the slope equal to -0.42 $^{o}/_{oo}$ per °C for Hong Kong and -0.10 $^{o}/_{oo}$ per °C for New Delhi. This confirms a predominant role of the amount effect in establishing the observed seasonal variations of $\delta^{18}O$ in precipitation at these stations. The correlation coefficient of the monthly $\delta^{18}O$-precipitation relationship is equal to 0.45 and 0.71 for New Delhi and Hong Kong, respectively [*IAEA*, 1992].

The role of local temperature

The apparent link between local surface air temperature and the heavy isotope composition of precipitation has attracted much attention since the very beginning of isotope studies. This interest was stimulated mainly by the potential importance of stable isotopes as palaeoclimatic indicators. Numerous studies carried out during the past three decades were directed towards reconstruction of past climatic changes from records of isotopic composition of ancient precipitation preserved in various environmental archives such as glacier ice, sediments, groundwater, organic matter, and others [e.g. *Dansgaard et al.*, 1982; *Jouzel at al.*, 1987b; *Eicher and Siegenthaler*, 1976; *Winograd et al.*, 1988; *Yapp and Epstein*, 1977; *Becker et al.*, 1991; *Stute et al.*, 1992].

Dansgaard [1964] in his classical review presented the empirical relationship between the annual averages of $\delta^{18}O$ of precipitation and local surface air temperature, derived from the data gathered during the first three years of operation of the IAEA/WMO network. The relationship was developed for mid- and high northern latitude coastal stations. The slope of this relationship is 0.69$^{o}/_{oo}$ per °C for $\delta^{18}O$ and 5.6$^{o}/_{oo}$ per °C for δD. This relationship was frequently used in isotope-aided palaeoclimatic reconstructions. However, doubts often arose whether spatial relations between isotopic composition of precipitation and climatic variables, derived for the present-day conditions, can be used with confidence to interpret isotope records preserved in various environmental archives, as they usually reflect long-term linkage between isotopic composition of precipitation and climate on a given area.

In principle, three different types of the isotope-temperature relationship can be derived from the database of the IAEA/WMO network: (1) spatial relation between the long-term (annual) averages of $\delta^{18}O$ (δD) of precipitation and surface air temperature for different stations; (2) temporal relation between short-term (seasonal) changes of $\delta^{18}O$ (δD) and temperature for a single station or group of stations, and (3) temporal relation between long-term (interannual) changes of $\delta^{18}O$ (δD) and temperature at a given location.

Figure 18 shows the spatial relation between long-term annual arithmetic means of $\delta^{18}O$ and surface air temperature, derived for the entire set of the IAEA/WMO stations. It contains also the best fit lines of the published data for polar regions (Greenland, Antarctica). The data presented in Figure 18 confirm the temperature dependence of the isotope-temperature coefficient expected from theoretical

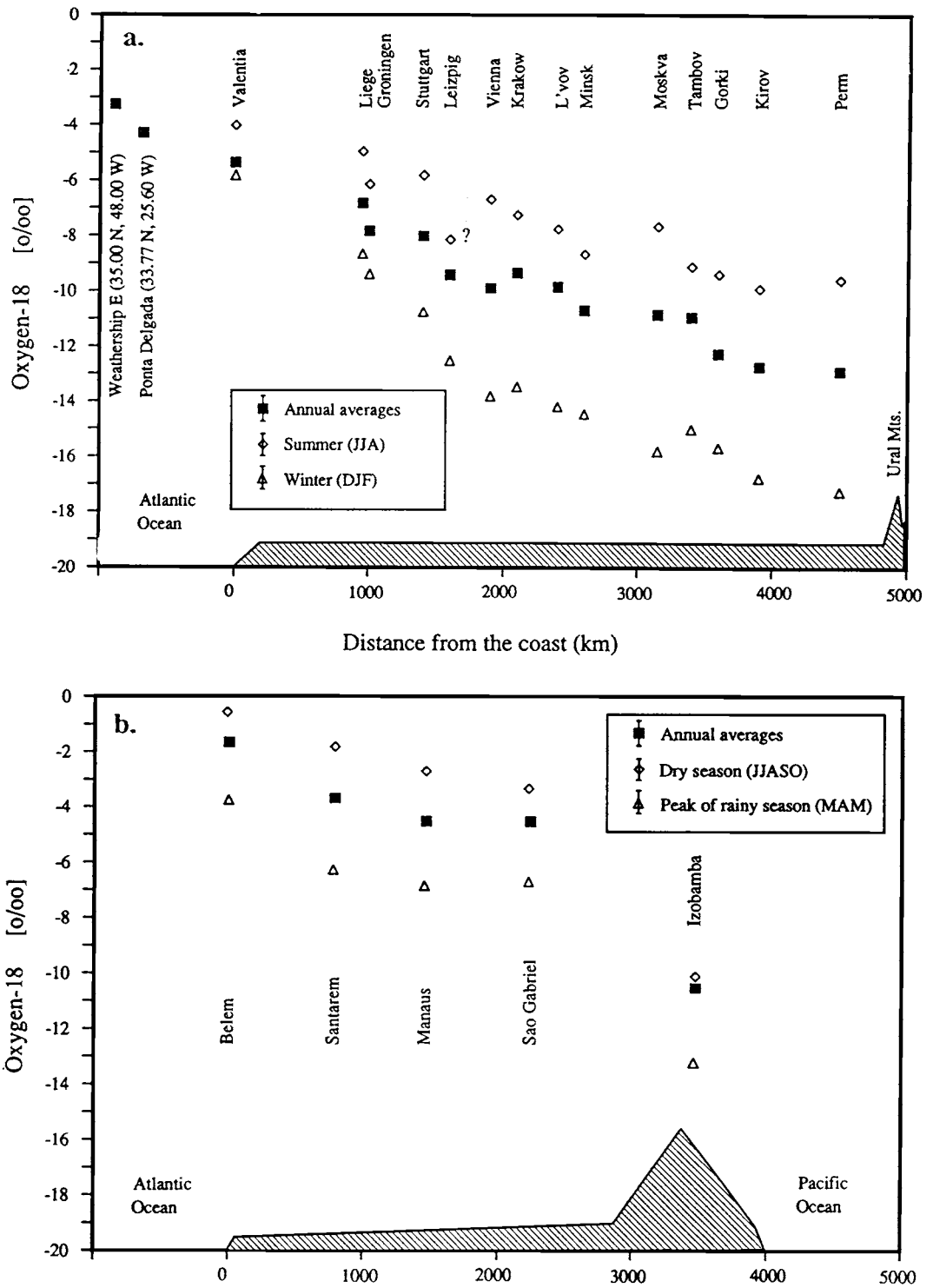

Fig. 11. (a) ^{18}O content of precipitation for selected European stations of the IAEA/WMO global network, plotted as a function of the distance from the Atlantic coast. Long-term annual, summer (June, July, August) and winter (December, January, February) mean $\delta^{18}O$ values are indicated for each station; (b) ^{18}O content of precipitation for selected stations of the network located in the Amazon Basin. The mean annual and seasonal $\delta^{18}O$ values are indicated for each station.

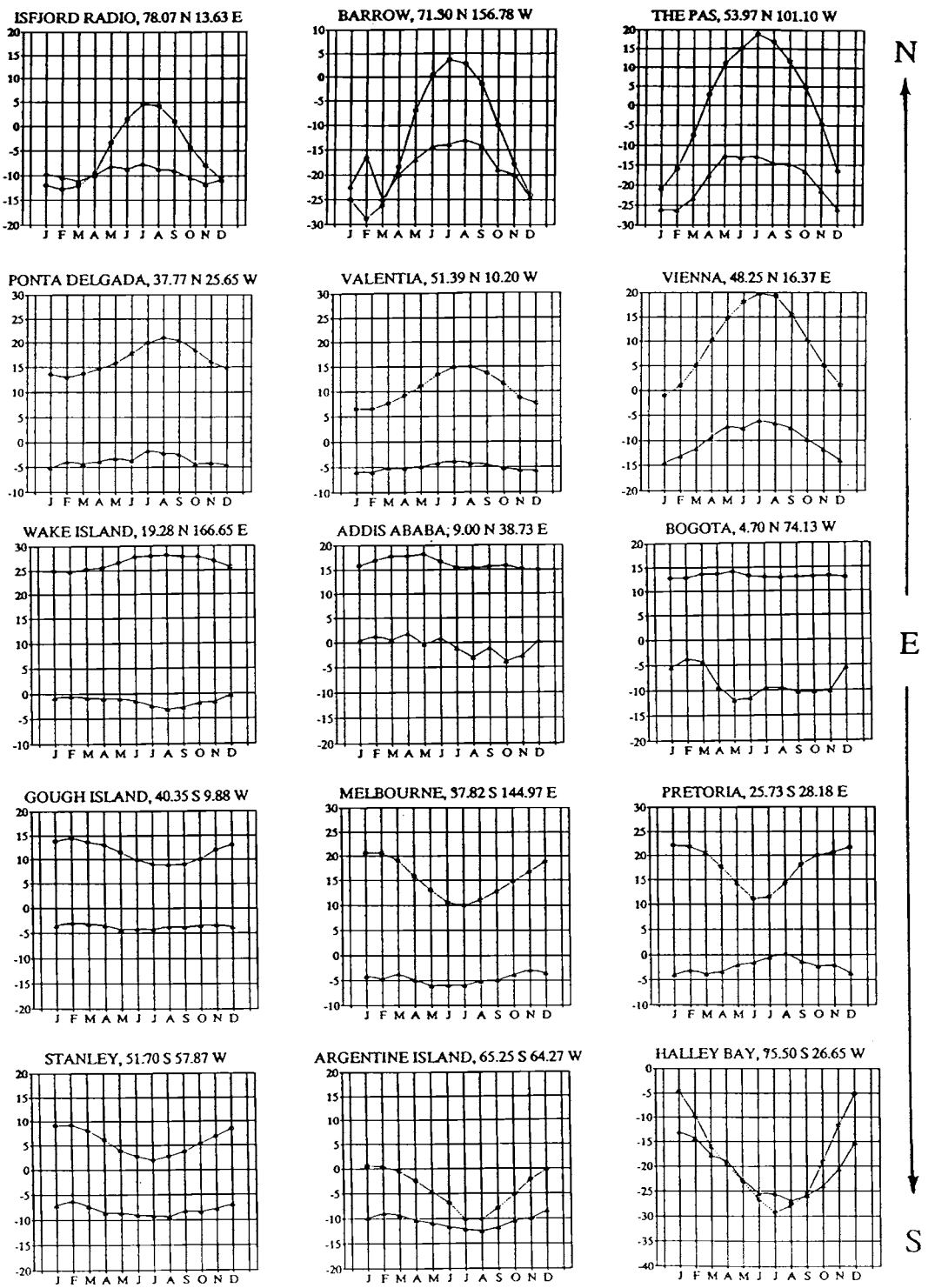

Fig. 12. Seasonal variations of $\delta^{18}O$ of precipitation and surface air temperature for selected stations of the IAEA/WMO global network, representing marine, coastal and continental environment of both hemispheres. Full triangles stand for long-term monthly means of $\delta^{18}O$ whereas open squares represent long-term monthly average temperature.

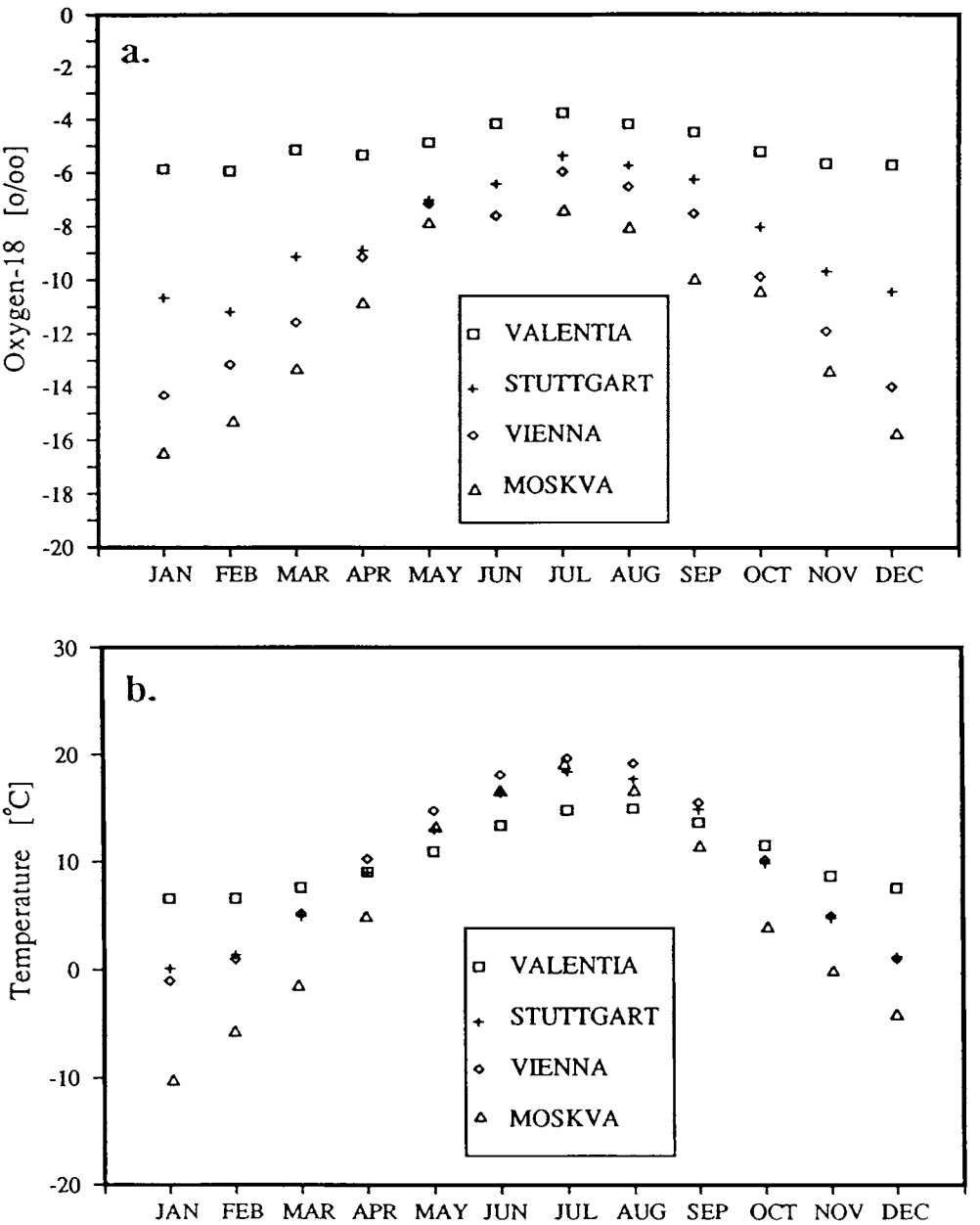

Fig. 13. Seasonal variations of $\delta^{18}O$ of precipitation (a) and surface air temperature (b), for selected European stations of the IAEA/WMO global network with increasing distance from the Atlantic coast.

considerations, with increasing slope of the $\delta^{18}O$-temperature relationship for reduced condensation temperatures. The slope of best fit line of the $\delta^{18}O$ data representing the temperature range between 0 and 20°C is equal to about 0.58‰ per °C, which is in close agreement with theoretical predictions for this temperature range [*Van der Straaten and Mook*, 1983], based on the Rayleigh condensation model with isobaric cooling of precipitating air masses. Lack of correlation for the high-temperature range (20 to 30°C) results from dominance of the amount effect in the tropics.

At polar regions the slope of the $\delta^{18}O$-temperature relation is substantially higher: the values reported in the literature range between 0.67‰ per °C for southern and western Greenland [*Johnsen et al.*, 1989], 0.76‰ per °C for East Antarctica [*Lorius and Merlivat*, 1977] and about 0.90‰ per °C for the Antarctic Peninsula [*Peel et al.*, 1988]. The slope of 0.9‰ per °C has also been reported by *Picciotto et al.* [1960] for the coastal Antarctic station (King Baudouin Base, 70.26°S, 24.19°E), using the temperature of the cloud sheet where precipitation was formed. Substantial spread of the data

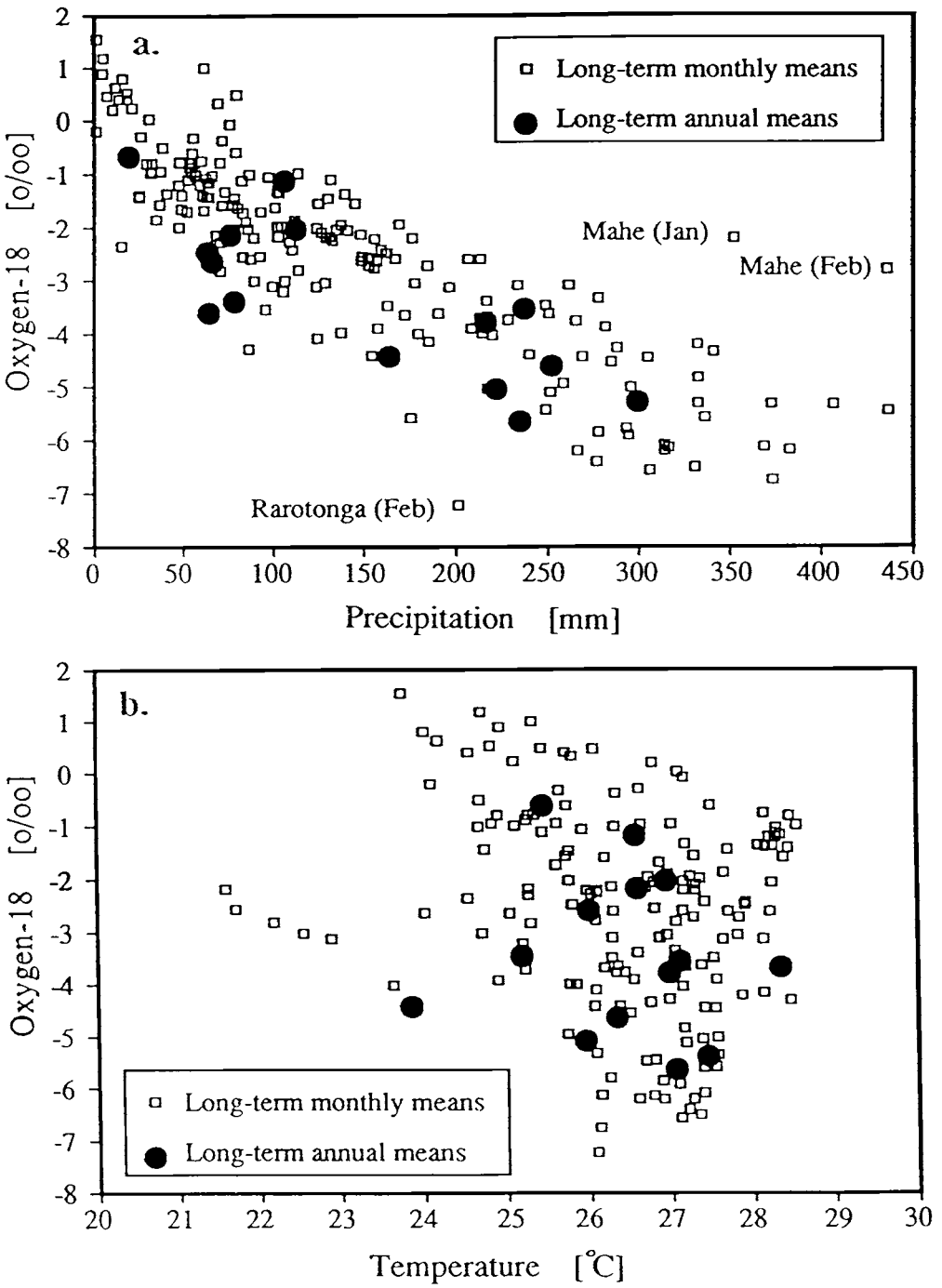

Fig. 14. (a) Long-term monthly and annual mean $\delta^{18}O$ values for tropical island stations of the IAEA/WMO global network (20°S to 20°N), plotted as a function of mean monthly precipitation. Annual mean $\delta^{18}O$ values are plotted as a function of the mean annual precipitation divided by 12; (b) Long-term monthly and annual mean $\delta^{18}O$ values for the same group of stations, plotted as a function of the mean monthly (annual) surface air temperature.

points, seen in Figure 18, confirms the fact that local surface air temperature is not always a good indicator of the average degree of rain-out of a given air mass. For instance, a comparison of the Whitehorse (60.72°N, 135.00°W) and Barrow (71.30°N, 156.70°W) stations shows that in spite of more than 10°C lower mean annual temperature at Barrow, the annual mean $\delta^{18}O$ of precipitation for this station is almost two per mil higher than at Whitehorse, with similar annual distribution of precipitation. This probably reflects a

substantially smaller average degree of rain-out of air masses precipitating at Barrow, with the moisture originating in the north Pacific and in the Arctic. The Whitehorse station, although situated only about 500 km from the Pacific, is effectively shielded from its direct influence by the Saint Elias Mountains, and receives moisture already isotopically depleted from both the south and south-east [*Holdsworth et al.*, 1991].

The seasonal relationship between $\delta^{18}O$ and temperature is summarized in Figure 19 and Table 2. Figure 19a shows relative changes of long-term monthly means of $\delta^{18}O$ and temperature for the mid-latitude IAEA/WMO network stations situated in the northern

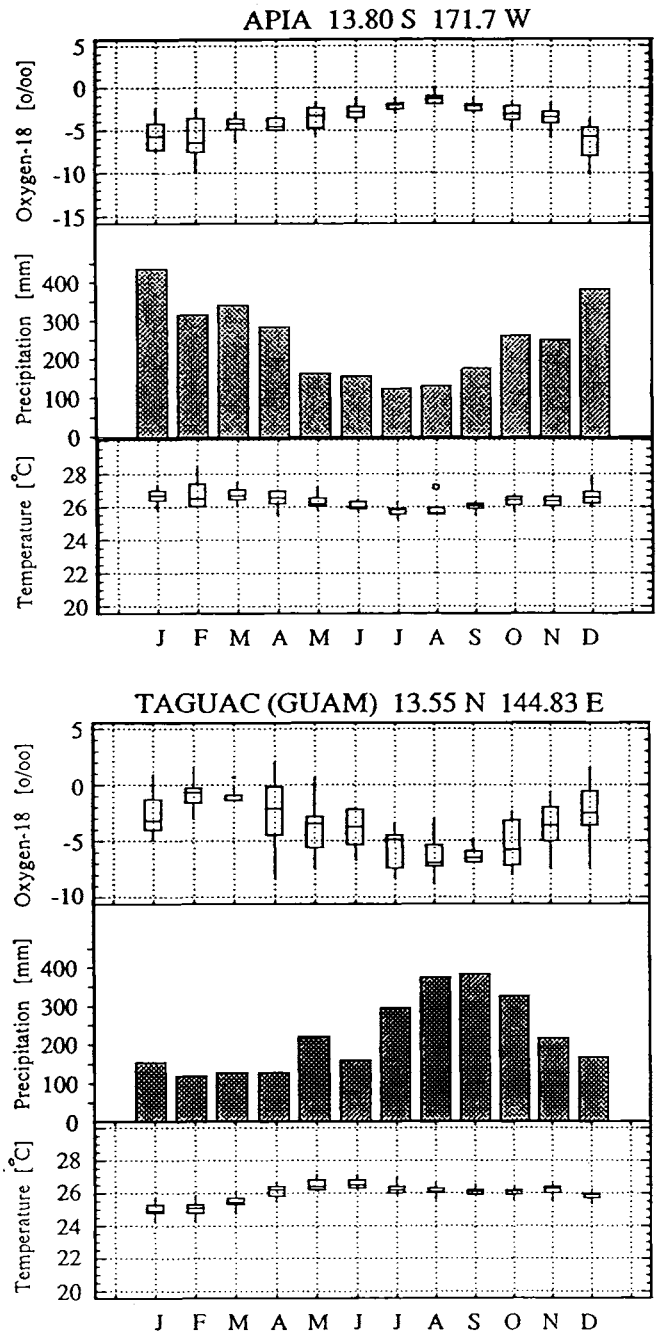

Fig. 15. Seasonal variations of $\delta^{18}O$, precipitation amount and surface air temperature for two tropical marine stations of the IAEA/WMO global network. The $\delta^{18}O$ and temperature data are presented in the form of box-and-whisker plots.

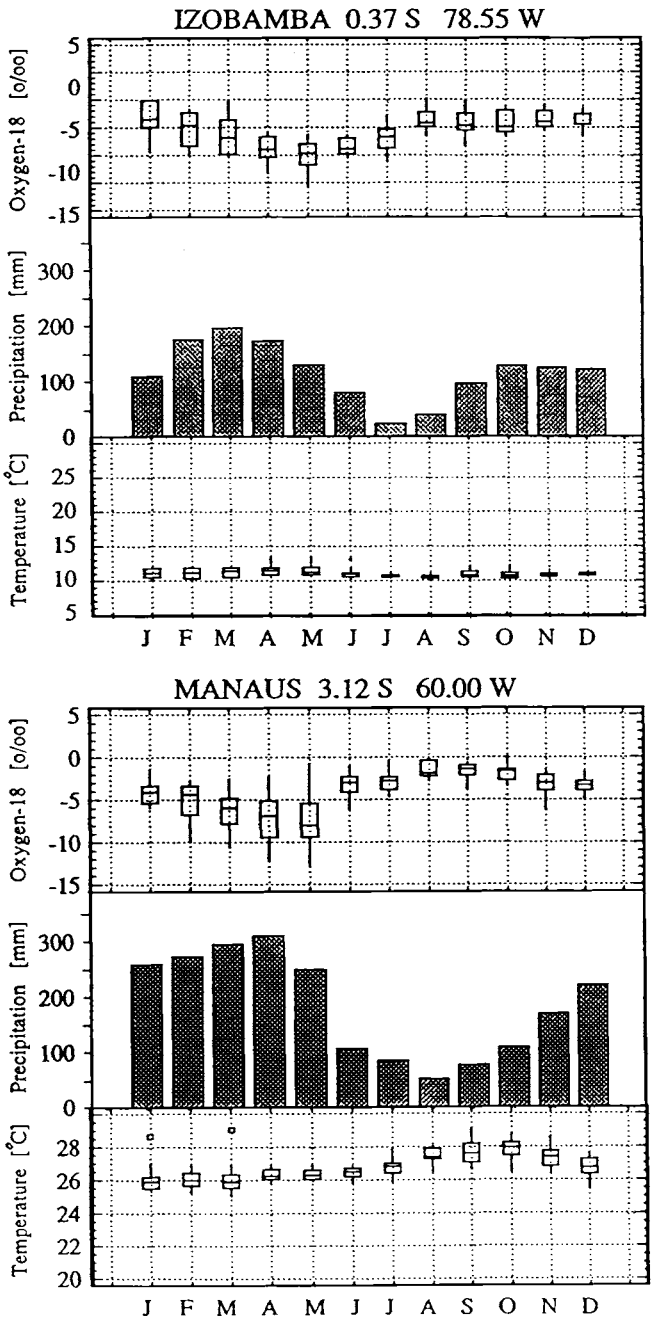

Fig. 16. Seasonal variations of $\delta^{18}O$, precipitation amount and surface air temperature for two stations of the IAEA/WMO global network located in the equatorial region of the south American continent. The $\delta^{18}O$ and temperature data are presented in the form of box-and-whisker plots.

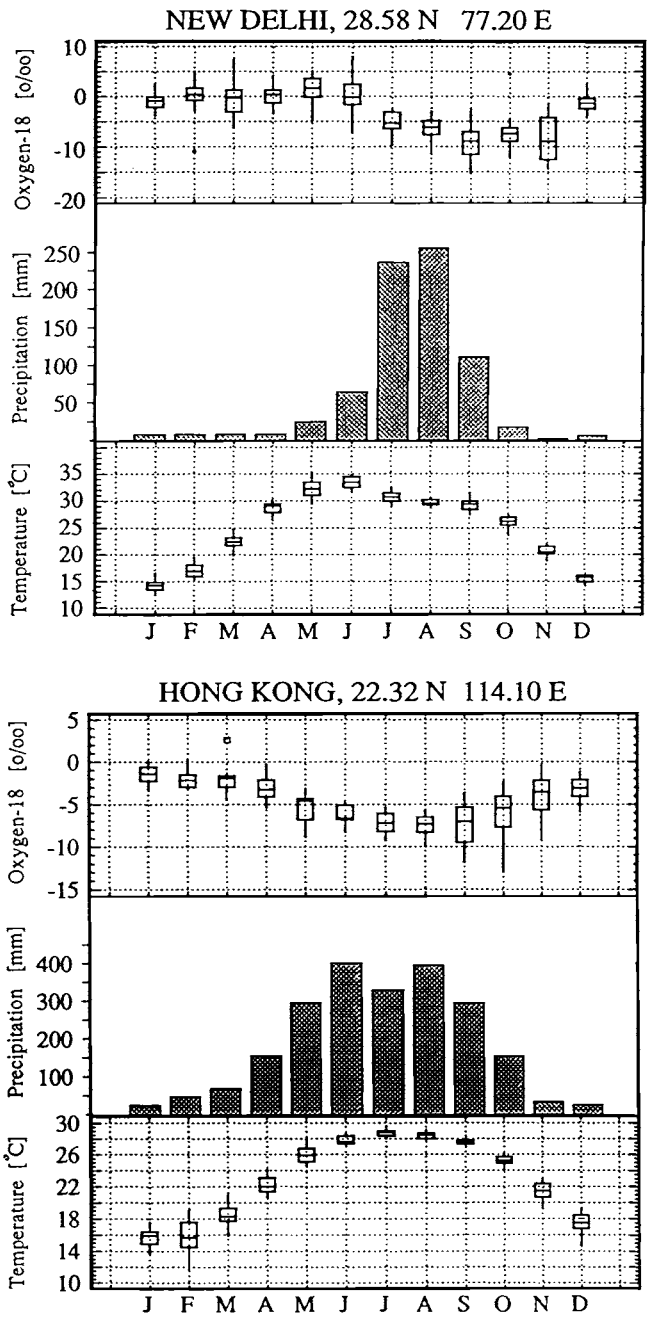

Fig. 17. Seasonal variations of $\delta^{18}O$, precipitation amount and surface air temperature for two tropical stations of the IAEA/WMO global network controlled by monsoon climate. The $\delta^{18}O$ and temperature data are presented in the form of box-and-whisker plots.

hemisphere (40°N to 60°N). The relative changes $\Delta\delta^{18}O$ and ΔT (long-term monthly minus long-term annual mean) were calculated in order to directly compare different stations. The same procedure was adopted to calculate seasonal $\Delta\delta^{18}O/\Delta P$ coefficients listed in Table 2. The slope of the best fit line is equal to 0.31‰ per °C, a substantially lower value than that derived from the spatial relationship (1). In fact, it is apparent from Figure 19 that the $\Delta\delta^{18}O$-ΔT relationship is nonlinear, with a higher slope for negative departures $\Delta\delta^{18}O$ and ΔT and only small changes of $\delta^{18}O$ for the upper end of the temperature range, in agreement with theoretical predictions. The slope of the $\Delta\delta^{18}O$-ΔT relationship, assuming linear dependence among these two variables, change from 0.66‰ per °C ($r^2 = 0.47$) to 0.17‰ per °C ($r^2 = 0.14$) for surface air temperatures lower than -10°C and higher than 10°C, respectively.

Very similar isotope variations have been observed in atmospheric water vapor sampled continuously at the ground level at Heidelberg, Germany (49.8°N, 8.7°E), between 1981 and 1988 [*Jacob and Sonntag*, 1991]. The authors conclude that the lack of a strong relationship between $\delta^{18}O$ and temperature in summer results mainly from an admixture of water vapor which is released by plant transpiration and has a relatively constant isotopic composition, close to weighted annual mean of precipitation. Higher slope of $\Delta\delta^{18}O$-ΔT relation for the low-temperature end is understood in view of a higher effective degree of rain-out of air masses in winter [*Rozanski et al.*, 1982] and a substantial contribution of snow, the formation of which is accompanied by an additional fractionation effect [*Jouzel and Merlivat*, 1984].

Figure 19b shows the relationship between amplitudes of seasonal changes of $\delta^{18}O$ and surface air temperature, defined as a difference between long-term averages of $\delta^{18}O$ and temperature for summer and winter months (JJA - DJF for the northern hemisphere and DJF - JJA for the southern hemisphere, respectively), for selected stations of the IAEA/WMO network. In general, more continental climate implies larger amplitude of seasonal variations of $\delta^{18}O$. The slope of the best fit line is equal to 0.40‰ per °C. However, for a number of stations the ratio $\Delta\delta^{18}O/\Delta T$ is negative. This indicates that seasonal changes of $\delta^{18}O$ at these stations are controlled by factors other than local surface air temperature (for instance, by seasonal changes of storm trajectories or the amount of precipitation).

Long-term trends

The relationship between long-term changes of the heavy isotope composition of precipitation and the surface air temperature at a given location is probably the most relevant as far as palaeoclimatic applications of stable isotopes are concerned. *Siegenthaler and Matter* [1983] investigated this relationship for selected stations of mid- and high latitudes and found significant correlations for only 4 out of 14 stations. However, the length of the analyzed records was rather short at that time (between 8 and 13 years). Recently, *Lawrence and White* [1991] examined in detail the available meteorological and isotope data for several stations of the IAEA/WMO network. They concluded that correlations between climate parameters (temperature, amount of precipitation) and the isotopic composition of precipitation, derived from the interannual variations of these parameters, are usually limited to certain seasons of the year.

At present, much longer records of isotope and meteorological data are available for a number of stations of the IAEA/WMO network, reaching in several cases three decades (cf. Table 1). Therefore, it was interesting to search for long-term trends in these records and to try to identify the response of isotope composition of precipitation to the postulated global warming trend during the past decade. The selection of stations for analysis was guided by several factors: (1)

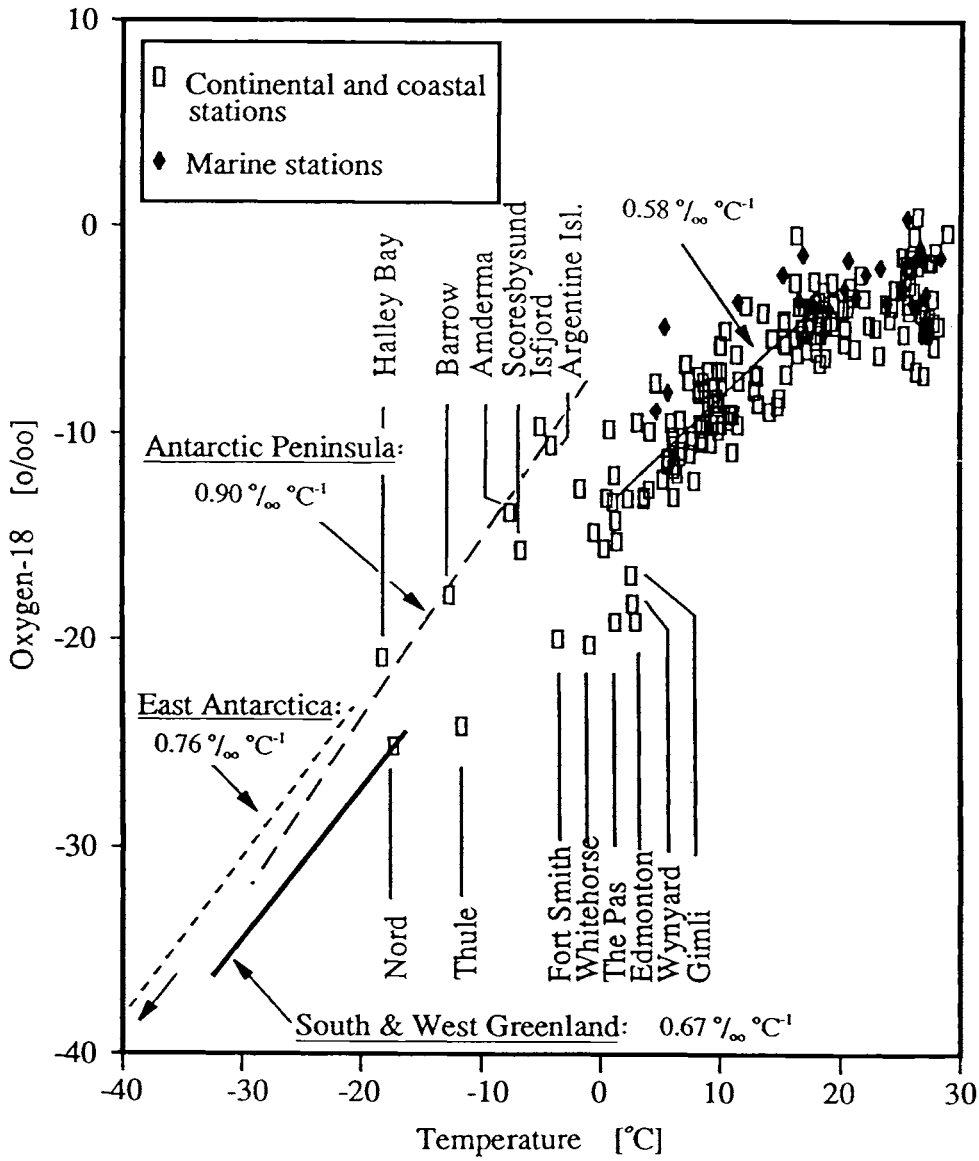

Fig. 18. Relationship between the long-term annual means of ^{18}O content in precipitation and surface air temperature for all stations of the IAEA/WMO global network. The best fit lines of the published data for southern and western Greenland [*Johnsen et al.*, 1989], East Antarctica [*Lorius and Merlivat*, 1977] and the Antarctic Peninsula [*Peel et al.*, 1988] are also shown.

length and quality of the available isotope and meteorological records; (2) continuity of the records, and (3) different climatic regimes represented by the stations. Twelve stations have been selected using the criteria outlined above. Eight of them are located in Europe: Meiringen, Guttannen, Grimsel and Bern (Switzerland), Thonon-les-Bains (France), Vienna (Austria), Groningen (The Netherlands) and Krakow (Poland). The remaining four stations are: Ottawa (Canada), Hong Kong (South East Asia), Taguac (Guam Island, West Pacific) and Argentine Island (Antarctic Peninsula).

The analysis of the available time series of monthly $\delta^{18}O$ and temperature data for the selected stations started by removing the seasonal component from the records. This was done by calculating a 12-month running average of $\delta^{18}O$ and temperature. Single-month gaps in the records were filled by the long-term mean monthly values. The calculation was interrupted whenever more than three consecutive months were missed in the records. Then, the differences $\Delta\delta^{18}O$ and ΔT were calculated for individual stations by subtracting the running average curves from the long-term annual means. Finally, the resulting curves were smoothed by again applying a 12-month running average. Spatial averaging of ^{18}O and temperature signals (composite curves for the Swiss stations and for the whole of Europe) was done by calculating average differences $\Delta\delta^{18}O$ and ΔT (arithmetic averaging of the differences for individual stations), the procedure usually adopted for calculation of spatially averaged temperature records [*Hansen and Lebedeff*, 1987].

Figure 20 shows the trend curves of $\Delta\delta^{18}O$ and ΔT calculated for

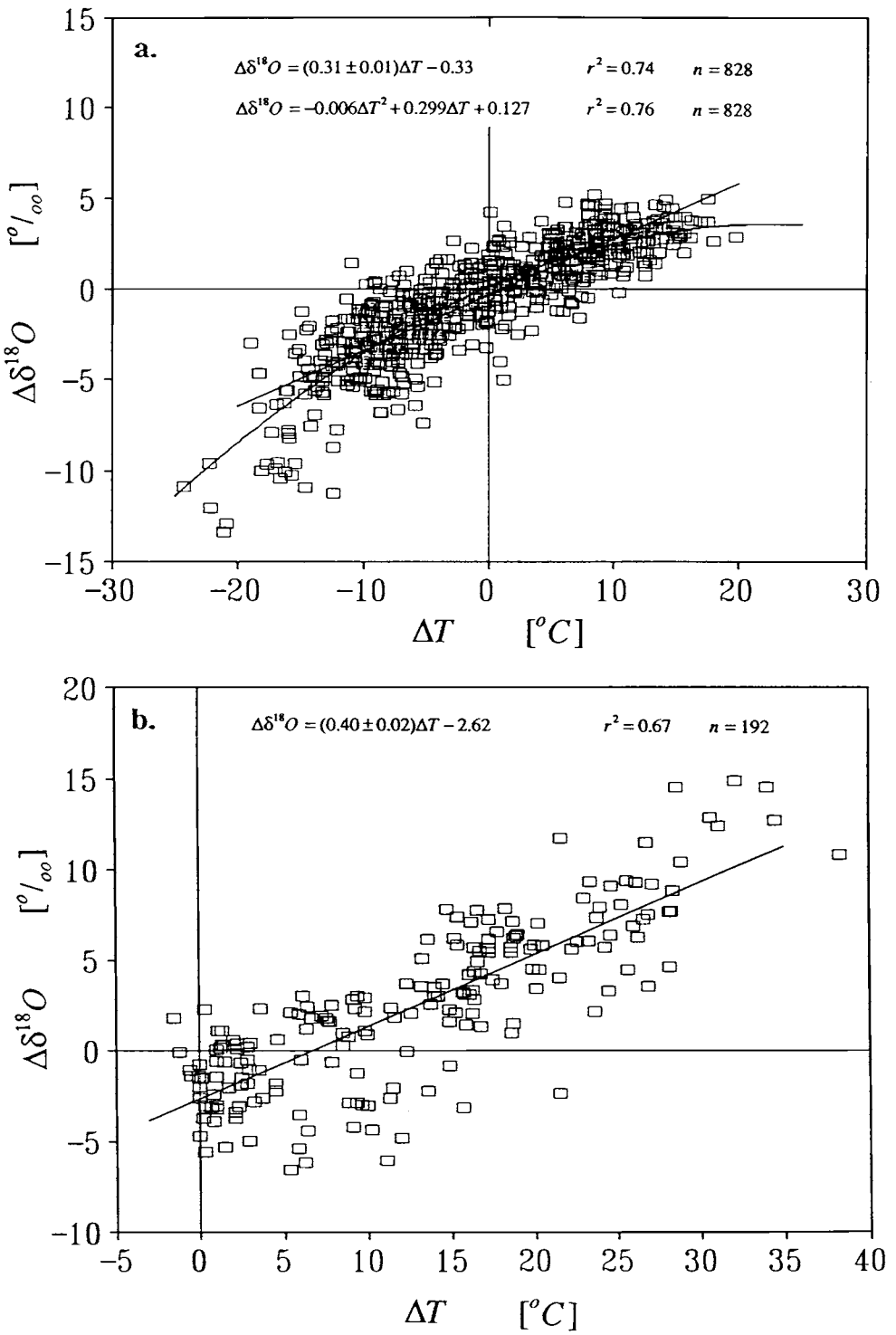

Fig. 19. (a) Seasonal correlation between $\delta^{18}O$ and surface air temperature derived for the stations of the IAEA/WMO global network situated between 40°N and 60°N. The differences between long-term monthly and long-term annual means of $\delta^{18}O$ and surface air temperature are plotted on the figure. (b) The relationship between amplitudes of seasonal changes of $\delta^{18}O$ and surface air temperature for the selected stations of the network, defined as a difference between long-term averages of $\delta^{18}O$ and temperature for summer and winter months (JJA - DJF for the northern hemisphere and DJF - JJA for the southern hemisphere, respectively).

TABLE 1. Summary of isotope and meteorological data for 219 stations of the IAEA/WMO network "Isotopes in Precipitation". The summary covers the time period 1961-1987. The stations marked by an asterisk continue operation after 1987. The isotope data are reported as per mil deviations from the standard V-SMOW. For calculation of the weighted means, weighing by amount of precipitation has been adopted. The number of available monthly data has been reported for both deuterium and ^{18}O data.

	Station name	Latitude	Longitude	Altitude	OXYGEN - 18 (per mil)						DEUTERIUM (per mil)						DEUTERIUM EXCESS			Prec	Temp	Vap. P.
		(deg.)	(deg.)	(m.a.s.l)	Mean	W. mean	n	Start	End		Mean	W. mean	n	Start	End		n	Mean	W. mean	(mm)	(C)	(mb)
1	Adak	51.88 N	176.65 W	4	-8.83	-8.89	68	62 - 01	73 - 05		-64.2	-64.4	61	62 - 01	73 - 05		60	6.5	6.4	1466	4.8	7.3
2	Adana	36.98 N	35.30 E	73	-4.70	-5.50	91	64 - 03	87 - 12	*	-24.3	-28.0	82	64 - 03	87 - 12	*	81	13.5	16.1	659	19.0	15.3
3	Addis Ababa	9.00 N	38.73 E	2360	-0.36	-1.31	102	61 - 03	87 - 09	*	8.5	1.8	95	61 - 03	87 - 09	*	93	11.6	13.2	1181	16.3	11.0
4	Adelaide	34.93 S	138.58 E	43	-4.06	-4.63	113	62 - 01	84 - 12	*	-20.7	-25.3	124	62 - 01	84 - 12	*	112	11.6	11.7	493	17.0	11.5
5	Alexandria	31.20 N	29.95 E	-3	-3.97	-4.60	73	61 - 10	73 - 03		-17.2	-21.9	64	61 - 10	73 - 03		63	14.6	16.4	191	20.2	16.4
6	Alice Springs	23.80 S	133.88 E	546	-2.84	-6.70	155	62 - 01	87 - 09	*	-14.8	-37.8	140	62 - 01	87 - 09	*	134	8.0	12.9	298	20.8	9.4
7	Amderma	69.46 N	61.41 E	53	-15.63	-15.82	36	80 - 04	83 - 12		-114.5	-114.0	27	81 - 01	83 - 12		26	15.0	14.5	456	-6.7	4.1
8	Amman	31.98 N	35.93 E	850	-5.07	-6.59	18	65 - 11	68 - 05		-20.0	-27.8	18	65 - 11	68 - 05		18	20.2	23.5	890	-	-
9	Ankara (Central)	39.95 N	32.88 E	902	-7.52	-8.34	212	63 - 07	87 - 12	*	-51.6	-56.7	186	64 - 03	87 - 12	*	185	9.0	10.5	401	11.7	8.3
10	Antalya	36.88 N	30.70 E	49	-4.70	-5.62	139	63 - 05	87 - 12	*	-24.6	-28.5	130	63 - 05	87 - 12	*	127	13.8	16.9	1098	18.5	14.2
11	Antananarivo	18.90 S	47.53 E	1300	-4.95	-6.41	71	61 - 12	75 - 10		-26.4	-36.0	67	61 - 12	75 - 04		66	13.9	15.4	1390	17.8	15.8
12	Apia	13.80 S	171.78 W	2	-3.75	-4.48	111	62 - 10	77 - 09		-17.8	-23.3	109	62 - 10	77 - 09		108	12.1	12.4	3024	26.4	28.6
13	Argentine Island	65.25 S	64.27 W	0	-10.54	-10.80	280	64 - 01	87 - 12	*	-84.5	-85.5	262	64 - 01	87 - 12	*	261	0.6	1.8	363	-4.0	4.1
14	Arkhangelsk	64.58 N	40.50 E	13	-13.21	-12.77	55	80 - 04	84 - 12	*	-99.8	-95.2	40	81 - 02	84 - 09	*	40	7.9	9.4	548	1.2	6.4
15	Ascension Island	7.92 S	14.42 W	15	0.29	-0.76	73	61 - 12	76 - 06		10.0	2.5	74	61 - 12	76 - 06		73	7.7	8.6	238	25.5	22.1
16	Astrakhan	46.25 N	48.03 E	-18	-8.99	-8.58	54	80 - 04	84 - 12		-68.5	-67.8	43	81 - 01	84 - 09		43	6.0	6.2	200	11.0	10.1
17	Asuncion	25.27 S	57.63 W	65	-4.45	-6.20	29	61 - 11	67 - 11		-25.7	-37.8	29	61 - 11	67 - 11		29	10.5	11.5	1417	24.1	20.4
18	Athens	37.90 N	23.73 E	27	-6.03	-6.30	55	60 - 11	76 - 01		-33.2	-34.2	50	60 - 11	74 - 03		38	13.2	13.1	395	18.0	12.5
19	Atikokan	48.75 N	91.62 W	393	-15.19	-12.61	76	75 - 08	82 - 07		-111.7	-91.5	75	75 - 08	82 - 07		75	10.3	9.7	683	1.4	-
20	Bad Salzuflen	52.10 N	8.73 E	100	-7.99	-8.22	119	78 - 01	87 - 12	*	-56.2	-58.1	119	78 - 01	87 - 12	*	119	7.8	7.7	859	8.8	-
21	Bahrain	26.27 N	50.62 E	2	0.57	-0.97	89	61 - 11	87 - 03	*	13.6	4.6	91	61 - 11	87 - 03	*	84	8.9	14.1	66	26.5	23.5
22	Bamako	12.63 N	8.03 E	329	-1.88	-4.44	111	62 - 05	79 - 08		-15.8	-30.7	103	62 - 05	79 - 08		103	4.3	7.0	917	27.6	18.4
23	Bangkok	13.73 N	100.50 E	2	-4.84	-6.60	185	68 - 07	87 - 11	*	-31.9	-43.6	157	68 - 08	87 - 11	*	152	8.6	8.9	1425	28.2	29.1
24	Barbados	13.07 N	59.48 W	50	-1.03	-1.14	186	61 - 02	87 - 12	*	-0.9	-4.0	188	61 - 02	87 - 12	*	170	7.6	8.0	1257	26.6	26.9
25	Barcelona	41.38 N	2.11 E	65	-5.23	-6.11	35	84 - 01	87 - 02	*	-27.7	-38.2	21	85 - 04	87 - 02	*	21	11.4	11.6	520	16.1	13.0
26	Barranquilla	10.88 N	74.78 W	14	-4.60	-5.09	85	71 - 07	87 - 06	*	-29.3	-33.9	77	72 - 08	87 - 06	*	75	7.2	8.0	743	27.4	28.9
27	Barrow	71.30 N	156.78 W	7	-18.54	-19.61	49	62 - 02	69 - 10		-132.9	-131.1	51	62 - 02	69 - 11		47	10.3	10.4	133	-12.7	2.9
28	Batumi	41.39 N	41.38 E	6	-8.61	-9.09	54	80 - 04	84 - 12		-54.2	-57.5	44	81 - 01	84 - 08		42	14.7	15.4	2612	14.8	14.0
29	Belem	1.43 S	48.48 W	24	-1.78	-2.71	233	65 - 03	87 - 09	*	-6.4	-13.9	201	65 - 03	87 - 02	*	189	8.6	9.1	2845	26.0	29.6
30	Berlin	52.47 N	13.40 E	50	-8.66	-8.67	114	78 - 01	87 - 12	*	-61.4	-61.6	114	78 - 01	87 - 12	*	114	7.9	7.9	584	8.7	9.0
31	Bermuda Island	32.37 N	64.68 W	6	-3.35	-3.53	48	62 - 01	66 - 01		-16.1	-16.7	45	62 - 01	65 - 12		45	10.5	11.5	1372	21.5	18.3
32	Bern	46.92 N	7.50 E	511	-10.40	-10.25	204	71 - 01	87 - 12	*	-	-	-	-	-		-	-	-	1090	8.5	8.3
33	Bet Dagan	32.00 N	34.82 E	30	-4.30	-5.02	137	60 - 11	87 - 12	*	-17.1	-21.8	99	60 - 11	87 - 12	*	95	16.8	18.4	531	19.2	15.9
34	Bethel	60.78 N	161.80 W	41	-12.52	-11.95	50	62 - 01	66 - 02		-98.7	-94.5	48	62 - 01	65 - 12		48	1.6	1.2	325	-1.9	5.0
35	Bogota	4.70 N	74.13 W	2547	-8.35	-9.50	120	71 - 08	87 - 06	*	-57.1	-65.5	113	72 - 06	87 - 06	*	112	9.8	10.6	781	13.2	12.1
36	Bombay	18.90 N	72.82 E	10	-1.72	-1.51	50	61 - 06	77 - 09		-5.1	-4.1	48	61 - 06	77 - 09		48	8.8	8.7	1984	27.4	26.9
37	Brasilia	15.85 S	47.93 W	1061	-4.07	-4.96	136	65 - 03	87 - 06	*	-22.2	-29.9	122	65 - 03	87 - 06	*	118	11.7	11.4	1474	20.6	16.6
38	Braunschweig	52.30 N	10.45 E	88	-7.98	-8.10	118	78 - 01	87 - 12	*	-57.6	-58.5	117	78 - 01	87 - 12	*	117	6.1	6.2	643	8.3	-
39	Brest	52.07 N	23.41 E	142	-9.71	-9.40	44	80 - 04	83 - 12		-73.4	-71.1	35	81 - 01	83 - 12		35	7.4	7.2	591	8.5	9.2
40	Brisbane	27.43 S	153.08 E	0	-3.50	-4.49	226	62 - 01	87 - 12	*	-13.3	-21.1	218	62 - 01	87 - 12	*	215	13.8	13.3	1197	21.0	16.5
41	Buenos Aires	34.58 S	58.48 W	24	-5.03	-5.01	106	61 - 07	85 - 04		-26.1	-26.0	87	61 - 07	84 - 12		87	10.7	10.4	1113	17.5	14.9
42	Canton Island	2.77 S	171.72 W	2	-1.51	-3.65	47	62 - 01	66 - 02		-6.5	-24.7	50	62 - 01	66 - 04		47	6.7	7.7	798	28.3	27.5
43	Cape Grim	40.68 S	144.69 E	90	-3.80	-4.41	95	79 - 09	87 - 12	*	-20.3	-24.3	90	79 - 09	87 - 12	*	90	9.8	10.6	782	12.3	11.8
44	Cayenne	4.83 N	52.37 W	8	-1.67	-2.09	91	62 - 05	75 - 08		-7.6	-10.0	60	62 - 05	75 - 08		60	8.9	10.4	3737	25.5	28.0
45	Ceara Mirim	5.80 S	35.20 W	8	-1.58	-2.30	148	61 - 12	82 - 12	*	-3.1	-9.1	115	61 - 12	82 - 12	*	113	10.3	11.0	1324	25.7	25.6
46	Chicago (Midway)	41.78 N	87.75 W	189	-6.90	-6.04	192	62 - 01	79 - 10		-50.0	-43.0	170	62 - 01	79 - 10		169	7.0	7.0	908	10.2	10.0
47	Chihuahua	28.63 N	106.07 W	1423	-6.41	-6.69	127	62 - 06	87 - 08	*	-41.7	-42.9	122	62 - 06	87 - 08	*	121	9.0	10.4	345	18.2	10.8
48	Christmas Island	1.98 N	157.46 W	3	-1.83	-2.43	23	62 - 03	64 - 04		-7.9	-11.4	23	62 - 03	64 - 04		23	6.9	8.1	845	-	-
49	Corrientes	24.47 S	58.83 W	55	-5.86	-6.75	33	81 - 09	84 - 12		-32.6	-37.3	13	81 - 09	83 - 02		13	10.8	11.8	1520	21.2	19.4
50	Coshocton	40.37 N	81.80 W	344	-7.90	-7.49	65	66 - 01	71 - 06		-50.7	-47.3	64	66 - 01	71 - 06		64	12.4	12.5	977	-	-
51	Cuiaba	15.60 S	56.10 W	165	-4.07	-5.33	203	61 - 11	87 - 06	*	-22.5	-31.9	190	61 - 11	87 - 06	*	187	9.6	10.4	1273	25.8	24.2
52	Cuxhaven	53.87 N	8.72 E	12	-7.20	-7.29	119	78 - 01	87 - 12	*	-51.8	-52.1	119	78 - 01	87 - 12	*	119	5.8	6.2	829	8.3	-
53	Dar Es Salaam	6.88 S	39.20 E	55	-2.03	-2.83	126	61 - 01	73 - 10		-7.1	-13.3	119	61 - 01	73 - 10		119	8.5	9.3	1139	25.7	25.6
54	Darwin	12.43 S	130.87 E	26	-3.49	-4.90	161	62 - 01	87 - 12	*	-18.7	-28.2	144	63 - 01	87 - 12	*	143	10.8	11.5	1775	27.7	24.8
55	Destruction Island	47.67 N	124.48 W	21	-6.88	-7.47	48	62 - 04	66 - 03		-49.5	-52.9	48	62 - 04	66 - 03		48	5.6	7.0	2012	-	-
56	Diego Garcia Island	7.32 S	72.40 E	1	-3.46	-4.03	182	62 - 01	87 - 12	*	-20.0	-23.7	170	62 - 01	87 - 12	*	159	9.1	9.6	2195	26.9	29.0
57	Djajapura	2.53 S	140.72 E	3	-4.98	-5.24	268	61 - 02	87 - 12	*	-31.6	-32.9	234	61 - 02	87 - 12	*	234	6.7	6.9	2332	27.2	29.9
58	Djakarta	6.18 S	106.83 E	8	-5.02	-5.58	168	62 - 01	87 - 12	*	-30.9	-34.8	169	62 - 01	87 - 12	*	167	9.7	9.7	1710	27.1	28.2
59	Edmonton (Industrial)	53.57 N	113.52 W	671	-19.14	-17.05	52	61 - 05	66 - 02		-149.0	-130.9	53	61 - 05	66 - 03		52	5.6	5.3	430	3.2	6.3
60	Emmerich	51.83 N	6.60 E	43	-6.98	-7.30	94	80 - 01	87 - 12	*	-50.0	-52.5	94	80 - 01	87 - 12	*	94	5.8	5.9	744	9.1	-
61	Entebbe (Airport)	0.05 N	32.45 E	1155	-2.26	-2.91	120	61 - 02	74 - 09		-5.8	-11.2	115	60 - 03	74 - 09		105	12.6	12.4	1613	21.6	20.5

TABLE 1. Continued

	Station name	Latitude		Longitude		Altitude	OXYGEN - 18 (per mil)						DEUTERIUM (per mil)						DEUTERIUM EXCESS			Prec	Temp	Vap. P.
		(deg.)		(deg.)		(m.a.s.l)	Mean	W. mean	n	Start	End		Mean	W. mean	n	Start	End		n	Mean	W. mean	(mm)	(C)	(mb)
62	Faro	37.01	N	7.96	W	9	-3.93	-4.39	68	78 - 11	87 - 12	*	-21.7	-25.2	63	78 - 11	87 - 12	*	60	9.5	10.0	365	17.5	14.0
63	Feldberg/Schwarzwald	47.52	N	8.00	E	1493	-9.35	-10.57	50	81 - 01	85 - 08	*	-65.0	-73.0	50	81 - 01	85 - 08	*	50	11.5	11.5	1879	3.1	-
64	Flagstaff	35.13	N	111.67	W	2137	-7.26	-8.07	114	61 - 12	74 - 07		-59.8	-65.9	101	61 - 12	74 - 07		101	-1.6	3.5	533	7.5	5.5
65	Fort Smith	3.72	S	38.55	W	27	-1.83	-2.65	41	61 - 08	65 - 09	*	-4.4	-11.8	72	61 - 08	69 - 06	*	41	5.5	7.6	1705	26.4	27.3
66	Fortaleza	60.02	N	111.97	W	203	-19.95	-18.10	126	65 - 04	85 - 12		-162.0	-146.4	97	65 - 04	84 - 12		97	9.0	8.3	360	-3.2	5.4
67	Garmisch-Partenk.	47.48	N	11.07	E	720	-11.49	-10.95	119	78 - 01	87 - 12	*	-84.6	-79.9	119	78 - 01	87 - 12	*	119	7.4	7.8	1383	6.4	-
68	Geneina	13.48	N	22.45	E	805	-0.44	-1.92	48	68 - 06	76 - 09		2.0	-8.5	36	68 - 06	76 - 09		36	5.5	5.9	455	26.2	11.1
69	Genoa (Sestri)	44.42	N	8.85	E	2	-5.41	-5.78	216	61 - 11	87 - 12	*	-33.1	-35.1	216	61 - 11	87 - 12	*	213	9.9	10.3	1117	14.5	13.2
70	Gibraltar	36.15	N	5.35	W	5	-4.18	-4.70	145	61 - 10	87 - 12	*	-22.6	-25.7	142	61 - 10	87 - 12	*	139	10.8	11.5	747	18.2	15.5
71	Gimli	50.62	N	96.98	W	223	-16.87	-14.15	76	75 - 08	82 - 07		-124.3	-103.7	73	75 - 08	82 - 07		72	9.3	9.0	551	2.6	-
72	Goose Bay	53.32	N	60.42	W	46	-15.54	-15.08	57	61 - 05	66 - 02		-112.4	-109.8	85	61 - 05	69 - 06		54	12.9	12.3	960	0.5	5.7
73	Gor'kij	56.13	N	43.49	E	82	-12.16	-12.27	42	80 - 05	83 - 12		-90.4	-89.8	33	81 - 01	83 - 12		32	9.8	11.5	662	5.3	7.8
74	Gough Island	40.35	S	9.88	W	54	-3.63	-3.73	236	61 - 04	87 - 09	*	-20.3	-20.8	76	61 - 04	74 - 09		76	7.7	8.0	3193	11.6	11.2
75	Grimsel	46.57	N	8.33	E	1950	-14.23	-14.69	209	70 - 08	87 - 12	*	-	-	-	-	-		-	-	-	2079	1.3	4.8
76	Groennedal	61.22	N	48.12	W	27	-11.47	-11.29	97	61 - 01	74 - 08		-88.0	-87.7	74	62 - 05	74 - 08		67	3.3	2.8	1018	1.2	5.0
77	Groningen	53.21	N	6.57	E	0	-7.70	-7.84	284	64 - 03	87 - 12	*	-50.2	-51.2	280	64 - 03	87 - 12	*	280	11.4	11.6	758	9.5	-
78	Guangzhou	23.13	N	113.32	E	7	-4.71	-5.18	16	86 - 04	87 - 11	*	-30.4	-34.2	16	86 - 04	87 - 11	*	16	7.3	7.0	1748	23.2	-
79	Guttannen	46.65	N	8.30	E	1055	-13.06	-12.87	208	70 - 08	87 - 12	*	-	-	-	-	-		-	-	-	1683	6.2	7.8
80	Halley Bay	75.50	S	26.65	W	0	-20.87	-20.67	232	65 - 07	87 - 12	*	-158.0	-155.4	213	65 - 07	87 - 12	*	212	7.1	7.5	432	-18.2	1.8
81	Har Kna'an (Tirat Yael)	32.97	N	35.50	E	964	-6.21	-6.74	77	64 - 03	87 - 12	*	-27.8	-28.7	45	64 - 03	87 - 12	*	44	21.2	23.2	734	16.5	10.6
82	Harare	17.83	S	31.02	E	1471	-3.88	-6.14	175	60 - 11	83 - 12	*	-16.1	-32.4	110	60 - 11	75 - 10	*	106	12.1	13.4	809	18.0	12.9
83	Hatteras	35.27	N	77.55	W	3	-3.82	-4.29	93	62 - 01	76 - 12		-19.0	-22.5	93	62 - 01	76 - 12		93	11.6	11.9	1386	16.6	16.3
84	Hawaii	19.72	N	155.07	W	9	-2.02	-2.29	87	62 - 02	69 - 10		-4.8	-6.4	85	62 - 02	69 - 10		85	10.9	11.4	3312	23.3	21.5
85	Heraklion (Yraklion)	35.33	N	25.18	E	47	-6.29	-6.61	22	63 - 05	74 - 02		-32.8	-35.5	23	63 - 05	74 - 02		22	16.9	15.8	524	18.8	13.5
86	Hof-Hohensaas	50.32	N	11.88	E	567	-9.44	-9.30	60	83 - 01	87 - 12	*	-67.8	-66.6	60	83 - 01	87 - 12	*	60	7.8	7.7	738	6.2	8.2
87	Hohenpeissenberg	47.80	N	11.02	E	977	-11.93	-11.38	168	74 - 01	87 - 12	*	-84.2	-80.2	209	70 - 07	87 - 12	*	168	10.4	10.3	1053	6.5	9.0
88	Hong Kong	22.32	N	114.17	E	65	-5.01	-6.70	193	61 - 01	87 - 11	*	-30.0	-43.2	193	61 - 01	87 - 11	*	185	9.7	10.0	2156	23.0	22.7
89	Howard Afb	8.92	N	79.60	W	13	-4.56	-5.65	165	68 - 07	87 - 12	*	-28.8	-37.0	150	68 - 07	87 - 12	*	138	8.0	8.8	1626	27.0	28.7
90	Invercargill	46.42	S	168.32	E	2	-6.95	-7.11	113	77 - 04	87 - 12	*	-46.7	-47.3	107	63 - 12	87 - 12	*	103	9.0	9.3	1037	9.8	10.0
91	Isfjord Radio	78.07	N	13.63	E	6	-9.55	-9.17	98	61 - 07	75 - 05		-63.3	-59.9	75	61 - 07	75 - 05		75	8.2	7.7	488	-5.1	3.9
92	Isla De Pascua	27.17	S	109.43	W	41	-1.57	-1.57	26	65 - 09	75 - 10		-3.6	-5.1	17	69 - 02	75 - 10		13	12.8	13.1	989	20.6	19.2
93	Izobamba	0.37	S	78.55	W	3059	-10.68	-11.05	111	73 - 06	84 - 11	*	-75.8	-78.9	102	73 - 06	84 - 11	*	101	9.8	10.0	1287	11.1	10.5
94	Johnston Island	16.73	N	169.52	W	2	-1.72	-2.58	93	62 - 01	76 - 12		-6.4	-13.6	90	62 - 01	76 - 12		90	7.6	7.3	798	26.0	25.2
95	Juan Fernandez Island	33.62	S	78.83	W	6	-2.50	-2.99	24	64 - 01	75 - 11		-13.7	-16.8	21	64 - 01	75 - 11		21	2.1	3.8	1062	15.1	12.8
96	Kabul (Karizimir)	34.67	N	69.08	E	1860	-6.01	-7.15	93	62 - 01	87 - 12	*	-33.2	-36.1	70	62 - 01	87 - 12	*	70	14.6	17.2	327	11.5	7.1
97	Kaitaia	35.07	S	173.28	E	76	-4.54	-5.01	193	62 - 10	87 - 12	*	-24.7	-28.6	180	62 - 10	87 - 12	*	180	11.7	11.7	1382	15.4	14.3
98	Kalinin	56.54	N	35.54	E	31	-12.19	-11.57	51	80 - 04	84 - 08		-93.3	-86.7	43	81 - 01	84 - 07		42	8.8	10.0	723	5.3	8.1
99	Kano	12.05	N	8.53	E	476	-2.88	-3.81	39	61 - 05	73 - 09		-19.1	-27.2	33	61 - 05	73 - 09		33	5.6	5.2	763	26.2	16.0
100	Karachi	24.90	N	67.13	E	23	-2.96	-3.93	45	61 - 07	75 - 08		-19.2	-23.5	43	61 - 07	75 - 08		39	6.2	9.0	195	25.7	22.0
101	Karlsruhe	49.02	N	8.38	E	120	-8.44	-8.48	79	81 - 01	87 - 11	*	-59.5	-59.8	79	81 - 01	87 - 11	*	79	8.1	8.1	851	9.8	-
102	Kericho	0.37	N	35.35	E	2130	-2.90	-3.83	24	67 - 11	70 - 05		-10.0	-16.3	19	67 - 11	69 - 12		19	11.5	13.4	1037	-	-
103	Khartoum	15.60	N	32.55	E	382	-0.44	-2.10	40	62 - 06	78 - 08		1.7	-10.0	37	62 - 06	78 - 08		36	3.6	6.1	147	29.0	12.9
104	Kinshasa (Binza)	4.37	S	15.25	E	438	-3.88	-4.70	60	61 - 03	68 - 05		-17.9	-24.2	59	61 - 03	68 - 05		59	13.2	13.5	1285	24.3	25.0
105	Kirov	58.39	N	49.37	E	164	-13.01	-12.73	43	80 - 04	83 - 10		-104.0	-101.3	32	81 - 01	83 - 10		32	3.5	3.2	679	3.7	7.1
106	Koblenz	50.35	N	7.58	E	97	-7.68	-7.45	36	81 - 03	87 - 12	*	-56.2	-54.6	29	81 - 03	87 - 12	*	80	5.2	5.1	637	10.2	-
107	Konstanz	47.68	N	9.18	E	447	-10.43	-10.18	15	78 - 01	87 - 12	*	-77.0	-74.7	14	78 - 01	87 - 12	*	118	6.5	6.8	873	8.8	9.4
108	Ko Samui	9.28	N	100.03	E	7	-4.64	-5.75	80	79 - 02	83 - 11		-24.2	-27.7	80	79 - 02	83 - 11		28	10.6	10.8	1442	27.8	29.4
109	Ko Sichang	13.17	N	100.80	E	0	-5.79	-6.28	118	84 - 06	87 - 11	*	-35.0	-38.9	118	84 - 06	87 - 11	*	14	-	-	1239	27.8	28.0
110	Krakow	50.07	N	19.88	E	205	-10.06	-9.35	154	75 - 03	87 - 12	*	-72.2	-66.5	154	75 - 03	87 - 12	*	154	8.4	8.3	619	7.7	9.4
111	Kunming	23.02	N	102.68	E	1841	-8.22	-10.61	19	86 - 04	87 - 11	*	-51.8	-71.0	19	86 - 04	87 - 11	*	19	13.9	14.6	1115	15.5	-
112	La Suela	30.58	S	64.58	W	900	-5.16	-5.99	22	81 - 08	84 - 03		-	-	-	-	-		-	-	-	1122	18.3	13.8
113	Leipzig	51.35	N	12.43	E	125	-9.56	-9.41	24	86 - 01	87 - 12	*	-62.5	-61.8	178	73 - 01	87 - 12	*	24	11.5	12.4	552	9.0	9.4
114	Liege	50.70	N	5.47	E	190	-6.82	-6.83	52	66 - 01	70 - 11		-47.5	-47.5	51	66 - 01	70 - 12		50	7.2	7.3	821	-	-
115	Lista	58.10	N	6.57	E	13	-6.66	-6.89	129	61 - 02	77 - 08		-46.2	-48.6	109	61 - 02	77 - 08		109	7.3	7.5	1025	7.4	9.0
116	Ljubljana	46.04	N	14.31	E	299	-9.28	-9.24	48	84 - 01	87 - 12	*	-64.9	-64.4	48	84 - 01	87 - 12	*	48	9.3	9.5	1474	9.9	10.1
117	Locamo	46.17	N	8.78	E	379	-9.47	-8.64	179	72 - 09	87 - 12	*	-	-	-	-	-		-	-	-	1850	11.6	9.1
118	Luang-Prabang	19.88	N	102.13	E	305	-6.39	-7.62	26	61 - 03	64 - 11		-42.5	-50.9	26	61 - 03	64 - 11		26	7.9	8.4	1257	25.7	26.1
119	L'vov	49.49	N	23.57	E	329	-10.28	-9.86	45	80 - 04	83 - 12	*	-75.8	-71.8	35	81 - 01	83 - 12		35	8.5	9.0	708	7.8	8.9
120	Madang	5.22	S	145.80	E	4	-7.04	-7.70	125	68 - 08	82 - 07	*	-44.8	-49.7	105	68 - 08	82 - 07		102	11.3	11.7	3218	27.0	29.5
121	Mahe	4.62	S	55.45	E	1	-3.29	-3.57	20	61 - 02	63 - 08	*	-14.2	-15.0	20	61 - 02	63 - 08		20	12.8	15.6	2597	27.1	28.6
122	Malan (Cape Town)	33.97	S	18.60	E	44	-2.81	-3.45	217	61 - 04	83 - 04		-8.9	-12.9	127	61 - 04	75 - 09		126	13.5	14.7	513	16.3	13.9
123	Malange	9.55	S	16.37	E	1139	-3.67	-4.48	86	69 - 01	83 - 03		-21.1	-26.1	66	69 - 01	83 - 04		63	12.3	12.0	1060	21.9	17.5
124	Manaus	3.12	S	60.02	W	60	-4.55	-5.52	183	65 - 07	87 - 08	*	-25.9	-33.1	156	65 - 07	87 - 08	*	152	12.0	11.8	2211	26.8	29.0
125	Manila	14.52	N	121.00	E	14	-5.11	-6.74	48	61 - 02	76 - 03		-34.6	-44.2	46	61 - 02	76 - 03		46	5.6	8.8	1955	27.0	27.3

TABLE 1. Continued

	Station name	Latitude	Longitude	Altitude	OXYGEN - 18 (per mil)						DEUTERIUM (per mil)						DEUTERIUM EXCESS			Prec	Temp	Vap. P.
		(deg.)	(deg.)	(m.a.s.l)	Mean	W. mean	n	Start	End		Mean	W. mean	n	Start	End		n	Mean	W. mean	(mm)	(C)	(mb)
126	Maracay	10.25 N	67.65 W	442	-3.91	-4.01	64	61 - 05	75 - 08		-25.5	-27.9	48	61 - 05	75 - 08		48	5.8	4.2	806	24.5	22.5
127	Marion Island	46.88 S	37.87 E	26	-4.91	-4.93	194	61 - 04	87 - 12	*	-33.4	-33.5	79	61 - 04	76 - 03		79	7.0	7.0	2452	5.5	7.6
128	Meiringen	46.73 N	8.20 E	632	-12.29	-11.77	209	70 - 08	87 - 12	*	-	-	-	-	-		-	-	-	1278	7.9	8.9
129	Melbourne	37.82 S	144.97 E	28	-4.68	-5.13	248	62 - 01	87 - 12	*	-25.5	-28.2	211	62 - 01	87 - 12	*	200	11.3	11.5	635	15.4	11.4
130	Mendoza	32.88 S	68.85 W	827	-5.90	-5.59	27	81 - 10	84 - 12		-	-	-	-	-		-	-	-	363	17.1	11.1
131	Menongue	14.67 S	17.70 E	1348	-4.82	-6.18	59	69 - 01	83 - 03		-28.8	-38.0	46	69 - 01	83 - 03		45	9.6	11.2	895	20.4	13.4
132	Midway Is.	28.22 N	177.37 W	13	-2.33	-2.52	264	62 - 02	87 - 12	*	-8.8	-10.6	233	62 - 02	87 - 12	*	218	9.4	9.7	1090	22.3	20.6
133	Minsk	52.52 N	27.32 E	225	-10.79	-10.70	44	80 - 04	83 - 12		-77.7	-78.6	36	81 - 01	83 - 12		36	10.9	10.3	676	6.8	8.2
134	Moskva	55.75 N	37.57 E	157	-11.42	-10.99	63	70 - 01	79 - 12		-91.4	-89.1	115	70 - 01	79 - 12		63	5.4	5.4	693	5.4	7.5
135	Muguga	1.22 S	36.63 E	2070	-3.56	-4.38	14	67 - 02	68 - 06		-13.7	-20.6	14	67 - 02	68 - 06		14	-	-	1268	-	-
136	Murmansk	68.58 N	33.03 E	46	-13.10	-12.68	42	80 - 04	83 - 09		-97.8	-93.2	34	81 - 01	83 - 12		31	7.2	8.2	489	0.6	5.7
137	Nancunan	34.03 S	67.97 W	572	-5.64	-5.77	30	81 - 10	84 - 12		-	-	-	-	-		-	-	-	427	15.4	10.1
138	N'djamena	12.13 N	15.03 E	294	-1.51	-4.11	81	64 - 03	78 - 09		-6.2	-22.5	70	64 - 03	78 - 09		68	7.4	11.6	557	27.9	16.6
139	Ndola	13.00 S	28.65 E	1331	-6.03	-6.59	79	68 - 11	85 - 05	*	-35.1	-39.5	69	68 - 11	85 - 04	*	68	12.5	13.3	1172	20.4	14.8
140	New Delhi	28.58 N	77.20 E	212	-3.40	-5.81	216	61 - 07	87 - 09	*	-19.3	-37.2	183	61 - 07	87 - 09	*	181	6.4	8.3	774	25.1	17.4
141	Nord	81.60 N	16.67 W	35	-25.01	-24.98	93	61 - 01	72 - 05		-185.6	-185.6	63	61 - 01	67 - 06		62	11.1	11.5	164	-17.1	1.9
142	Odessa	46.48 N	30.63 E	64	-8.44	-9.09	40	80 - 04	83 - 12	*	-60.5	-64.5	32	81 - 02	83 - 12	*	31	6.9	8.2	459	10.0	10.5
143	Ottawa	45.32 N	75.67 W	114	-11.18	-10.89	202	70 - 02	87 - 12	*	-77.0	-74.2	188	67 - 06	87 - 12	*	164	11.2	11.3	881	5.8	8.3
144	Pechora	65.07 N	57.06 E	56	-14.74	-14.67	45	80 - 04	83 - 12		-111.2	-109.7	35	81 - 01	83 - 12		35	9.7	9.3	623	-0.5	5.7
145	Perm	58.01 N	56.18 E	161	-13.02	-12.90	42	80 - 04	83 - 12	*	-93.2	-92.1	32	81 - 01	83 - 12	*	32	14.9	14.0	630	2.4	7.0
146	Perth	31.95 S	115.97 E	17	-3.12	-3.87	98	62 - 02	76 - 12		-12.0	-14.9	93	62 - 02	76 - 12		93	13.0	16.2	809	18.6	13.2
147	Petzenkirchen	48.15 N	15.15 E	252	-9.45	-8.68	64	66 - 03	71 - 08		-68.5	-63.4	61	66 - 03	71 - 08		60	8.8	7.8	726	8.6	9.4
148	Podersdorf	47.85 N	16.85 E	120	-9.57	-8.73	24	65 - 05	68 - 12		-68.9	-63.4	41	65 - 05	68 - 12		24	-	-	566	-	-
149	Pohang	36.03 N	129.38 E	6	-7.31	-7.78	110	61 - 03	76 - 12		-44.5	-51.0	118	61 - 03	76 - 12		110	12.3	10.1	1106	13.2	12.4
150	Ponta Delgada	33.77 N	25.65 W	175	-3.53	-4.20	70	62 - 02	74 - 12		-16.0	-19.9	72	62 - 02	74 - 12		70	12.3	13.7	1058	16.6	15.5
151	Porto Alegre	30.08 S	51.18 W	7	-4.63	-4.71	200	65 - 03	83 - 07	*	-24.8	-25.2	175	65 - 03	83 - 07	*	172	12.4	12.6	1305	19.6	17.8
152	Porto Velho	8.77 S	63.92 W	105	-5.74	-6.82	86	65 - 08	81 - 10	*	-34.4	-43.0	73	65 - 08	81 - 10	*	72	11.3	11.4	2210	25.3	28.1
153	Pretoria	25.73 S	28.18 E	1330	-2.57	-3.70	190	61 - 04	83 - 01		-9.2	-16.8	121	61 - 04	75 - 04		121	9.8	12.1	682	17.8	11.9
154	Prins Christians Sund	60.02 N	43.07 W	76	-9.76	-10.30	16	76 - 03	78 - 05		-63.5	-64.5	7	76 - 03	78 - 05		7	-	-	2928	1.2	8.1
155	Puerto Montt	41.47 S	72.93 W	13	-5.72	-6.07	40	64 - 05	75 - 09		-39.5	-41.9	27	64 - 05	75 - 09		27	6.4	7.7	1884	10.0	10.3
156	Rabba	31.20 N	35.75 E	970	-4.55	-4.81	12	65 - 12	68 - 02		-16.0	-16.9	12	65 - 12	68 - 02		12	22.6	23.6	700	-	-
157	Rarotonga	21.20 S	159.80 W	6	-3.47	-4.26	85	79 - 04	87 - 12	*	-17.8	-23.7	85	79 - 04	87 - 12	*	85	10.0	10.5	1953	23.9	24.2
158	Regensburg	49.02 N	12.07 E	377	-10.29	-10.02	119	78 - 01	87 - 12	*	-76.0	-73.5	119	78 - 01	87 - 12	*	119	6.4	6.7	639	7.7	-
159	Reykjavik	64.13 N	21.93 W	14	-7.49	-7.65	147	61 - 04	76 - 12		-53.7	-55.2	98	61 - 04	76 - 12		98	6.5	6.8	870	4.7	7.2
160	Rhodes (Maritsai)	36.38 N	28.10 E	42	-5.11	-4.95	23	63 - 05	76 - 03		-25.3	-23.5	18	63 - 05	72 - 10		18	17.5	19.6	647	18.6	13.9
161	Riga	56.97 N	24.07 E	3	-10.12	-10.34	55	80 - 04	84 - 12		-71.3	-73.3	44	81 - 01	84 - 09		42	10.9	11.0	646	6.5	8.4
162	Rio De Janeiro	22.90 S	43.17 W	26	-3.81	-4.54	182	61 - 11	87 - 09	*	-18.4	-26.2	135	61 - 11	85 - 09	*	132	12.3	12.0	1167	23.8	22.7
163	Rjazan	54.37 N	39.43 E	135	-11.45	-10.99	42	80 - 05	83 - 12		-87.6	-83.3	36	81 - 01	83 - 12		35	5.6	6.9	617	5.7	8.0
164	Rostov-Na-Donu	47.25 N	39.82 E	77	-8.29	-8.83	51	80 - 04	84 - 09	*	-64.5	-67.1	36	81 - 01	84 - 09	*	36	8.8	9.6	641	9.8	10.1
165	Ryori	39.02 N	141.50 E	260	-8.37	-8.13	86	79 - 01	86 - 06	*	-53.2	-53.0	89	79 - 01	86 - 06	*	86	13.5	12.1	1124	10.0	10.5
166	Salta	24.78 S	65.40 W	1187	-4.01	-4.53	19	81 - 11	83 - 12		-	-	-	-	-	*	-	-	-	697	17.7	14.8
167	Salvador (Ondina)	13.00 S	38.52 W	45	-1.45	-1.73	169	65 - 02	87 - 07	*	-1.3	-2.9	118	65 - 02	85 - 04	*	112	11.1	11.4	2106	25.2	25.7
168	San Andres	34.57 S	58.55 W	0	-4.40	-3.52	35	79 - 05	82 - 03		-	-	-	-	-		-	-	-	1368	-	-
169	San Juan (Puerto Rico)	18.43 N	66.00 W	4	-1.57	-2.19	45	68 - 08	73 - 04		-3.8	-5.6	18	68 - 08	73 - 04		18	8.7	8.3	1356	27.0	25.7
170	San Luis	33.30 S	66.35 W	709	-5.17	-4.08	17	81 - 09	83 - 07		-	-	-	-	-		-	-	-	792	16.8	11.2
171	S. Petersburg	59.58 N	30.18 E	4	-11.66	-11.80	44	80 - 04	83 - 11		-87.1	-86.8	34	81 - 01	83 - 10		34	7.1	8.4	672	6.2	8.3
172	San Salvador (Ilopango)	13.70 N	89.12 W	615	-6.46	-6.67	98	68 - 07	84 - 08	*	-42.3	-45.8	74	68 - 07	84 - 07	*	73	10.1	9.5	1509	23.2	20.6
173	Santa Maria	34.90 N	120.45 W	79	-4.22	-6.01	62	62 - 01	76 - 12		-26.5	-38.7	60	62 - 01	76 - 12		60	7.3	9.4	312	13.7	11.3
174	Santiago	33.45 S	70.70 W	520	-8.87	-10.16	13	72 - 08	75 - 07		-63.5	-69.0	13	72 - 08	75 - 07		12	16.0	17.8	323	14.0	11.4
175	Santiago Del Estero	27.78 S	64.27 W	187	-3.90	-4.90	21	81 - 12	84 - 08		-	-	-	-	-		-	-	-	775	20.1	17.1
176	Sao Gabriel	0.13 S	67.08 W	87	-4.39	-4.65	100	61 - 11	83 - 01	*	-26.3	-28.8	101	61 - 11	83 - 01	*	89	9.2	9.1	2764	25.5	28.1
177	Sao Tome	0.38 N	6.72 E	8	-2.84	-3.39	123	62 - 01	76 - 12		-12.5	-17.7	94	62 - 01	76 - 12		94	8.8	9.2	939	25.2	26.2
178	Saratov	51.34 N	46.02 E	166	-10.94	-11.27	45	80 - 09	84 - 12		-72.4	-74.5	38	81 - 01	84 - 09		36	6.2	6.8	422	7.5	7.9
179	Scoresbysund	70.50 N	22.00 W	0	-13.65	-13.67	40	61 - 01	65 - 08		-	-	-	-	-		-	-	-	442	-7.3	3.2
180	Shijiazhuang	38.02 N	114.25 E	80	-7.85	-7.77	29	85 - 07	87 - 11	*	-53.1	-53.3	29	85 - 07	87 - 11	*	29	10.6	8.8	472	13.8	-
181	Shillong	25.57 N	91.88 E	1598	-4.59	-3.67	31	69 - 01	78 - 10		-27.5	-28.5	30	69 - 01	78 - 10		30	12.7	13.2	2187	17.4	15.1
182	Sidi Barrani	31.63 N	25.96 E	23	-3.65	-4.18	45	78 - 10	87 - 12	*	-17.2	-20.4	46	78 - 10	87 - 12	*	45	11.5	12.7	152	19.5	12.7
183	Simcoe	42.85 N	80.27 W	240	-10.26	-9.27	81	75 - 08	82 - 07		-69.1	-62.2	78	75 - 08	82 - 07		78	11.5	11.4	941	8.6	-
184	Singapore (Airport)	1.35 N	103.90 E	32	-6.89	-7.26	97	68 - 06	76 - 12		-43.9	-46.2	52	68 - 06	75 - 12		52	13.4	13.7	2164	26.3	29.2
185	St. Helena	15.97 S	5.70 W	604	-1.31	-1.42	80	62 - 05	75 - 12		3.1	2.4	74	62 - 05	75 - 12		74	13.9	14.1	893	16.9	16.6
186	Stanley	51.70 S	57.87 W	51	-7.99	-8.08	95	61 - 11	76 - 12		-57.5	-58.0	94	61 - 11	76 - 12		92	6.4	6.4	605	5.7	8.0
187	Ste. Agathe	46.05 N	74.28 W	395	-12.66	-12.55	82	75 - 08	82 - 07		-89.0	-87.8	80	75 - 08	82 - 07		80	13.5	13.6	1200	4.1	-
188	Stuttgart (Cannstatt)	48.83 N	9.20 E	315	-8.19	-8.01	226	61 - 02	87 - 12	*	-59.9	-58.4	223	61 - 02	87 - 12	*	223	5.8	5.7	655	9.3	9.4
189	Taastrup	55.67 N	12.30 E	28	-9.76	-10.02	50	65 - 11	71 - 03		-68.5	-70.7	51	65 - 11	71 - 03		50	9.1	9.2	515	-	-

TABLE 1. Continued

	Station name	Latitude		Longitude		Altitude	OXYGEN - 18 (per mil)						DEUTERIUM (per mil)						DEUTERIUM EXCESS			Prec	Temp	Vap. P.
		(deg.)		(deg.)		(m.a.s.l)	Mean	W. mean	n	Start	End		Mean	W. mean	n	Start	End		n	Mean	W. mean	(mm)	(C)	(mb)
190	Taguac	13.55	N	144.83	E	110	-3.73	-5.21	112	61 - 12	77 - 03		-20.3	-31.1	106	61 - 12	77 - 03		106	9.7	10.8	2659	26.0	28.2
191	Tambov	52.44	N	41.28	E	139	-11.05	-10.95	22	80 - 04	83 - 12		-84.9	-86.4	15	82 - 08	83 - 12		15	5.8	7.6	558	6.7	7.9
192	Teheran	35.68	N	51.32	E	1200	-5.22	-6.76	159	61 - 02	87 - 03	*	-30.3	-41.4	137	61 - 02	87 - 03	*	136	8.8	11.3	211	16.8	6.7
193	The Pas	53.97	N	101.10	W	272	-19.47	-16.31	73	75 - 08	82 - 07		-144.5	-122.8	70	75 - 08	82 - 07		70	7.8	6.8	379	1.5	-
194	Thonon-Les-Bains	46.22	N	6.28	E	385	-9.62	-9.69	196	63 - 06	87 - 01	*	-	-	2	85 - 01	87 - 03	*	1	-	-	1008	10.2	-
195	Thule	76.52	N	68.83	W	77	-24.14	-22.72	59	66 - 01	71 - 09		-184.2	-171.9	45	66 - 01	70 - 03		43	9.3	8.6	189	-11.6	2.3
196	Tokyo	35.68	N	139.77	E	4	-7.10	-7.30	219	61 - 03	79 - 12		-43.8	-46.4	184	61 - 03	79 - 12		183	12.7	11.4	1378	15.5	13.3
197	Trier	49.75	N	6.07	E	273	-7.48	-7.75	118	78 - 01	87 - 12	*	-53.3	-55.2	118	78 - 01	87 - 12	*	118	6.6	6.8	829	8.7	-
198	Truk	7.47	N	151.85	E	2	-4.94	-5.35	93	68 - 03	77 - 05		-30.1	-32.9	72	68 - 03	77 - 05		72	9.8	10.3	3582	27.5	29.9
199	Truro	45.37	N	63.27	W	40	-9.48	-9.53	91	75 - 08	83 - 12		-65.8	-66.1	91	75 - 08	83 - 12		91	10.1	10.2	1008	10.1	7.0
200	Tunis (Carthage)	36.83	N	10.23	E	4	-3.58	-4.54	145	68 - 04	87 - 11	*	-21.5	-26.6	129	68 - 04	87 - 11	*	129	7.5	10.8	481	18.2	15.0
201	Ushuaia	54.78	S	68.28	W	10	-10.53	-10.41	36	81 - 10	85 - 04		-80.3	-73.8	4	82 - 05	82 - 08		4	-	-	299	6.2	7.3
202	Valentia (Observatory)	51.93	N	10.25	W	9	-5.01	-5.34	209	60 - 03	87 - 12	*	-33.6	-35.7	179	60 - 03	87 - 12	*	175	6.8	7.1	1426	10.5	10.9
203	Veracruz	19.20	N	96.13	W	16	-2.86	-4.13	169	62 - 04	87 - 06	*	-16.1	-27.1	136	62 - 04	87 - 06	*	133	7.7	7.5	1518	25.4	25.9
204	Victoria	48.25	N	16.37	E	203	-9.87	-9.96	72	75 - 08	82 - 07		-70.9	-70.8	70	75 - 08	82 - 07		70	3.8	5.0	610	10.0	9.5
205	Vienna (Hohe Warte)	48.65	N	123.43	W	20	-9.32	-10.31	306	61 - 02	87 - 12	*	-71.2	-76.8	302	61 - 02	87 - 12	*	302	7.7	8.0	909	10.7	-
206	Vologda	59.17	N	39.52	E	118	-13.16	-12.75	45	80 - 04	83 - 12		-101.2	-98.9	35	81 - 01	83 - 12		35	6.4	6.6	565	3.6	7.5
207	Waco	31.62	N	97.22	W	156	-3.75	-4.04	96	62 - 01	76 - 12		-19.8	-22.9	96	62 - 01	76 - 12		96	10.2	9.4	810	19.4	16.1
208	Wake Island	19.28	N	166.65	E	3	-1.46	-2.11	151	62 - 02	76 - 12		-3.9	-10.3	132	62 - 02	76 - 12		122	8.1	8.0	908	26.6	25.7
209	Wasserkuppe Rhoen	50.50	N	9.95	E	921	-9.88	-9.78	120	78 - 01	87 - 12	*	-68.3	-67.6	120	78 - 01	87 - 12	*	120	10.8	10.7	1127	4.2	-
210	Weathership E	35.00	N	48.00	W	0	-2.90	-3.16	129	62 - 01	73 - 06		-14.9	-16.4	102	62 - 01	73 - 06		101	9.5	9.5	527	20.4	18.9
211	Weathership V	31.00	N	164.00	E	0	-3.99	-4.35	96	62 - 11	71 - 09		-22.8	-23.7	84	62 - 11	69 - 12		83	8.9	10.7	832	19.1	18.1
212	Whitehorse	60.72	N	135.07	W	702	-20.86	-20.95	54	61 - 05	66 - 01		-162.6	-162.2	54	61 - 05	66 - 01		54	4.4	5.4	269	-1.1	4.7
213	Windhoek	22.57	S	17.10	E	1728	-2.59	-5.03	135	61 - 04	80 - 12		-11.3	-24.5	91	61 - 04	75 - 04		87	10.1	12.6	385	19.3	7.6
214	Wuerzburg	49.80	N	9.90	E	259	-8.07	-8.10	120	78 - 01	87 - 12	*	-59.0	-58.9	120	78 - 01	87 - 12	*	120	5.6	6.0	612	8.3	-
215	Wynyard	51.77	N	104.20	W	561	-17.84	-15.55	77	75 - 08	82 - 07		-139.2	-119.3	76	75 - 08	82 - 07		72	6.4	7.9	354	3.0	-
216	Xian	34.30	N	108.93	E	397	-7.12	-6.74	19	85 - 09	87 - 10	*	-45.7	-43.0	19	85 - 09	87 - 10	*	19	12.4	9.4	530	13.9	-
217	Yangoon	16.77	N	96.17	E	20	-4.79	-4.34	20	61 - 05	63 - 12		-32.0	-28.9	20	61 - 05	63 - 12		20	6.3	6.0	2456	27.3	27.7
218	Yap	9.49	N	138.09	E	0	-4.98	-5.65	99	68 - 06	76 - 12		-29.1	-34.7	65	68 - 06	76 - 12		65	8.6	9.5	2812	27.1	29.1
219	Zagreb	45.49	N	15.59	E	165	-9.08	-9.08	94	80 - 01	87 - 12	*	-64.5	-64.3	94	80 - 01	87 - 12	*	94	8.2	8.4	840	11.0	10.4

TABLE 2. Seasonal and long-term $\delta^{18}O$-temperature and $\delta^{18}O$-precipitation coefficients derived for selected stations of the IAEA/WMO global network. See text for definition of $\Delta\delta^{18}O$, ΔT and ΔP for both seasonal and long-term relationships.

STATION	$\overline{T}$ (°C)	$\overline{P}$ (mm)	Seasonal $\Delta\delta^{18}O/\Delta T$ (‰/°C)	r^2	Long-term $\Delta\delta^{18}O/\Delta T$ (‰/°C)	r^2	Seasonal $\Delta\delta^{18}O/\Delta P$ (‰/10 mm)	r^2	Long-term $\Delta\delta^{18}O/\Delta P$ (‰/10 mm)	r^2
1. Vienna (1961-1990) 48.25°N, 16.30°E; 203 m.a.s.l.	9.9	610	0.39 ± 0.02	0.93	0.65 ± 0.05	0.36	1.83 ± 0.60	0.48	-0.18 ± 0.05	0.039
2. Ottawa (1970-1990) 45.32°N, 75.60°W; 114 m.a.s.l.	5.8	884	0.31 ± 0.02	0.94	0.49 ± 0.08	0.14	2.49 ± 0.88	0.44	0.11 ± 0.05	0.017
3. Argentine Island (1965-1987) 65.25°S, 64.20°W; 0 m.a.s.l.	-4.1	377	0.31 ± 0.03	0.89	0.59 ± 0.04	0.45	-0.88 ± 0.64	0.16	0.10 ± 0.06	0.015
4. Hong Kong (1961-1965) (1973-1987) 22.32°N, 114.10°E; 65 m.a.s.l	22.9	2219	-0.42 ± 0.04	0.91	0.25 ± 0.13	0.02	-0.13 ± 0.02	0.75	-0.06 ± 0.01	0.310
5. Taguac (Guam Isl.) (1961-1967) (1973-1977) 13.55 N, 144.80 E; 110 m.a.s.l.	26.0	2659	-2.43 ± 0.98	0.38	-1.28 ± 0.83	0.02	-0.19 ± 0.02	0.89	-0.17 ± 0.01	0.750
6. Apia (1962-1967) (1972-1977) 13.80 S, 171.70 W 2 m.a.s.l.	26.4	3024	-4.29 ± 0.51	0.88	-1.15 ± 0.19	0.29	-0.13 ± 0.02	0.78	0.03 ± 0.01	0.070

the Vienna station, having the longest $\delta^{18}O$ record in the network. It is clear that the smoothing does not change the character of the trend curves. The trend curves of $\Delta\delta^{18}O$ for the Swiss stations are shown in Figure 21a. They reveal a strong coherence among the four stations (correlation coefficient between each pair of stations higher than 0.8). This indicates the presence of common mechanisms controlling the long-term behaviour of ^{18}O content in precipitation in this region.

The composite trend curve of ΔT for the Swiss stations (Figure 22a) indicates a warming trend in the order of 1.5°C between 1986 and 1990, associated with an increase of $\Delta\delta^{18}O$ by about 2‰ above the 1970-1990 average, during the same time interval. The composite trend curve of temperature for all European stations shown in Figure 22b reveals the same trend and is in qualitative agreement with regional estimates published by *Hansen and Lebedeff* [1987], based on a much larger data set. Correlation analysis suggests that up to 45 per cent of the variations observed for trend curves of $\Delta\delta^{18}O$ representing European stations can be attributed to temperature changes, although the strength of this coupling may vary substantially from place to place, even on a regional scale [*Rozanski et al.*, 1992]. Figure 23 illustrates the correlation between $\Delta\delta^{18}O$ and ΔT for the Vienna station, derived from the trend curves shown in Figure 20. The slope of the best fit line is equal to 0.65±0.05 ‰ per °C.

The trend curves for stations representing other regions reveal a different behaviour. The Ottawa station, although located at a similar latitude to the Vienna station, does not reveal any warming trend over the last decade. To the contrary, a general cooling is visible (Figure 22c). There is a poor correlation between $\Delta\delta^{18}O$ and ΔT for this station (see Table 2). The Hong Kong data, representing tropical, monsoon-type climate, shows relatively small fluctuations of $\Delta\delta^{18}O$ and ΔT, without apparent correlation among them (Fig. 22d). The Taguac data (tropical, oceanic climate) reveal similar behaviour.

Argentine Island, located at a high latitude in the southern hemisphere, is characterized by the strongest link between ^{18}O and temperature among the stations analyzed. The trend curves show a very distinct maximum around 1985. The $\Delta\delta^{18}O/\Delta T$ coefficient derived from the trend curves of ^{18}O and temperature amounts to 0.59±0.04 ‰ per °C. This is in excellent agreement with an independent estimate of this coefficient based on comparison of δD variations measured in the snow core collected at Dalinger Dome (Antarctic Peninsula) and covering the time period 1953-1980, with instrumental records of temperature in this region [*Aristarain et al.*, 1986]

The trend curves of the long-term changes of precipitation amount (ΔP) at selected stations were calculated in an analogous way as for the temperature and $\delta^{18}O$. They are compared with the $\Delta\delta^{18}O$ curves in Figure 24. The slopes $\Delta\delta^{18}O/\Delta T$ and $\Delta\delta^{18}O/\Delta P$ derived from regression analysis of the trend curves are summarized in Table 2. For the analyzed continental stations (Vienna, Ottawa, Argentine

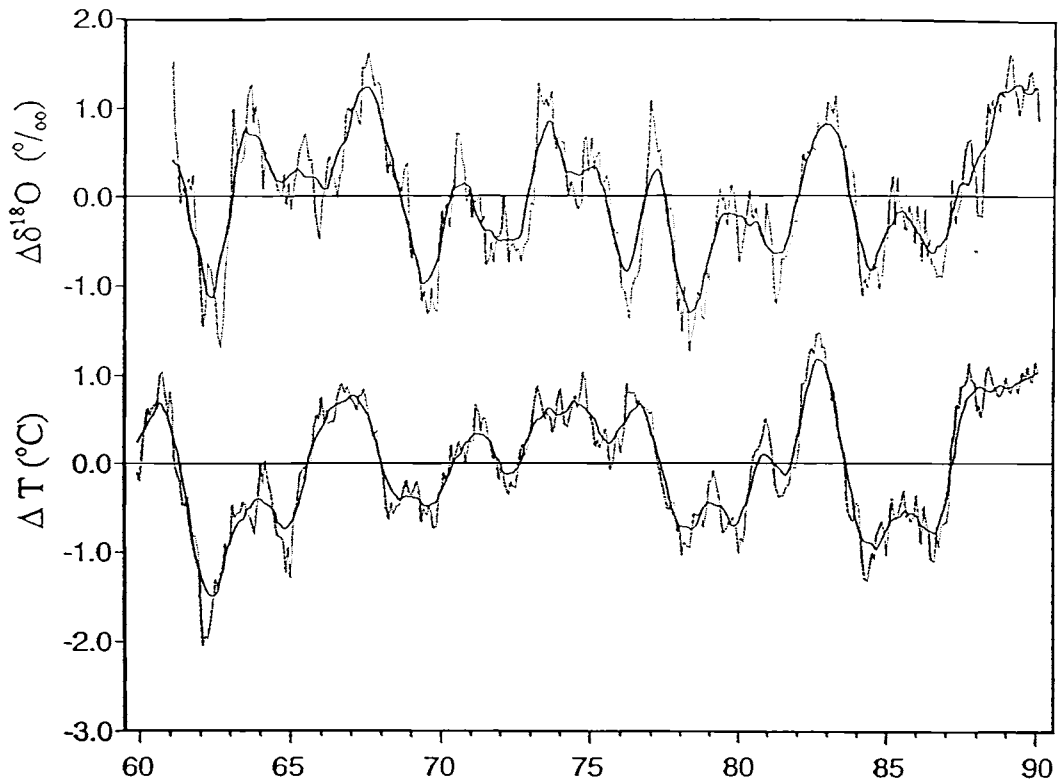

Fig. 20. Long-term trend curves of $\delta^{18}O$ and surface air temperature for the Vienna station. The trend curves $\Delta\delta^{18}O$ and ΔT were calculated by applying a 12-month running average over the monthly time series and subtracting the resulting curves from the long-term annual means of $\delta^{18}O$ and temperature (broken lines). The resulting curves were then smoothed by applying again a 12-month running average (heavy lines).

Island) there is no significant correlation between long-term changes of $\delta^{18}O$ and the amount of precipitation. Temperature appears to be a major parameter controlling long-term behaviour of isotopic composition of precipitation in a continental environment. On the contrary, Taguac and Hong Kong data reveal significant correlation between long-term changes of $\delta^{18}O$ and precipitation amount with no apparent link to the fluctuations of temperature at these stations. Exceptionally strong correlation between $\Delta\delta^{18}O$ and ΔP for Taguac station ($r^2 = 0.75$) has already been noted by *Lawrence and White* [1991].

δD - $\delta^{18}O$ relationship

A close relationship between deuterium and oxygen-18 isotopic composition of freshwaters (including precipitation) when plotted on the δD - $\delta^{18}O$ diagram, was first noted by *Friedman* [1953]. Craig, in his global survey of deuterium and oxygen-18 content of freshwaters [*Craig*, 1961], suggested the best fit line of his data points, $\delta D = 8 \cdot \delta^{18}O + 10$, which was later named the Global Meteoric Water Line (GMWL). A few years later, Dansgaard [*Dansgaard*, 1964] introduced the concept of "deuterium excess", defined as $d = \delta D - 8 \cdot \delta^{18}O$.

A clear distinction has to be made between the deuterium excess calculated using the above equation which defines location of individual data points on the δD-$\delta^{18}O$ plot with respect to the GMWL, and the intercept of the best fit line of all data points available, which frequently has a different slope than the GMWL. Figure 25a shows the long-term annual mean $\delta^{18}O$ and δD values for all analyzed stations of the IAEA/WMO network, plotted on the δD - $\delta^{18}O$ diagram. The least square fit of the data points results in the following equations:

a) long-term arithmetic means:

$$\delta D_a = (8.17 \pm 0.06)\delta^{18}O + (10.35 \pm 0.65) \quad r^2 = 0.99 \quad n = 206 \quad (2)$$

b) long-term weighted means (weighing by amount of precipitation):

$$\delta D_w = (8.20 \pm 0.07)\delta^{18}O + (11.27 \pm 0.65) \quad r^2 = 0.98 \quad n = 205 \quad (3)$$

The above equations are identical, within the quoted errors, with the earlier estimates based on the IAEA database [*Dansgaard*, 1964; *Yurtsever and Gat*, 1981] and confirm that Craig's equation $\delta D = 8 \cdot \delta^{18}O + 10$ is a good approximation of the locus of points representing average isotopic composition of freshwaters worldwide.

The global δD - $\delta^{18}O$ relationship is well understood. It was properly reproduced by both "isolated air mass" models based on the Rayleigh approach [*Merlivat and Jouzel*, 1979] and by general circulation models [*Joussaume et al.*, 1984a; *Jouzel et al.*, 1987a]. It

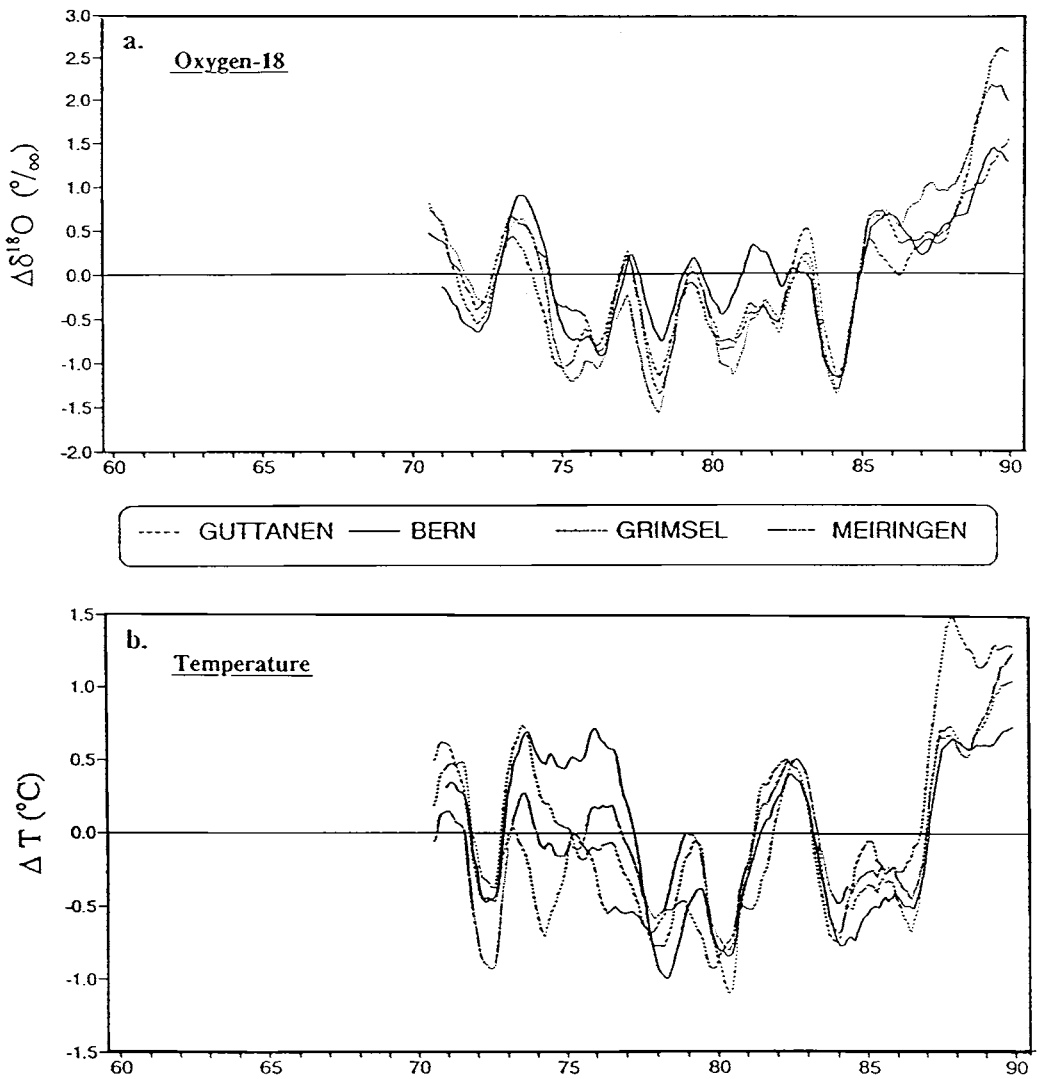

Fig. 21. The trend curves of $\delta^{18}O$ in precipitation (a) and surface air temperature (b) for four Swiss stations of the IAEA/WMO global network, derived from the available time series of monthly data (see text for details).

has been demonstrated that the value of the intercept of the global meteoric water line is controlled by the evaporation process in the major source regions of the vapor (subtropical ocean). The sea surface temperature, humidity of the air and the wind speed are the main controlling parameters. In-cloud processes in general do not modify significantly the deuterium excess value of the vapor, as long as formation of rain is considered. It has also been shown that the slope of the GMWL is controlled in the first instance by the ratio of equilibrium isotope enrichments for deuterium and oxygen-18, respectively [*Dansgaard*, 1964; *Merlivat and Jouzel*, 1979].

Comparison of the long-term annual means of $\delta^{18}O$ and δD (Figure 25a) with the long-term monthly means for the same set of stations (Figure 25b), reveals in the latter case a slightly lower slope of the δD - $\delta^{18}O$ relationship and generally higher spread of data points. This effect is more obvious when monthly data for individual stations are plotted on the δD - $\delta^{18}O$ diagram (Figures 26 and 27). The comparison of δD - $\delta^{18}O$ plots for selected marine (Figure 26) and continental (Figure 27) stations shows that in the former case the range of variations is smaller and a scatter of the data points is usually substantially larger. The regression equations with corresponding correlation coefficients for the monthly data presented in Figures 26 and 27 are summarized in Table 3. In an extreme situation, represented by the St. Helena station (see Figure 26), the monthly data points form a tight cluster, with a very poor correlation between δD and $\delta^{18}O$. At this station essentially all precipitation probably comes from nearby sources and represents the first stage of the rain-out process. This probably accounts for the poor correlation. Most of the data points have positive δD values. This reflects a higher evaporation temperature at the vapor source, when compared to average condensation temperatures. The generally weaker

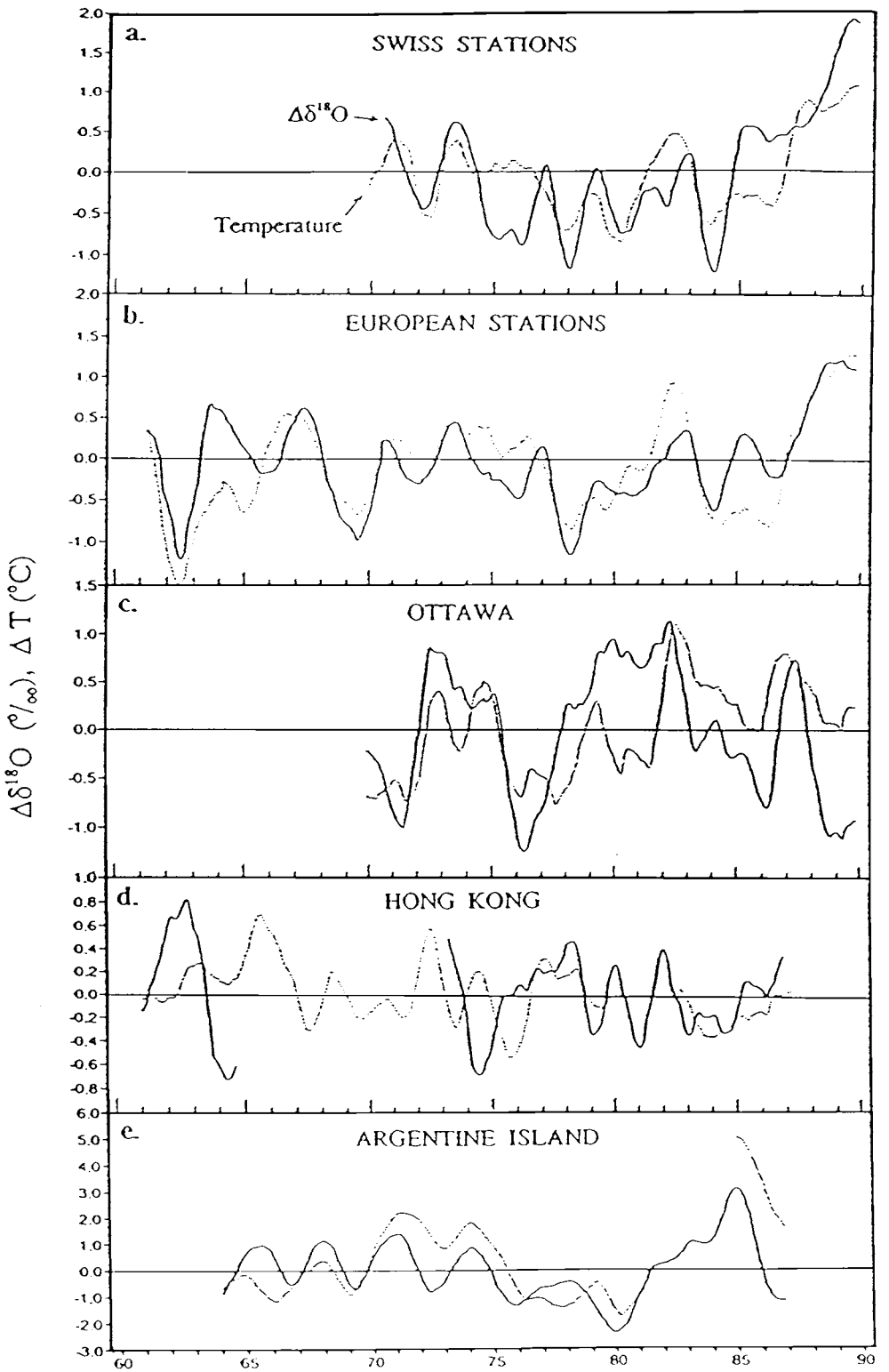

Fig. 22. The long-term trends of $\delta^{18}O$ in precipitation and surface air temperature for selected stations of the IAEA/WMO global network. (a) composite trend curves of $\Delta\delta^{18}O$ and ΔT for the four Swiss stations presented in Figure 21; (b) composite trend curves of $\Delta\delta^{18}O$ and ΔT for selected European stations; (c,d,e) trend curves of $\Delta\delta^{18}O$ and ΔT for Ottawa, Hong Kong and Argentine Island, respectively.

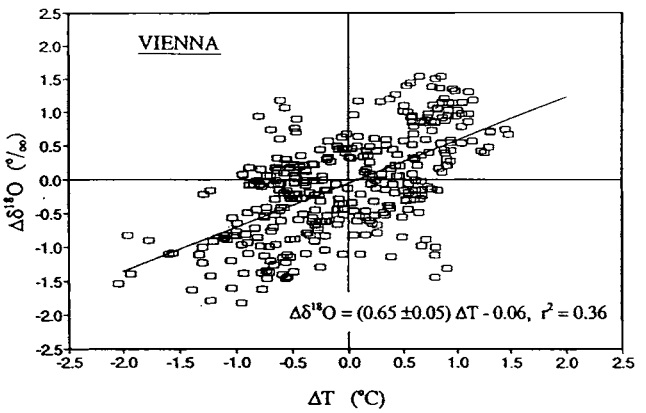

Fig. 23. Relationship between the trend curves of $\Delta\delta^{18}O$ and ΔT calculated for the Vienna station having the longest ^{18}O record among the stations of the IAEA/WMO global network.

correlation of δD and $\delta^{18}O$ values for the marine stations of the network [see *IAEA*, 1992] may reflect varying contributions of air masses with different source characteristics and a low degree of rain-out.

The imprint of local conditions at source regions of the vapor and different storm trajectories on the isotopic composition of precipitation can be seen also at a number of coastal and continental stations. For instance, the Bet Dagan station receives rains associated with Mediterranean or European air masses, each characterized by a different deuterium excess value [*Gat and Carmi*, 1987; *Rindsberger et al.*, 1983, 1990]. This results in a large spread of data points on the δD - $\delta^{18}O$ plot. A similar situation is observed for Tokyo station, which receives precipitation of Pacific origin in summer, whereas in winter the westerly circulation dominates bringing precipitation from the Japan Sea and the China Sea.

Even in cases where the stations receive precipitation essentially from one source, distinct seasonal trends can be identified on δD - $\delta^{18}O$ plots of monthly data. European stations of the network serve as an example of such a situation. The plot of the mean monthly values of the deuterium excess for the Valentia and Vienna stations (Figure 28) reveal significantly higher values of this parameter in winter than in summer. This, in turn, leads to the slope of δD - $\delta^{18}O$ relation distinctly lower than 8 when an attempt is made to fit the data with a straight line (see Table 3). It has been suggested [*Rozanski*, 1987] that this apparent seasonality of the d-excess values in Europe may be generated by two effects: (1) lower relative humidity of air (normalized to the sea surface temperature) in the source region in winter leads to enhanced kinetic fractionation during the evaporation process and, consequently, higher d-excess signature of the vapor. (2) lower relative humidity over the continent in summer facilitates partial evaporation of raindrops below the cloud base. This, in turn will lead to reduction of the deuterium excess values of summer rains. For stations with substantial contribution of snow precipitation, higher deuterium excess values during winter may result from additional kinetic fractionation during snow formation [*Jouzel and Merlivat*, 1984].

Fitting monthly isotope data of individual stations with a straight line is not always justified theoretically; the above examples have shown that seasonally varying influence of different sources of vapor with different isotope characteristics, different storm trajectories or evaporation and isotope exchange processes below the cloud base, may often lead to a more complex relationship between δD and $\delta^{18}O$ of precipitation recorded at a given station.

Figure 29a shows latitudinal distribution of the deuterium excess values derived from the long-term annual means of δD and $\delta^{18}O$ for the selected stations of the network. Stations of the northern hemisphere reveal a relatively large spread of the d-values, without any clear trend. An exception is the group of stations located in the Mediterranean region, which are characterized by distinctly higher deuterium excess values, reflecting specific conditions of vapor formation over the Mediterranean Sea [*Gat and Carmi*, 1970; *Rindsberger et al.*, 1983, 1990]. For the southern hemisphere, a slight increase of the d-values can be noted between the equatorial region and 30°S, followed by an apparent reduction of this parameter further south, with a distinct minimum around 65°S (Argentine Island). The Perth station (31.95°S. 115.90°E) constitutes an exception to this trend. Contrary to other Australian stations of the network, in Perth, as in the Mediterranean region, winter precipitation prevails. Although these apparent variations of the deuterium excess may properly reflect different conditions at vapor source regions (relative humidity, wind speed, sea surface temperature), scarcity of data documenting variability in these conditions does not allow any firm conclusions.

The role of vapor source regions in establishing the deuterium excess values observed in precipitation is illustrated by Figure 29b showing the d-values for selected stations of the network, as a function of a fraction of winter precipitation in the total precipitation collected at the given station. For the stations with dominating winter precipitation, an apparent increase of the deuterium excess is observed, probably due to lower relative humidity (normalized to the sea surface temperature) over the ocean in winter and/or substantial contribution of snow precipitation formed under non-equilibrium conditions.

Frequency distribution of monthly data

The above discussion demonstrated that the isotopic composition of monthly composite samples of precipitation collected throughout the year is controlled by a number of different processes, both of a regional and local nature. To illustrate the relative importance of these processes in formation of the average isotopic composition of precipitation at a given location, frequency distribution histograms of monthly $\delta^{18}O$ values have been constructed for several stations representing different environments. These histograms are shown in Figure 30. Two marine stations (Weathership E and Apia) reveal a rather symmetric distribution, coupled with a relatively small range for the $\delta^{18}O$ values. This appears to be a typical $\delta^{18}O$ distribution for oceanic islands [*IAEA*, 1992] . The mid-latitude continental stations in contrast are characterized by a much broader range of $\delta^{18}O$ values and a distribution which is usually skewed towards negative values (Vienna, Ottawa). An interesting example of bimodal distribution is represented by the data from the New Delhi station. Two distinct peaks are associated with two distinct modes of precipitation regime: the more negative peak represents abundant monsoon precipitation (June-September), whereas light rains occurring between October

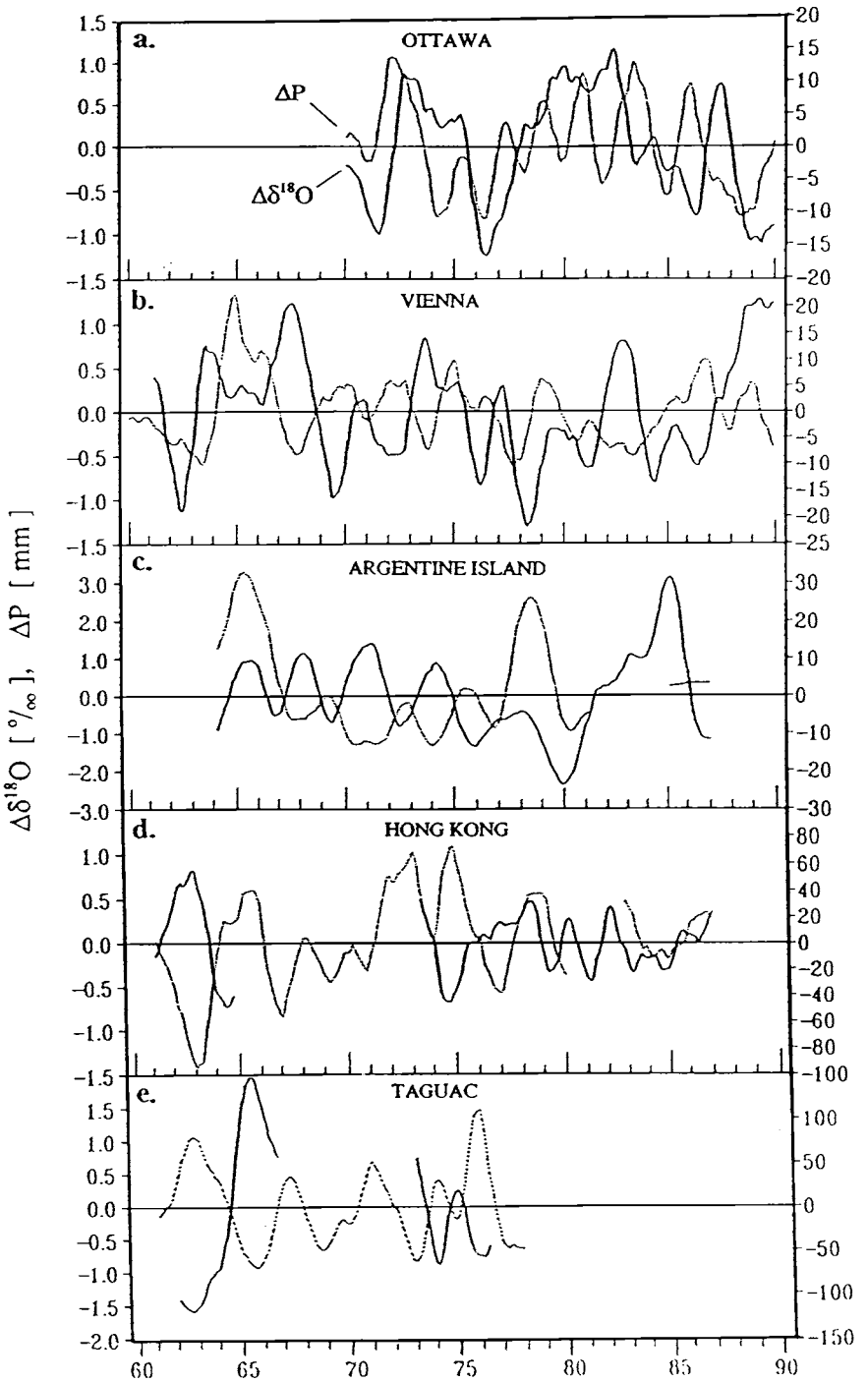

Fig. 24. The long-term trends of $\delta^{18}O$ and amount of precipitation, calculated for selected stations of the IAEA/WMO global network: Vienna (a), Ottawa (b), Argentine Island (c), Hong Kong (d) and Taguac (e). See text for details of calculation of $\Delta\delta^{18}O$ and ΔP.

and June form the second peak. Detailed analysis of isotope and precipitation data for this station suggests that isotopic composition of precipitation representing the dry period is probably modified by evaporation and isotope exchange below the cloud base [*Datta et al.*, 1991].

CONCLUDING REMARKS

The IAEA/WMO network "Isotopes in Precipitation" has accumulated during the past three decades a unique set of basic data on spatial and temporal distribution patterns of deuterium and oxygen-18 isotope composition of precipitation on the global scale.

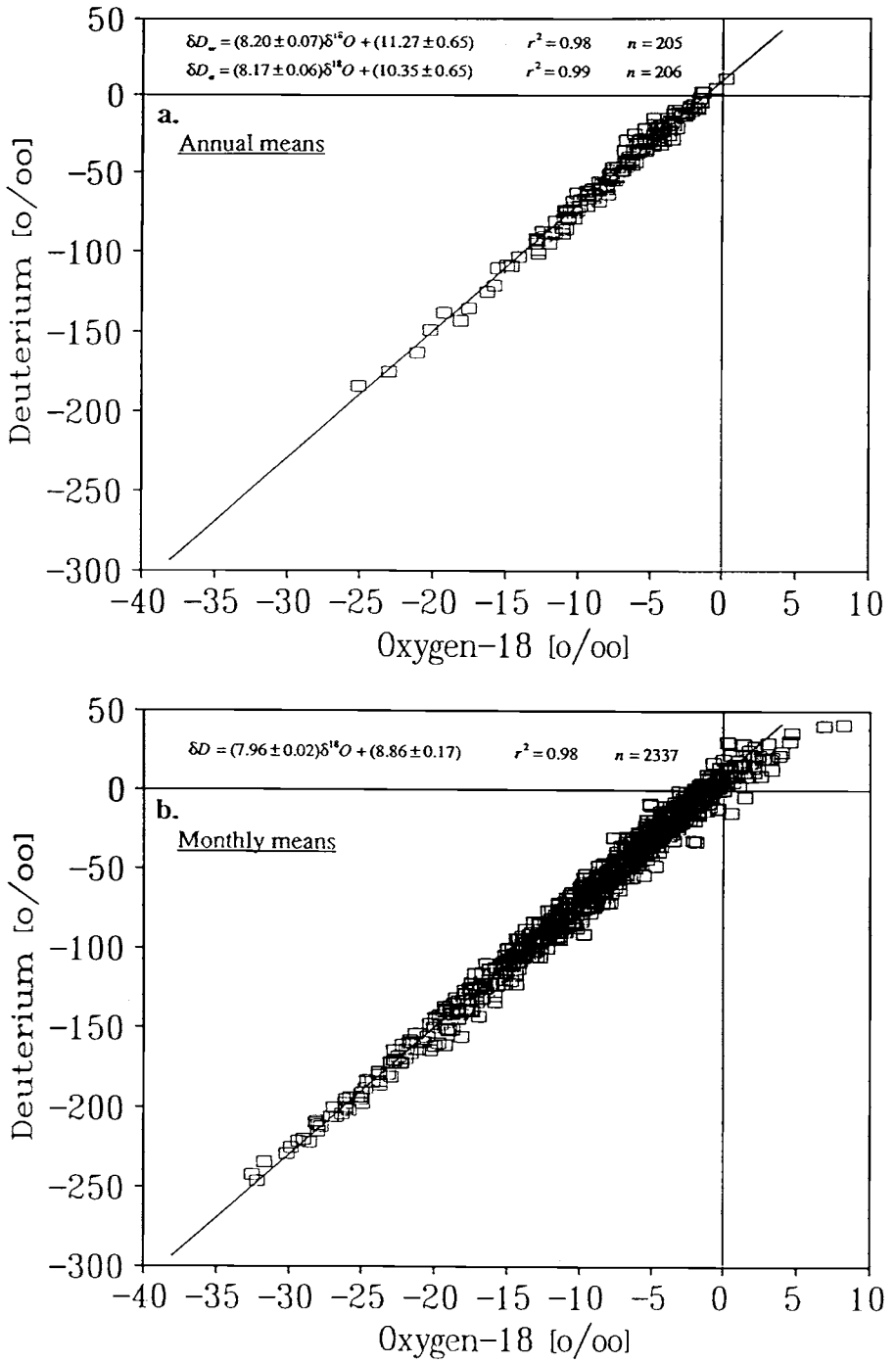

Fig. 25. Global relationship between long-term annual (a) and monthly (b) means of $\delta^{18}O$ and δD in precipitation, derived for all stations of the IAEA/WMO global network. Heavy lines indicate the position of the Global Meteoric Water Line: $\delta D = 8 \cdot \delta^{18}O + 10$.

This database has been extensively used in the past in numerous applications of environmental isotopes to hydrology, oceanography and climatology. The basic design and structure of the network appears to be correct, although certain modifications would be necessary to meet current needs of new fields of applications of stable isotope data, especially in climatology and global atmospheric modelling.

The present-day global distribution patterns of deuterium and oxygen-18 in meteoric waters reveal a close relationship between some climatically relevant meteorological parameters such as surface

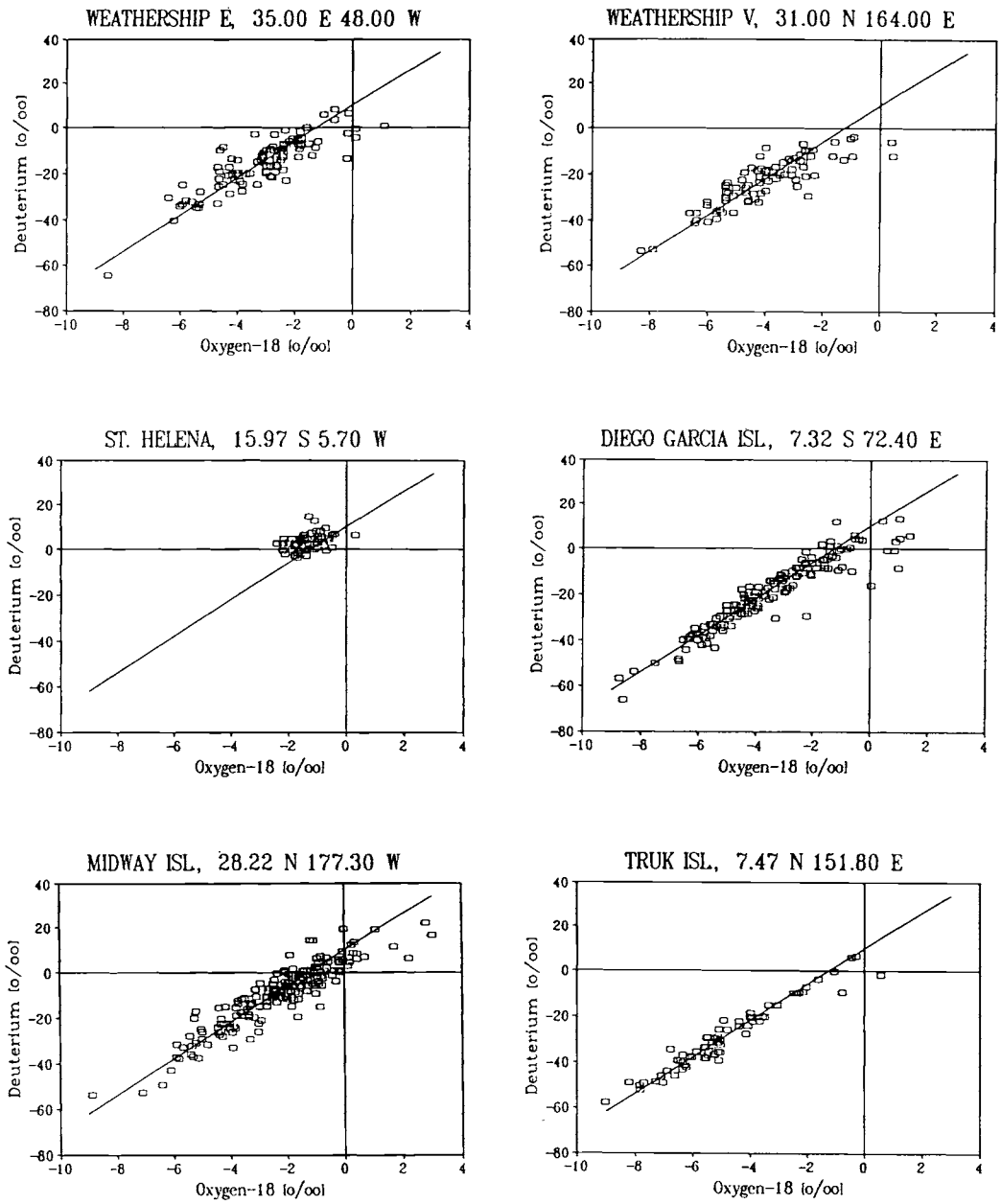

Fig. 26. δD - $\delta^{18}O$ relationships for the monthly data of the selected marine stations of the IAEA/WMO global network. The heavy line indicates the position of the Global Meteoric Water Line: $\delta D = 8 \cdot \delta^{18}O + 10$.

air temperature or amount of precipitation and isotopic composition of precipitation. These apparent correlations have been applied in numerous studies to extract palaeoclimatic information from records of isotopic composition of ancient precipitation preserved in various climatic archives (polar ice cores, lake deposits, groundwater, organic matter). Quantitative interpretation of these records is, however, hampered by our limited understanding of physical processes controlling global isotope behaviour. Whereas the link between isotope signature of precipitation and climate at polar regions is at present relatively well understood, this is much less the case for temperate and tropical areas. The IAEA/WMO network is providing ground-truth data needed to improve our knowledge of these processes.

Today, long records of isotope and meteorological data are available for a number of stations of the IAEA/WMO network, reaching in several cases three decades, a time scale comparable with climatic fluctuations. Therefore, a search for long-term trends in the isotope records is becoming meaningful. We have demonstrated that the long-term changes of ^{18}O content of precipitation in some regions closely follow long-term changes of surface air temperature and

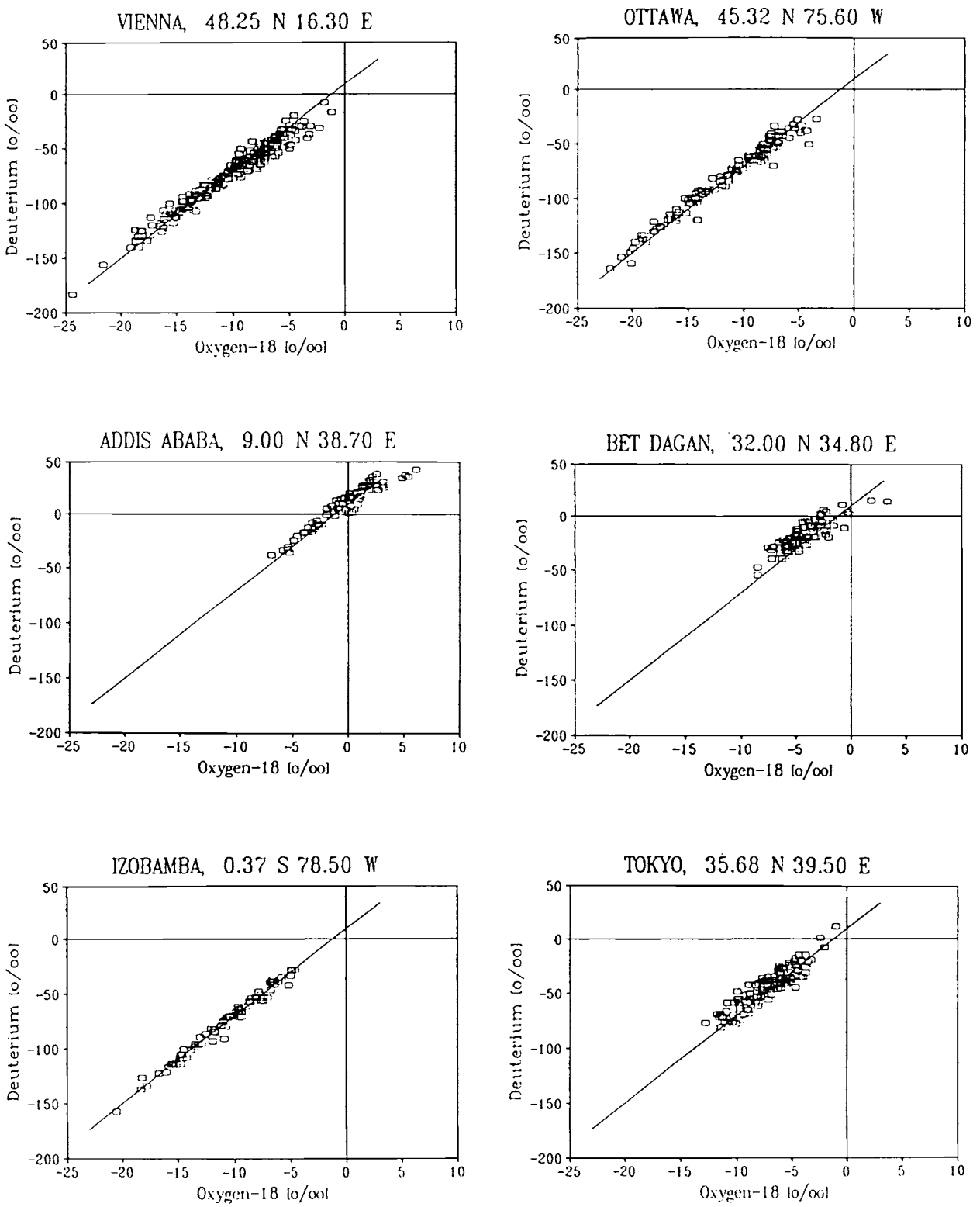

Fig. 27. δD - $\delta^{18}O$ relationships for the monthly data of selected continental stations of the IAEA/WMO global network. The heavy line indicates the position of the Global Meteoric Water Line: $\delta D = 8 \cdot \delta^{18}O + 10$.

TABLE 3. Regression equations of δD and $\delta^{18}O$ monthly data for selected stations of the IAEA/WMO global network.

STATION	Regression equation	r^2	STATION	Regression equation	r^2
Continental and coastal stations			Marine stations		
Vienna	$\delta D = 7.07\,\delta^{18}O - 1.38$	0.961	Weathership E	$\delta D = 5.96\,\delta^{18}O + 2.99$	0.738
Ottawa	$\delta D = 7.44\,\delta^{18}O + 5.01$	0.973	Weathership V	$\delta D = 5.51\,\delta^{18}O - 1.10$	0.737
Addis Ababa	$\delta D = 6.95\,\delta^{18}O + 11.51$	0.918	St. Helene	$\delta D = 2.80\,\delta^{18}O + 6.61$	0.158
Bet Dagan	$\delta D = 5.48\,\delta^{18}O + 6.87$	0.695	Diego García Isl.	$\delta D = 6.93\,\delta^{18}O + 4.66$	0.880
Izobamba	$\delta D = 8.01\,\delta^{18}O + 10.09$	0.984	Midway Isl.	$\delta D = 6.80\,\delta^{18}O + 6.15$	0.840
Tokyo	$\delta D = 6.87\,\delta^{18}O + 4.70$	0.835	Truk Isl.	$\delta D = 7.07\,\delta^{18}O + 5.05$	0.940

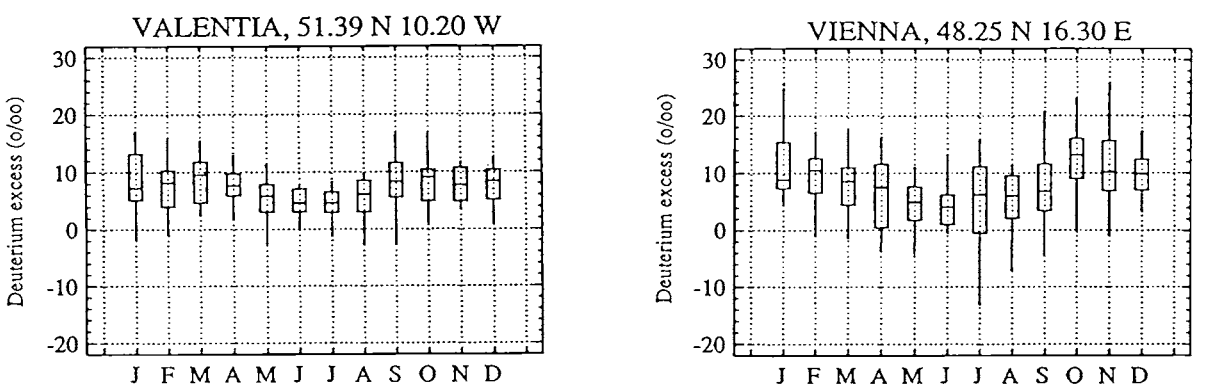

Fig. 28. Seasonal variations of the deuterium excess values in precipitation collected at two European stations of the IAEA/WMO global network: Valentia and Vienna. The data are presented in the form of box-and-whisker plots.

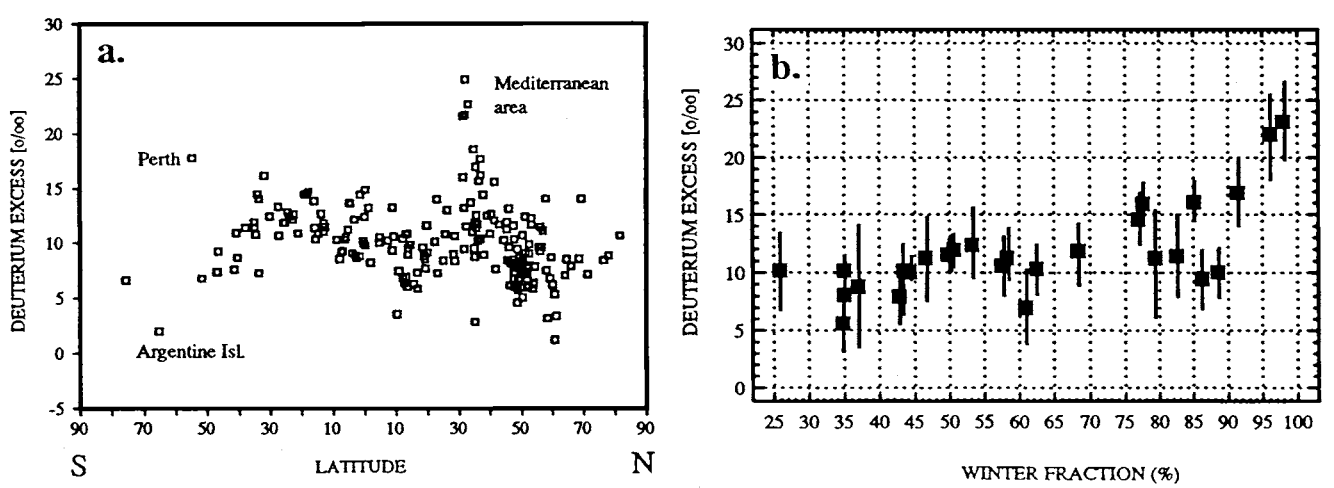

Fig. 29. (a) Latitudinal distribution of deuterium excess values calculated from the long-term annual means of $\delta^{18}O$ and δD in precipitation, available for the stations of the IAEA/WMO global network; (b) the deuterium excess values calculated from the long-term annual means of $\delta^{18}O$ and δD in precipitation for selected stations of the network and plotted as a function of the fraction of winter precipitation in the mean annual precipitation recorded at the given station.

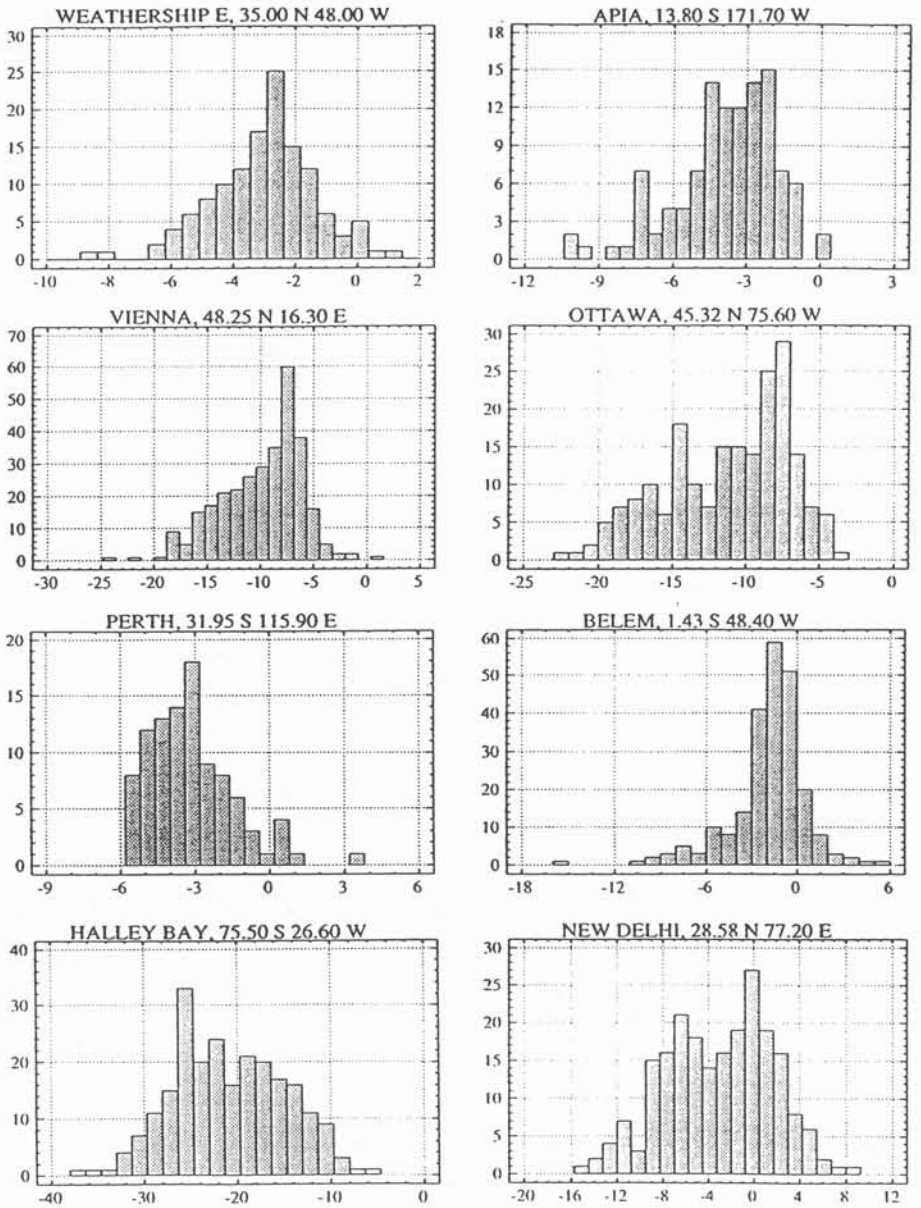

Fig. 30. Frequency distribution histograms of $\delta^{18}O$ in monthly precipitation, calculated for selected stations of the IAEA/WMO global network.

amount of precipitation, confirming the importance of stable isotopes as climatic indicators.

Acknowledgements. The continuous support and cooperation of numerous individuals and institutions in the IAEA and WMO Member States in maintaining the network activities is highly acknowledged. Thorough reviews of Carol Kendall and James R. Lawrence greatly improved the manuscript.

REFERENCES

Ambach, W., M. Elsässer, H. Moser, W. Rauert, W. Stichler, and P. Trimborn, Variationen des Gehaltes an Deuterium, Sauerstoff-18 und Tritium während einzelner Niederschläge, *Wasser und Leben, 27*, 186-192, (1975).

Aristarain, A.J., J. Jouzel, and M. Pourchet, Past Antarctic Peninsula climate (1850-1980) deduced from an ice core isotope record, *Clim. Change, 8*, 69-89, 1986.

Becker, B., B. Kromer, and P. Trimborn, A stable-isotope tree-ring timescale of the Late Glacial/Holocene boundary, *Nature, 353*, 647-649, 1991.

Bryson, R.A., and F.K. Hare, Climates of North America, in *World Survey of Climatology*, edited by H.E. Landsberg, pp. 321-356, Elsevier, Amsterdam, 1974.

Covey, C., and P.L. Haagenson, A model of oxygen isotope composition of precipitation: Implication for paleoclimate data, *J. Geophys. Res.*, 89, 4647-4655, 1984.

Craig, H., Isotopic variation in meteoric waters, *Science, 133*, 1702-1703, 1961.

Craig, H., and L. Gordon, Deuterium and oxygen 18 variation in the ocean and marine atmosphere, in *Stable Isotopes in Oceanographic Studies and Palaeotemperatures, Spoleto 1965*, edited by E. Tongiorgi, pp. 9-130, Consiglio Nazionale della Richerche, Pisa, Italy, 1965.

Dansgaard, W., The abundance of ^{18}O in atmospheric water and water vapour, *Tellus, 5*, 461-469, 1953.

Dansgaard, W., The ^{18}O abundance of fresh water, *Geochim. Cosmochim. Acta, 6*, 241-260, 1954.

Dansgaard, W., Stable isotopes in precipitation. *Tellus, 16*, 436-468, 1964.

Dansgaard, W., H. Clausen, N. Gundestrup, C. Hammer, S. Johnsen, P. Kristinsdottir, and N. Reeh, A new Greenland deep ice core, *Science, 218*, 1273-1277, 1982.

Datta, P.S., S.K. Tyagi, and H. Chandrasekharan, Factors controlling stable isotope composition of rainfall in New Delhi, India, *J. Hydrol., 128*, 223-236, 1991.

Eicher, U., and U. Siegenthaler, Palynological and oxygen isotope investigations on Late-Glacial sediment cores from Swiss lakes, *Boreas, 5*, 109-117, 1976.

Ehhalt, D.H., Vertical profiles of HTO, HDO and H_2O in the troposphere. *NCAR Technical Note, NCAR-TN/STR-100*, 133pp., 1974.

Epstein, S., and T. Mayeda, Variations of the ^{18}O content of waters from natural sources, *Geochim. Cosmochim. Acta, 4*, 213-224, 1953.

Eriksson, E., Deuterium and oxygen 18 in precipitation and other natural waters: Some theoretical considerations, *Tellus, 27*, 498-512, 1965.

Fisher, D.A., and B.T. Alt, A global oxygen isotope model, semiempirical, zonally averaged, *Ann. Glaciol., 7*, 117-124, 1985.

Fisher, D.A., A zonally-averaged stable-isotope model coupled to a regional variable-elevation stable-isotope model, *Ann. Glaciol., 14*, 65-71, 1990.

Friedman, I., Deuterium content of natural waters and other substances, *Geochim. Cosmochim. Acta, 4*, 89-103, 1953.

Friedman, I., A.C. Redfield, B. Schoen, and J. Harris, The variation of the deuterium content of natural waters in the hydrologic cycle, *Rev. Geophys., 2*, 1-124, 1964.

Friedman, I., G.I. Smith, J.D. Gleason, A. Warden, and J.M. Harris. Stable isotope composition of waters in southeastern California, 1. Modern precipitation, *J. Geophys. Res., 97*, 5795-5812, 1992.

Fritz, P., R.J. Drimmie, S.K. Frape, and K. O'Shea, The isotopic composition of precipitation and groundwater in Canada, in *Isotope Techniques in Water Resources Development*, pp. 539-550, International Atomic Energy Agency, Vienna, Austria, 1987.

Gambell, A.W., and I. Friedman, Note on the great variation of deuterium/hydrogen ratios in rainfall for a single storm event, *J. Appl. Meteorol., 4*, 533-535, 1965.

Gat, J.R., and W. Dansgaard, Stable isotope survey of the fresh water occurrences in Israel and the northern Jordan rift valley, *J. Hydrol., 16*, 177-212, 1972.

Gat, J.R., and I. Carmi, Effect of climate changes on the precipitation patterns and isotopic composition of water in a climate transition zone: Case of the Eastern Mediterranean Sea area. in *The Influence of Climatic Variability on the Hydrologic Regime and Water Resources*, IAHS Publ. No. 168, pp. 513-523, 1987.

Gat, J.R., and E. Matsui, Atmospheric water balance in the Amazon Basin: An isotopic evapotranspiration model, *J. Geophys. Res., 96*, 13,179-13,188, 1991.

Gedzelman, S.D., and J.R. Lawrence, The isotopic composition of cyclonic precipitation, *J. Appl. Meteorol., 21*, 1387-1404, 1982.

Gedzelman, S.D., Deuterium in water vapour above the atmospheric boundary layer, *Tellus, 40B*, 134-147, 1988.

Gedzelman, S.D., and J.R. Lawrence, The isotopic composition of precipitation from two extratropical cyclones, *Monthly Weather Review, 118*, 495-509, 1990.

Gonfiantini, R., On the isotopic composition of precipitation, *Rendiconti Soc. It. Miner. Petr., 38*, 1175-1187, 1982.

Gonfiantini, R., On the isotopic composition of precipitation in tropical stations, *Acta Amazonica, 15*, 121-139, 1985.

Hansen, J., and S. Lebedeff, Global trends of measured surface air temperature, *J. Geophys. Res., 92*, 13,345-13,372, 1987.

Holdsworth, G., S. Fogarasi, and H.R. Krouse, Variation of the stable isotopes of water with altitude in the Saint Elias Mountains of Canada, *J. Geophys. Res., 96*, 7483-7494, 1991.

IAEA, *World Survey of Isotope Concentrations in Precipitation*. Technical Report Series Nos. 69, 117, 129, 147, 165, 192, 226, 264, 311, International Atomic Energy Agency, Vienna, 1969, 1970, 1971, 1973, 1975, 1979, 1983, 1986, 1990.

IAEA, *Statistical treatment of environmental isotope data in precipitation*, Technical Report Series No. 206, 256pp., International Atomic Energy Agency, Vienna, 1981.

IAEA, *Statistical treatment of data on environmental isotopes in precipitation*, Technical Report Series, No. 331, 720pp., International Atomic Energy Agency, Vienna, 1992.

Ingraham, N.L., and B.E. Taylor, Hydrogen isotope study of large-scale meteoric water transport in northern California and Nevada, *J. Hydrol., 85*, 183-197, 1986.

Ingraham, N.L., and R.C. Craig, Isotopic evidence of the terrestrial recycling of meteoric water as validated by a climate model, (this volume).

Jacob, H., and C. Sonntag, An 8-year record of the seasonal variation of ^{2}H and ^{18}O in atmospheric water vapour and precipitation at Heidelberg, Germany, *Tellus, 43B*, 291-300, 1991.

Johnsen, S.J., W. Dansgaard, and J.W.C. White, The origin of Arctic precipitation under present and glacial conditions, *Tellus, 41B*, 452-468, 1989.

Joseph, A., J.P. Frangi and J.F. Aranyossy, Isotope characteristics of meteoric water and groundwater in the Sahelo-Sudanese Zone, *J. Geophys. Res., 97*, 7543-7551, 1992.

Joussaume, S., J. Jouzel, and R. Sadourny, Water isotope cycles in the atmosphere: First simulation using a general circulation model, *Nature, 311*, 24-29, 1984a.

Joussaume, S., R. Sadourny, and J. Jouzel, Simulation of the HDO and $H^{18}O$ cycles in an atmospheric general circulation model, *Ann. Glaciol., 5*, 208-210, 1984b.

Jouzel, J., and L. Merlivat, Deuterium and oxygen 18 in precipitation: Modelling of the isotopic effect during snow formation, *J. Geophys. Res., 89*, 11,749-11,757, 1984.

Jouzel, J., Isotopes in cloud physics: multiphase and multistage condensation processes, in *Handbook of Environmental Isotope Geochemistry, Vol. 2 The Terrestrial Environment, B*, pp. 61-105, Elsevier, Amsterdam-Oxford-New York-Boston, 1986.

Jouzel, J., G.L. Russel, R.J. Suozzo, R.D. Koster, J.W.C. White, and W.S. Broecker, Simulations of the HDO and $H^{18}O$ atmospheric cycles using the NASA GISS general circulation model: The seasonal cycle for present-day conditions, *J. Geophys. Res., 92*, 14,739-14,760, 1987a.

Jouzel, J., C. Lorius, J. Petit, C. Genthon, N. Barkov, V. Kotlyakov, and V. Petrov, Vostok ice core: a continuous isotope temperature record over the last climatic cycle (160,000 years), *Nature, 329*, 403-408, 1987b.

Jouzel, J., R.D. Koster, R.J. Suozzo, G.L. Russel, J.W.C. White and W.S. Broecker, Simulations of the HDO and $H_2^{18}O$ atmospheric cycles using the NASA GISS general circulation model: Sensitivity experiments for present-day conditions, *J. Geophys. Res., 96*, 7495-7507, 1991.

Korzun, V.I. (Ed.) *World Water Balance and Water Resources of the Earth*. Report of the USRR Committee for the IHD, 663pp, Gidromet. Izdatel., Leningrad, 1974, (English translation: *Studies and Reports in Hydrology, No. 25*, UNESCO, Paris, 1978.)

Kuznetsova, L.P., Use of data on atmospheric moisture transport over continents and large river basins for the estimation of water balances and other purposes. *Technical Documents in Hydrology*, 105pp., UNESCO, Paris, 1990.

Lacaux, J.P., R. Delmas, G. Kouadio, B. Cros, and M.O. Andreae, Precipitation chemistry in the Mayombé forest of equatorial Africa, *J. Geophys. Res. 97*, 6195-6206, 1992.

Lawrence, J.R., S.D. Gedzelman, J.W.C. White, D. Smiley, and P. Lazov, Storm trajectories in eastern U.S.: D/H isotopic composition of precipitation, *Nature, 296*, 638-640, 1982.

Lawrence, J.R., and J.W.C. White, The elusive climate signal in the isotopic composition of precipitation, in *Stable Isotope Geochemistry: A Tribute to Samuel Epstein*, edited by H.P. Taylor, Jr., J.R. O'Neil and I.R. Kaplan, pp. 169-185, The Geochemical Society, Special Publication No. 3, 1991.

Lorius, C., and L. Merlivat. Distribution of mean surface stable isotope values

in East Antarctica: observed changes with depth in the coastal area. in *Isotopes and Impurities in Snow and Ice*, IAHS Publ. No. 118, pp. 127-137, 1977.

Matsui, E., E. Salati, M.N.G. Ribeiro, M.C. Reis, A.C. Tancredi, and J.R. Gat, Precipitation in the central Amazon Basin: The isotopic composition of rain and atmospheric moisture at Belém and Manaus, *Acta Amazonica, 13*, 307-369, 1983.

Matsuo, S., and I. Friedman, Deuterium content in fractionally collected rain, *J. Geophys. Res., 72*, 6374-6376, 1967.

McKinney, C.R., J.M. McCrea, S. Epstein, H.A. Allen, and H.C. Urey, Improvements in mass spectrometers for the measurement of small differences in isotope abundance ratios, *Rev. Sci. Instrum., 21*, 724-756, 1950.

Merlivat, M., and J. Jouzel, Global climatic interpretation of the deuterium - oxygen-18 relationship for precipitation, *J. Geophys. Res., 84*, 5029-5033, 1979.

Miyake, Y., O. Matsubaya and C. Nishihara, An isotopic study on meteoric precipitation, *Pap. Meteor. Geophys., 19*, 243-266, 1968.

Mook, W.G., D.J. Groeneveld, A.E., Brown, and A.J. Van Ganswijk, Analysis of a run-off hydrograph by means of natural ^{18}O, in *Isotope Techniques in Groundwater Hydrology, Vol. I*, pp. 145-153, International Atomic Energy Agency, Vienna, 1974.

Nativ, R., and R. Riggio, Precipitation in the southern High Plains: Meteorologic and isotopic patterns, *J. Geophys. Res., 95*, 22,559-22,564, 1990.

Nier, A.O., A mass spectrometer for isotope and gas analysis, *Rev. Sci. Instrum., 18*, 398-404, 1947.

Nier, A.O., E.P. Ney, and M.G. Inghram, A null method for the comparison of two ion currents in a mass spectrometer, *Rev. Sci. Instrum., 18*, 294-301, 1947.

Peel, D.A., R. Mulvaney, and B.M. Davison. Stable-isotope/air-temperature relationship in ice cores from Dolleman Island and the Palmer Land Plateau, Antarctic Peninsula, *Ann. Glaciol., 10*, 130-136, 1988.

Peixoto, J.P., and A.H. Oort, The atmospheric branch of the hydrological cycle and climate, in *Variations in the Global Water Budget*, edited by A. Street-Perrott et al., pp. 5-65, D. Reidel Publishing Company, 1983.

Petit, J.R., J.W.C. White, N.W. Young, J. Jouzel, and Y.S. Korotkevich, Deuterium excess in recent Antarctic snow, *J. Geophys. Res., 96*, 5113-5122, 1991.

Picciotto. E., X. De Maere and I. Friedman, Isotopic composition and temperature of formation of Antarctic snows, *Nature, 187*, 857-859, 1960.

Ratisbona, L.R., The climate of Brazil, in *Climates of Central and South America*, edited by W. Schwerdtfeger, pp. 219-293, Elsevier-Science, New York, 1976.

Rindsberger, M., M. Magaritz, I. Carmi, and D. Gilad, The relation between air mass trajectories and the water isotope composition of rain in the Mediterranean Sea area, *Geophys. Res. Lett., 10*, 43-46, 1983.

Rindsberger, M., S. Jaffe, S. Rahamin, and J.R. Gat, Patterns of the isotopic composition of precipitation in time and space: data from the Israeli storm water collection program, *Tellus, 42B*, 263-271, 1990.

Rozanski, K., and C. Sonntag, Vertical distribution of deuterium in atmospheric water vapour, *Tellus, 34*, 135-141, 1982.

Rozanski, K., C. Sonntag and K.O. Münnich, Factors controlling stable isotope composition of modern European precipitation, *Tellus, 34*, 142-150, 1982.

Rozanski, K., D, ^{18}O and ^{3}H in atmospheric water vapour and precipitation collected at Krakow station during the time period June 1981 - Dezember 1985, *Report INT 202/I*, Institute of Physics and Nuclear Techniques, Academy of Mining and Metallurgy, Krakow, 1986.

Rozanski, K., Deuterium and oxygen-18 in atmospheric part of hydrological cycle, *Scientific Bulletins of Academy of Mining and Metallurgy, No. 1098*, 1-100pp., (in Polish), 1987.

Rozanski, K., L. Araguás-Araguás, and R. Gonfiantini, Relation between long-term trends of oxygen-18 isotope composition of precipitation and climate, Science, (in press), 1992.

Salati, E., A. Dall'Olio, E. Matsui, and J.R. Gat, Recycling of water in the Amazon Basin: An isotopic study, *Water Resour. Res., 15*, 1250-1258, 1979.

Schoch-Fischer, H., K. Rozanski, H. Jacob, C. Sonntag, J. Jouzel, G. Östlund and M.A. Geyh, Hydrometeorological factors controlling the time variation of D, ^{18}O and ^{3}H in atmospheric water vapour and precipitation in the northern westwind belt, in Isotope Hydrology 1983, pp. 3-31, International Atomic Energy Agency, Vienna, 1984.

Siegenthaler, U., and H. Matter, Dependence of $\delta^{18}O$ and δD in precipitation on climate, in *Paleoclimate and Paleowaters: A Collection of Environmental Isotope Studies*, pp. 37-51, International Atomic Energy Agency, Vienna, Austria, 1983.

Sonntag, C. E. Klitzsch, E.P. Löhnert, E.M. El-Shazly, K.O. Münnich, Ch. Junghans, U. Thorweihe, K. Weistroffer and F.M. Swailem, Palaeoclimatic information from deuterium and oxygen-18 in carbon-14 dated north Saharian groundwaters, in *Isotope Hydrology 1978, Vol. II*, pp. 569-581, International Atomic Energy Agency, Vienna, 1979.

Sonntag, C., K. Rozanski, K.O. Münnich, and H. Jacob, Variations of deuterium and oxygen-18 in continental precipitation and groundwater and their causes, in *Variations in the Global Water Budget*, edited by A.Street-Perrott et al., pp. 107-124, D. Reidel Publishing Company, 1983.

Steward, M.K., Stable isotope fractionation due to evaporation and isotopic exchange of falling water drops: Applications to atmospheric processes and evaporation of lakes, *J. Geophys. Res., 80*, 1133-1146, 1975.

Stute, M., P. Schlosser, J.F. Clark, and W.S. Broecker, Paleotemperatures in the southwestern United States derived from noble gases in ground water, *Science, 256*, 1000-1003, 1992.

Taylor, C.B., The vertical variations of the isotopic concentrations of tropospheric water vapour over continental Europe and their relationship to tropospheric structure, *DSIR Report INS-R-107*, 44pp., Lower Hutt, New Zealand, 1972.

Taylor, C.B., Stable isotope composition of monthly precipitation samples collected in New Zealand and Rarotonga, DSIR Physical Sciences Report No. 3, 102pp., Lower Hutt, New Zealand, 1990.

White, J.W.C., and S.D. Gedzelman, The isotopic composition of atmospheric water vapor and the concurrent meteorological conditions, *J. Geophys. Res., 89*, 4937-4939, 1984.

Winograd, I.J., B.J. Szabo, T.B. Coplen, and A.C. Riggs, A 250,000-year climatic record from Great Basin vein calcite: implications for Milankovitch theory, *Science, 242*, 1275-1280, 1988.

Van der Straaten C.M., and W.G. Mook, Stable isotope composition of precipitation and climatic variability, in *Paleoclimate and Paleowaters: A Collection of Environmental Isotope Studies*, pp. 53-64, International Atomic Energy Agency, Vienna, 1983.

Yapp, C.J., and S. Epstein, Climatic implications of D/H ratios of meteoric water over North America (9.500-22.000 B.P.) as inferred from ancient wood cellulose C-H hydrogen, *Earth Planet. Sci. Lett., 34*, 333-350, 1977.

Yapp, C.J., A model for the relationships between precipitation D/H ratios and precipitation intensity, *J. Geophys. Res., 87*, 9614-9620, 1982.

Yonge, C.J., L. Goldenberg, and H.R. Krouse, An isotope study of water bodies along a traverse of southwestern Canada, *J. Hydrol., 106*, 245-255, 1989.

Yurtsever, Y., and J.R. Gat, Atmospheric waters. in *Stable Isotope Hydrology: Deuterium and Oxygen-18 in the Water Cycle*, edited by J.R. Gat and R. Gonfiantini, Technical Report Series, No. 210, pp. 103-142, International Atomic Energy Agency, Vienna, 1981.

Zimmermann, U., D.H. Ehhalt, and K.O. Münnich. Soil water movement and evapotranspiration: Changes in the isotopic composition of water, in *Isotopes in Hydrology*, pp. 567-585, International Atomic Energy Agency, Vienna, 1967.

K. Rozanski, L. Araguás-Araguás and R. Gonfiantini, International Atomic Energy Agency, P.O. Box 100, 1400-Vienna, Austria.